Characterization of Polylactic Acid Degradation in Rotary Drum Composting Systems: From Laboratory Respirometry to Industrial-Scale Performance

By

Jacob Harvey

A Thesis submitted to the Faculty of Graduate and Postdoctoral Studies of The University of Manitoba in partial fulfilment of the requirements of the degree of

MASTER OF SCIENCE

Department of Biosystems Engineering

University of Manitoba

Winnipeg

Copyright © 2026 by Jacob Harvey

Author's Declaration

I certify that this thesis is my own original work. This document is an accurate copy of the thesis, including all required final revisions, as approved by my examining committee. I acknowledge that the thesis may be made publicly available in electronic form.

Supervisory Committee

Dr. David B. Levin - Department of Biosystems Engineering, University of Manitoba

Dr. Richard Sparling - Department of Microbiology, University of Manitoba

Dr. Ryan Sestric - Department of Biosystems Engineering, University of Manitoba

Dr. Warren Blunt - Department of Biosystems Engineering, University of Manitoba

Dr. Michael Snowdon - National Research Council of Canada

Abstract

This thesis characterizes polylactic acid (PLA) degradation in Rotary Drum Composting (RDC) systems through laboratory respirometry and industrial-scale composting. Laboratory respirometry was conducted in 2 L vessels containing ~5 g of PLA in 275 g of PLA-adapted compost sourced from a local operating RDC. At 58 °C, complete mineralization was achieved within 45 days. At 30 °C, there was negligible mineralization within 81 days regardless of biostimulation or bioaugmentation. RDC trials, the first characterization of PLA degradation in rotating in-vessel composters, showed rapid physical degradation of PLA. Most films degraded beyond recoverable mass within two to four weeks under intermittent thermophilic exposure. Outcomes were bimodal; some films were completely degraded, while others remained intact over six weeks despite identical residence time. This was hypothesized to result from spatial thermal heterogeneity within the vessel, which was supported by per-bag temperature sensor data, and was reduced but not eliminated through increased vessel rotation. As abiotic hydrolysis and molecular weight reduction are the rate-limiting steps in PLA degradation, UV-C pretreatment was investigated and achieved in hours the degree of molecular weight reduction that required weeks under thermophilic composting, though without a corresponding reduction in PLA mass. Across composting experiments, cumulative thermal exposure was the strongest predictor of PLA degradation, and residence time alone was not a reliable metric in heterogeneous composting environments. Future work should prioritize per-sample thermal tracking in full-length RDC trials, with continuous rotation, and integration of UV-C pretreatment with composting to determine whether accelerated molecular weight reduction translates to faster mineralization.

Table of Contents

Author's Declaration *1*

Supervisory Committee *2*

Abstract *3*

Acknowledgements *9*

List of Abbreviations *11*

List of Tables *14*

List of Figures *16*

List of Equations *18*

Chapter 1: Introduction and Background on PLA Biodegradation *19*

1.1 Plastics and the environment **19**

1.2 PLA – uses and structure **20**

1.3 Composting, Landfilling, and Standards for PLA Compostability **21**

1.4 Degradation of PLA – Chemical and Environmental Factors **24**

1.4.1 Initial Hydrolysis Step 24

1.4.2 Effect of Polymer Properties 25

1.4.3 Effect of environment pH on PLA degradation 27

1.5 Microbial and Enzymatic Degradation of PLA **28**

1.5.1 Enzymatic Approaches 28

1.5.2 Inducers 28

1.5.3 Bacteria 30

1.6 Pretreatment of PLA **31**

1.7 Rotary Drum Compost Systems **33**

1.8 Research Questions, Hypotheses, and Objectives **35**

1.8.1 Rationale of the Research 35

1.8.2 Research Questions 35

1.8.3 Hypotheses 36

1.8.4 Objectives 37

Chapter 2: Materials and Methods *38*

2.1 PLA Films **38**

2.2 Polymer Characterization Techniques 39
2.2.1 Mass Loss Analysis 39
2.2.2 Differential Scanning Calorimetry (DSC) 40
2.2.3 Intrinsic Viscosity (Viscometry) Molecular Weight Determination 42
2.2.4 Scanning Electron Microscopy (SEM) 44

Chapter 3: Influence of Temperature, Crystallinity, and Biological Enhancement on PLA Mineralization in Laboratory Composting 46

3.1 Introduction 46

3.2 Experimental Design and Methods 48
3.2.1 Respirometry Setup 48
3.2.2 Compost Source and Preparation 48
3.2.3 Calculation of Biodegradation via CO_2 Evolution 49
3.2.4 Statistical Analyses 50
3.2.5 Thermophilic Degradation 52
3.2.6 Mesophilic Degradation 53
3.2.7 Mesophilic Degradation with Bacterial Inoculation 54

3.3 Results 56
3.3.1 Thermophilic Degradation 56
3.3.2 Mesophilic Degradation 64
3.3.3 Mesophilic Degradation with Bacterial Inoculation 68

3.4 Discussion 73
3.4.1 Thermophilic Degradation of PLA 73
3.4.2 Mesophilic Conditions and Biostimulation/Bioaugmentation 75
3.4.3 Crystallinity 76

3.5 Conclusions 77

3.6 Recommendations for Experimental Refinement 78
3.6.1 Controls and Baseline Characterization 78
3.6.2 Replication, Sampling, and Analytical Gaps 79
3.6.3 Bioaugmentation Validation 80

Chapter 4: PLA Degradation and Thermal Variability in Rotary Drum Composting Systems 82

4.1 Introduction 82

4.2 Experimental Design and Methods 85
4.2.1 RDC System and Operating Conditions 85
4.2.2 SIAF RDC Experiment 1 Operating Conditions 90
4.2.3 SIAF RDC Experiment 2 Operating Conditions 91
4.2.4 SIAF RDC Experiment 3 Operating Conditions 92

4.2.5 Forks RDC Operating Conditions 93
4.3 Results 94
4.3.1 SIAF RDC Experiment 1 94
4.3.2 SIAF RDC Experiment 2 99
4.3.3 SIAF RDC Experiment 3 103
4.3.4 The Forks RDC Experiments 108
4.3.5 Thermal and Crystalline Changes in PLA Recovered from RDC Composting 112
4.4 Discussion 114
4.4.1 Mesh Bag Recovery Method 114
4.4.2 PLA Degradation 114
4.4.3 RDC Scale 116
4.5 Conclusions 117
4.6 Recommendations for Experimental Refinement 117
4.6.1 Recovery Method Validation 117
4.6.2 Environmental Monitoring 118
4.6.3 Forks PLA Characterization 119
Chapter 5: Molecular Weight Reduction of PLA Following UV-C Treatment 120
5.1 Introduction 120
5.2 Experimental Design and Methods 122
5.3 Results 124
5.3.1 Mass loss 124
5.3.2 Molecular-weight (Mv) response to UV-C exposure 124
5.3.3 Thermal and Crystalline Changes in PLA Following UV-C Exposure (DSC Analysis) 128
5.4 Discussion 130
5.4.1 Comparison to prior UV degradation studies 130
5.4.2 Context within composting-based degradation 133
5.5 Conclusions 134
5.6 Recommendations for Experimental Refinement 135
5.6.1 Validation of UV Pretreatment Effects 135
5.6.2 Refinement of Exposure Parameters 135
Chapter 6: Synthesis and Engineering Significance 137
6.1 Cross-Chapter Synthesis 137
6.2 Engineering Significance 139
6.3 Scope Limitations 140

6.4 Recommendations for Future Work **141**

References ***143***

Appendix ***154***

Appendix A – Raw mass recovery and film condition data **154**
Table A1 – SIAF RDC Experiment 1: individual film recovery data 154
Table A2 – SIAF RDC Experiment 2: individual film recovery data 157
Table A3 – Forks RDC Experiment (grouped-bag method): individual film recovery data 160
Figure A1 – Lightly fragmented PLA film with 100% recovery 162
Figure A2 – Heavily fragmented/powderized PLA film with 22% recovery 163

Appendix B – Molecular weight and DSC raw outputs **164**
Table B1 – Respirometer PLA Mv Data (30 °C Experiments) 164
Table B2 – SIAF RDC PLA Mv Data 166
Table B3 – Forks RDC PLA Mv Data 167
Table B4 – UV-C Exposure PLA Mv Data 168
Table B5 – DSC outputs for composted PLA samples 172
Table B6 – DSC outputs for UV-treated PLA samples 172
Figure B7 – DSC first heating thermograms of amorphous PLA films after 8 and 24 hours of UV-C exposure 173
Figure B8 – DSC first heating thermograms of crystalline (annealed) PLA films after 0, 1, 2, 8, and 24 hours of UV-C exposure 174
Figure B9 – DSC first heating thermograms of Forks PLA films after 0, 8, and 24 hours of UV-C exposure 175
Figure B10 – DSC first heating thermograms of Forks PLA samples before and after 3 and 6 weeks in the Forks RDC 176
Figure B11 – DSC first heating thermograms of crystalline PLA recovered after 4 weeks in the SIAF RDC (SBE1 4w C) 177
Figure B12 – DSC first heating thermograms of Forks PLA recovered after 4 weeks in the SIAF RDC (SBE1 4w F) 178
Figure B13 – DSC first heating thermogram of amorphous PLA recovered after 4 weeks in the SIAF RDC (SBE1 4w A) 179

Appendix C – RDC Temperature Data **180**
Table C1 – SIAF RDC Experiment 1 Daily Internal Temperature Data 180
Table C2 – SIAF RDC Experiment 2 Daily Internal Temperature Data 181
Table C3 – Forks RDC Experiment 2 Daily Internal Temperature Data 183

Appendix D – Statistical outputs and calculation examples **184**
Table D1 – Two-way ANOVA (58 °C respirometer) 184
Table D2 – One-way ANOVA (30 °C respirometer) 184
Table D3 – One-way ANOVA (30 °C inoculation experiment) 184
Table D4 – Tukey HSD pairwise comparisons (58 °C) 185
Table D5 – Tukey HSD pairwise comparisons (30 °C) 185

Table D6 – Tukey HSD pairwise comparisons (inoculated study)..... 187
Table D7 – Two-way ANOVA on Mv - 30 °C Experiment (Crystallinity × Gelatin) 188
Table D8 – Tukey HSD pairwise comparisons on Mv (30 °C Experiment) 189
Table D9 – One-way ANOVA on Mv - 30 °C Inoculation Experiment 189
Table D10 – Welch's t-test on Mv - Forks RDC (3 vs 6 weeks)..... 190
Table D11 – Two-way ANOVA on Mv - UV-C 1h exposure (Material × Irradiance)..... 190
Table D12 – Two-way ANOVA on Mv - UV-C 2h exposure (Material × Irradiance)..... 190
Table D13 – Two-way ANOVA on Mv - UV-C 8h exposure (Material × Irradiance)..... 191
Table D14 – Two-way ANOVA on Mv - UV-C 24h exposure (Material × Irradiance)..... 192
Table D15 – Tukey HSD pairwise comparisons on Material (UV-C, 24 h)..... 192
Table D16 – Unconstrained kinetic model parameters..... 193
Table D17 – Constrained kinetic model parameters..... 195
D18 – CO_2 → % biodegradation calculation example for Annealed PLA (Experiment 1)..... 197
D19 – Intrinsic viscosity → Mark–Houwink molecular weight calculation example for Amorphous PLA (baseline) 199
D20 – Single-point intrinsic viscosity estimate → Mark–Houwink molecular weight example for UV Experiment sample 201

Acknowledgements

Firstly, I would like to thank the members of my advisory committee. I am very grateful to Dr. Levin for being my advisor and for his support through the entire experience, always responding quickly and helpfully. I thank Dr. Sparling for his very helpful feedback during committee and lab meetings. I also thank Dr. Warren Blunt for mentoring me in the lab and starting my journey with research, and Dr. Ryan Sestric for his mentorship and support throughout my research experience as well. I am grateful to Dr. Sarita Shrestha for her help with various project elements I was unfamiliar with. I am also extremely grateful to the whole lab for it being a great space to work in.

My thanks also go to Dr. Joe Ackerman for his knowledge, support, and company throughout my work at the SIAF rotary drum composter. I am thankful to Daniel Benedet and Minami Maeda for continuously helping with technical problems throughout the thesis, and Dale Bourns for helping me construct the UV chamber. I am also grateful to Jen Beaudoin and Caitlin Jacques for their knowledge regarding the program requirements and help with vehicle bookings, reimbursements, shipment tracking, and order processing.

I would also like to thank Helga Jakobson and Dave Pancoe for allowing me to conduct experiments with the Forks rotary drum composter, and all their help in doing so.

I thank the NRC – Dr. Michael Snowdon, Sarah Low Ying, Dash Yetirajula, and Dr. Abbas Ghanbari – for helping me with respirometer experiments and their great support and company throughout those experiments. I am also grateful to the NRC for funding the project and their great communication with me throughout its duration.

Finally, I would like to thank my wife, mother, father, sister, and extended family for their unwavering support, encouragement, and patience throughout this work.

List of Abbreviations

ANOVA	Analysis of Variance
ASTM	American Society for Testing and Materials
CFU	Colony-Forming Units
CO_2	Carbon Dioxide
DSC	Differential Scanning Calorimetry
GC	Gas Chromatograph
H_2	Hydrogen
HSD	Honestly Significant Difference
LB	Lysogeny Broth
MM	Minimal Medium
Mn	Number-Average Molecular Weight
Mv	Viscosity-Average Molecular Weight
Mw	Weight-Average Molecular Weight
N_2	Nitrogen
NRC	National Research Council (of Canada)
O_2	Oxygen
PBS	Phosphate-Buffered Saline
PE	Polyethylene

PET	Polyethylene Terephthalate
PHBV	Poly(3-hydroxybutyrate-co-valerate)
PLA	Polylactic Acid / Polylactide
PLLA	Poly(L-lactic acid)
PDLA	Poly(D-lactic acid)
RDC	Rotary Drum Composter
RH	Relative Humidity
SD	Standard Deviation
SEM	Scanning Electron Microscopy
SIAF	Sustainability in Action Facility (Building, University of Manitoba)
Tcc	Cold Crystallization Temperature
Tc	Crystallization Temperature
Tg	Glass Transition Temperature
Tm	Melting Temperature
TOC	Theoretical Organic Carbon
U of M	University of Manitoba
UV	Ultraviolet
UV-A	Ultraviolet A (315–400 nm)
UV-C	Ultraviolet C (100–280 nm)
w/v	Weight per Volume

Xc	Percent Crystallinity
ΔHcc	Enthalpy of Cold Crystallization
ΔHm	Enthalpy of Melting
[η]	Intrinsic Viscosity

List of Tables

Table 1.1 Comparative Overview of Crystallinity Effects on PLA Degradation Rates under Composting, Hydrolytic, and Enzymatic Conditions. 26

Table 3.1 Summary of published studies on aerobic biodegradation of PLA in compost respirometry systems. 47

Table 3.2 Summary of respirometer conditions for Experiment 1, evaluating the effects of PLA crystallinity and biostimulation on aerobic biodegradation at 58 °C. 53

Table 3.3 End-point CO_2 values & calculated percentage of biodegradation for aerobic composting at 58 °C. 58

Table 3.4 Kinetic parameters for PLA biodegradation during aerobic composting at 58 °C over 45 days, based on first-order kinetic model. 61

Table 3.5 End-point CO_2 values & calculated percentage of biodegradation for aerobic composting at 30 °C. 66

Table 3.6 Viscosity-average molecular weight (Mv) of PLA films (n = 3) following mesophilic composting at 30 °C. 67

Table 3.7 End-point CO_2 values & calculated biodegradation percentage for PLA-containing compost inoculated with different bacterial strains at 30 °C for 90 days. 70

Table 3.8 Viscosity-average molecular weight (Mv) of PLA films following mesophilic composting with bacterial inoculation at 30 °C. 71

Table 4.1 Summary of published studies on PLA degradation under industrially relevant composting conditions. 83

Table 4.2 Distribution of PLA film recovery outcomes for SIAF Experiment 1 at 2, 4 and 6 weeks. 95

Table 4.3 Viscosity-average molecular weight of PLA recovered from SIAF RDC Experiment 1.... 97

Table 4.4 Distribution of PLA film recovery outcomes for Experiment 2 at 2, 4 and 6 weeks. 100

Table 4.5 Viscosity-average molecular weight of PLA recovered from SIAF RDC Experiment 2.. 101

Table 4.6 Summary of thermal exposure metrics by sensor for SIAF RDC Experiment 3. 104

Table 4.7 Summary of thermal exposure and viscosity-average molecular weight loss by sensor for SIAF RDC Experiment 3. 106

Table 4.8 Distribution of PLA film recovery outcomes following Forks RDC composting at 3 and 6 weeks. 108

Table 4.9 Viscosity-average molecular weight of PLA recovered from Forks RDC experiment. 110

Table 4.10 Differential scanning calorimetry (DSC) results for PLA samples recovered from RDC composting experiments. 112

Table 5.1 Mean irradiance relative to the UV-lamp position in the chamber. 123

Table 5.2 Molecular weight reduction of PLA films under 2300 μW cm^{-2} UV exposure. 126

Table 5.3 Molecular weight reduction of PLA films under 1750 μW cm^{-2} UV exposure. 127

Table 5.4 Differential scanning calorimetry (DSC) results for PLA films following UV-C exposure at varying durations. 130
Table 5.5 Summary of published studies investigating UV-induced degradation of polylactic acid (PLA) under varying wavelengths, irradiance levels, and material forms. 131
Table A1 SIAF RDC Experiment 1: individual film recovery data 154
Table A2 SIAF RDC Experiment 2: individual film recovery data 157
Table A3 Forks RDC Experiment (grouped-bag method): individual film recovery data 160
Table B1 Respirometer PLA Mv Data (30 °C Experiments) 164
Table B2 SIAF RDC PLA Mv Data 166
Table B3 Forks RDC PLA Mv Data 167
Table B4 UV-C Exposure PLA Mv Data 168
Table B5 DSC outputs for composted PLA samples 172
Table B6 DSC outputs for UV-treated PLA samples 172
Table C1 SIAF RDC Experiment 1 Daily Internal Temperature Data 180
Table C2 SIAF RDC Experiment 2 Daily Internal Temperature Data 181
Table C3 Forks RDC Experiment 2 Daily Internal Temperature Data 183
Table D1 Two-way ANOVA (58 °C respirometer) 184
Table D2 One-way ANOVA (30 °C respirometer) 184
Table D3 One-way ANOVA (30 °C inoculation experiment) 184
Table D4 Tukey HSD pairwise comparisons (58 °C) 185
Table D5 Tukey HSD pairwise comparisons (30 °C) 185
Table D6 Tukey HSD pairwise comparisons (inoculated study) 187
Table D7 Two-way ANOVA on Mv - 30 °C Experiment (Crystallinity × Gelatin) 188
Table D8 Tukey HSD pairwise comparisons on Mv (30 °C Experiment) 189
Table D9 One-way ANOVA on Mv - 30 °C Inoculation Experiment 189
Table D10 Welch's t-test on Mv - Forks RDC (3 vs 6 weeks) 190
Table D11 Two-way ANOVA on Mv - UV-C 1h exposure (Material × Irradiance) 190
Table D12 Two-way ANOVA on Mv - UV-C 2h exposure (Material × Irradiance) 190
Table D13 Two-way ANOVA on Mv - UV-C 8h exposure (Material × Irradiance) 191
Table D14 Two-way ANOVA on Mv - UV-C 24h exposure (Material × Irradiance) 192
Table D15 Tukey HSD pairwise comparisons on Material (UV-C, 24 h) 192
Table D16 Unconstrained kinetic model parameters 193
Table D17 Constrained kinetic model parameters 195

List of Figures

Figure 2.1 Representative DSC thermogram for annealed PLA showing a complete heat-cool-heat cycle. 41

Figure 3.1 Cumulative CO_2 evolution from different compost conditions after aerobic composting at 58 °C for 45 days. 57

Figure 3.2 Compost recovered from thermophilic respirometer vessels (58 °C) following complete PLA mineralization. White deposits on wood chip surfaces were observed equally across all conditions, including negative controls without PLA, and are attributed to mineral precipitates. 59

Figure 3.3 First-order kinetic model fits for untreated and inducer-included amorphous PLA biodegradation at 58 °C. 62

Figure 3.4 First-order kinetic model fits for untreated annealed PLA biodegradation and inducer conditions at 58 °C. 62

Figure 3.5 First-order kinetic model fits for untreated cellulose biodegradation and inducer conditions at 58 °C. 63

Figure 3.6 Cumulative CO_2 evolution from different compost conditions after aerobic composting at 30 °C for 81 days. 65

Figure 3.7 Cumulative CO_2 evolution from PLA-containing compost inoculated with different bacterial strains at 30 °C for 90 days. 69

Figure 3.8 Scanning electron micrographs (2000×) of untreated amorphous and crystalline PLA films prior to composting. 72

Figure 3.9 Surface morphology of amorphous PLA films pre- and post-incubation with PLA-degrading microbes. 73

Figure 4.1 Schematic of Forks RDC, showing the inlet and outlet with unit length and diameter. 85

Figure 4.2 Diagram showing PLA within mesh bags along with identity tags. 87

Figure 4.3 Exterior view of the SIAF RDC (Winnipeg, MB), an 18-foot rotating in-vessel composting unit used in experiments. 90

Figure 4.4 Exterior view of the Forks Market RDC (Winnipeg, MB), a 42-foot rotating in-vessel composting unit used in experiments. 93

Figure 4.5 Internal temperature profile of the SIAF RDC compared to ambient temperature during Experiment 1. 98

Figure 4.6 Internal temperature profile of the SIAF RDC compared to ambient temperature during Experiment 2. 102
Figure 4.7 Temperature-time profiles for seven sensors in the SIAF RDC during Experiment 3. 103
Figure 4.8 Mean internal temperature of the SIAF RDC (seven sensors) compared to ambient temperature during Experiment 3. 107
Figure 4.9 Chamber temperature profiles of the Forks RDC compared to ambient temperature. 111
Figure 5.1 Inside of UV Chamber. 123
Figure 5.2 Kinetics of viscosity-average molecular weight (Mv) reduction of amorphous, crystalline, and field-recovered (Forks) PLA films during high-irradiance UV exposure. 125
Figure A1 Lightly fragmented PLA film with 100% recovery 162
Figure A2 Heavily fragmented/powderized PLA film with 22% recovery 163
Figure B7 DSC first heating thermograms of amorphous PLA films after 8 and 24 hours of UV-C exposure 173
Figure B8 DSC first heating thermograms of crystalline (annealed) PLA films after 0, 1, 2, 8, and 24 hours of UV-C exposure.....174
Figure B9 DSC first heating thermograms of Forks PLA films after 0, 8, and 24 hours of UV-C exposure 175
Figure B10 DSC first heating thermograms of Forks PLA samples before and after 3 and 6 weeks in the Forks RDC 176
Figure B11 DSC first heating thermograms of crystalline PLA recovered after 4 weeks in the SIAF RDC (SBE1 4w C). 177
Figure B12 DSC first heating thermograms of Forks PLA recovered after 4 weeks in the SIAF RDC (SBE1 4w F). 178
Figure B13 DSC first heating thermogram of amorphous PLA recovered after 4 weeks in the SIAF RDC (SBE1 4w A). 179

List of Equations

Eq. 1 Percent crystallinity....41
Eq. 2 Mark-Houwink-Sakurada equation....43
Eq. 3 Inherent viscosity....43
Eq. 4 Percent biodegradation (ASTM D5338)....49
Eq. 5 Standard error of biodegradation....49
Eq. 6 First-order kinetic model with lag phase....60

Chapter 1: Introduction and Background on PLA Biodegradation

1.1 Plastics and the environment

Plastics have become a ubiquitous and essential component of daily life due to their versatility, durability, and low cost. Their easy processability and widespread availability have made them integral in numerous sectors, including consumer goods, food and medical packaging, agriculture, construction, and automotive parts. These properties have significantly increased their demand and usage across various industries (Gautam et al., 2024).

The accumulation of plastic waste is a significant global environmental concern and is brought on by their large-scale usage and persistence in natural environments (Napper & Thompson. 2023). This persistence is primarily attributed to their molecular composition and contributes to significant ecological issues such as accumulation in landfills, oceans, and other natural habitats (Dhiman et al., 2022). Most common commodity plastics are synthesized from subunits derived from processing crude oil (petrochemicals), such as ethylene, and include common polymers like polyethylene (PE), polypropylene (PP), and polyvinyl chloride (PVC). These materials are specifically engineered for durability, incorporating strong carbon-carbon bonds that impart high resistance to physical and chemical degradation. Their inherent stability means that these plastics do not readily undergo natural degradation processes.

Biodegradable plastics are those that are degraded through biological means, primarily breakdown by microorganisms such as algae, bacteria, and fungi (Nizamuddin & Chen. 2024). These microorganisms secrete enzymes that degrade the polymers prior to and throughout assimilation, with abiotic factors influencing this process, such as exposure to UV-radiation and

wind-driven erosion. Biodegradation is a complex, multi-phase process in which abiotic and biotic factors combine to alter the chemical structure of the polymer chains. Conversion of all the carbon in the polymers to cell mass, carbon dioxide, water, and inorganic compounds results in mineralization, and complete biodegradation (Lucas et al., 2008). Complete mineralization of common commodity plastics like PE and PP has not yet been observed (Fakhrizada & Dahman. 2025). Complete mineralization of "compostable" plastics, like Poly(Lactic acid), or Polylactide (PLA), can be achieved, but only under specific conditions (Fakhrizada & Dahman. 2025).

1.2 PLA – uses and structure

PLA is a thermoplastic (remoldable when heated), aliphatic polyester typically derived from renewable materials and marketed as a biodegradable and industrially compostable polymer. Agricultural products such as corn, sugarcane, and cassava undergo processing to convert carbohydrates (e.g., starch or cellulose) into fermentable sugars, which are then fermented by specific strains of bacteria or yeast to produce lactic acid (Nampoothiri et al., 2010). The produced lactic acid is then polymerized to form PLA through either a condensation reaction or by the ring-opening polymerization (ROP) of lactide, the cyclic dimer of the lactic acid repeating unit. The method of polymerization affects the type of PLA produced, with ROP yielding high molecular weight PLA suitable for various applications, and condensation methods producing low molecular weight PLA often requiring further modification for practical use (Swetha et al., 2023). It is commonly produced in three stereochemical forms: poly(L-lactide) (PLLA), poly(D-lactide) (PDLA), and poly(DL-lactide) (PDLLA) (Nampoothiri et al., 2010).

The need for commercially viable degradable plastics derived from renewable feedstocks, instead of petrochemicals, has spurred the large-scale production of PLA, taking various compostable forms (Karamanlioglu et al., 2017). Its growing use can be attributed to its bio-based origin, biodegradability, and ease of processing; PLA can be molded into a wide range of forms through blending, reinforcement, and nanocomposite design both for common commodity usage as well as engineering, agricultural, and medical sectors (Ranakoti et al., 2022). PLA's stereochemical forms offer varying crystallinity and thermal properties, making it possible to tailor PLA grades for specific processing methods and high-performance applications (Fiori. 2014). From 2020 to the present, PLA has become the most widely-used bioplastic globally (Ceresana, 2023).

1.3 Composting, Landfilling, and Standards for PLA Compostability

PLA products are primarily landfilled or composted at end of life (Ghomi et al., 2021). Landfills are engineered containment systems in which waste is compacted, covered, and isolated from the environment (U.S. EPA, 2025), resulting in predominantly anaerobic conditions (Shi & Palfery, 2012). Internal landfill temperatures generally do reach peak temperatures around 55 °C, though this is not always the case, and over decades they stabilize between 25 and 55 °C (Yeşiller et al., 2015). In cases where they do not sustain thermophilic temperatures, the initial hydrolysis step required for subsequent microbial assimilation is limited (Quecholac-Piña et al., 2020; Olaya-Rincon et al., 2025). Composting is a managed aerobic process involving mesophilic and thermophilic degradation of organic matter (ASTM D6400, 2023). Effective composting requires a balanced carbon-to-nitrogen (C:N) ratio, typically between 25:1 and 35:1, which is maintained

through carbon-rich bulking agents such as wood chips and straw alongside nitrogen sources such as manure, food waste, and fresh grass. PLA is essentially a pure carbon substrate, and so high PLA-loading composting systems require a distinct nitrogen source, similar to conventional cellulose-based carbon sources. There are numerous ways to compost, ranging from passive, static piles and windrow systems, to actively aerated piles and in-vessel systems that use forced aeration and mechanical mixing to maintain controlled conditions (U.S. EPA, 2025). Industrial and municipal composting facilities typically employ windrow, aerated static pile, or in-vessel methods to process large volumes of organic waste, with windrow being the most common in North America (U.S. EPA, 2025; Environment Canada, 2013). PLA is considered compostable, and complete or near-complete degradation has been reported in both laboratory respirometers and industrial-scale composting systems at sustained temperatures above 55°C (Musioł et al., 2016; Maragkaki et al., 2023; Fogašová et al., 2022; Gastaldi et al., 2024).

A plastic material being considered compostable has a different meaning than the material being biodegradable; there are specific standards that establish definitions. ASTM D5338, *Standard Test Method for Determining Aerobic Biodegradation of Plastic Materials Under Controlled Composting Conditions, Incorporating Thermophilic Temperatures*, is a respirometry standard used to quantify biodegradation of plastics under simulated composting conditions (ASTM D5338, 2021). The test plastic is mixed with a compost inoculum and incubated at 58 °C for a minimum of 45 days, with CO_2 evolution measured relative to a negative control containing only the compost inoculum. A positive cellulose control is also required, where 70% biodegradation must be measured within 45 days with less than 20% standard deviation for the test to be valid. ASTM

D6400, *Standard Specification for Labeling of Plastics Designed to be Aerobically Composted in Municipal or Industrial Facilities*, sets the requirements for labeling a plastic as compostable, and requires physical disintegration (no more than 10% of original dry weight remaining on a 2.0 mm sieve after 12 weeks), conversion of at least 90% of organic carbon to CO_2 within 180 days, and no adverse effects on compost quality through ecotoxicity or regulated heavy metal content (ASTM D6400, 2023). These standards define the framework against which PLA compostability is formally evaluated, and ASTM D5338 informed the methodology of the respirometry experiments conducted in this thesis.

Incomplete degradation of PLA poses environmental risks. Ainali et al. (2022) reviewed the existing literature and report that fragmented PLA microplastics (MPs) can adsorb and transport pollutants and may contribute to ecological stress, similarly to conventional plastics. PLA has been found to produce comparatively high quantities of microplastic particles relative to some other polymers through environmental weathering and mechanical stresses (Lambert and Wagner. 2017). Studies report adverse effects of PLA MPs on various organisms, including algae, bacteria, worms, invertebrates, and fish (Ainali et al., 2022). These effects range from altered growth and photosynthesis to stress responses, behavioural changes, reduced reproduction, and microbiome disruptions. Real-world environmental concentrations and distribution of PLA MPs is not well understood.

1.4 Degradation of PLA – Chemical and Environmental Factors

1.4.1 Initial Hydrolysis Step

The hydrolytic degradation of solid PLA proceeds through surface reactions and/or bulk erosion, depending on rates of water diffusion and hydrolysis reactions (Elsawy et al., 2017; Iñiguez-Franco et al., 2018). During bulk degradation, hydrolysis of ester bonds generates oligomers and monomers such as carboxylic acid and hydrolysis end groups. Limited diffusion of the degradation leads to their accumulation in material which lowers the local pH and promotes autocatalytic hydrolysis, which increases the degradation rate (Pitt and Zhong-wei., 1987; Lizundia et al., 2017). The degradation of the PLA polymer matrix is restricted to its surface if the temperature remains below the glass transition (Tg) value, which for PLA is approximately 55 to 62 °C (Karamanlioglu et al., 2017). Sustained exposure to temperatures within this range increases the mobility of the polymer chains, thereby reducing the tightly aligned structure of crystalline regions in the polymer (Bher et al., 2022).

Highly ordered alignment of polymer chains results in regions of the polymer with high crystallinity. Crystalline regions of the polymer are often separated and connected by polymer chains that are more flexible and randomly orientated, resulting in amorphous regions. Enzymes that degrade PLA generally target the amorphous regions of the polymer and are less efficient at breaking down the highly crystalline areas (Shrestha et al., 2025). This initial hydrolysis, whether it occurs enzymatically or chemically, is the rate-limiting step. At lower temperatures, such as those found in agricultural soil environments (around 25 °C), the rate of chemical hydrolysis is

slower. This prolongs the initiation of the enzymatic hydrolysis process and the microbial assimilation of the hydrolysis products.

1.4.2 Effect of Polymer Properties

The degradation rate of PLA is significantly influenced by its polymer properties. High molecular weight and high crystallinity of PLA lead to slower PLA degradation (Tokiwa & Suzuki, 1977; Kun & Kálmán, 2013). Crystalline structures inhibit the diffusion of water and microbes, thereby reducing the rate at which these elements penetrate and degrade the polymer. Amorphous PLA absorbs water more quickly and in larger amounts, which leads to earlier and more significant swelling, facilitating faster biodegradation. Microorganisms find it difficult to assimilate polymer chain segments with higher molecular weights, which reduces the rate of biodegradation. The ratio of L- to D-lactic acid in PLA significantly affects its properties and degradation rate, with the addition of D-lactide units to 100% PLLA increasing hydrolysis due to decreased crystallinity (Höglund et al., 2012).

Table 1.1 Comparative Overview of Crystallinity Effects on PLA Degradation Rates under Composting, Hydrolytic, and Enzymatic Conditions.

Source	***PLA Properties***	***Temp (°C)***	***Medium/Conditions***	***Results***
Pantani and Sorrentino (2013)	Amorphous vs. Semi-crystalline PLA	58	Yard waste compost (Rome, Italy), ASTM D5338/ISO 14855	Amorphous: ~60% degraded in 35 days; Semi-crystalline: ~30% in 60 days. Powdered crystalline reached ~80%.
Kale et al. (2007)	PLA bottles (96% L-lactide) vs. deli containers (94%)	65	MSU composting facility	Lower crystallinity (deli containers, 94% L-lactide) degraded faster.
Gorrasi & Pantani (2017)	Amorphous vs. Semi-crystalline PLLA	37	Phosphate-buffered solution (pH 4.0 & 3.4)	Amorphous: ~14% weight loss in 18 weeks; Semi-crystalline took ~20 months.
MacDonald et al. (1996)	PLA films, varying crystallinity	37	Tris-HCl buffer (pH 8.6) with proteinase K	High crystallinity (PLA-95): 93% reduction in weight loss; Low crystallinity (PLA-90): 38% reduction.
Tsuji and Miyauchi (2001)	PLLA with varying crystallinity	37	Enzymatic hydrolysis	Increased crystallinity led to significantly reduced hydrolysis rate.

Table 1.1 summarizes studies comparing the effect of PLA crystallinity on degradation. Across composting, hydrolytic, and enzymatic conditions, lower crystallinity consistently enhanced degradation rates. Pantani and Sorrentino (2013) showed that amorphous PLA degraded twice as fast as semi-crystalline PLA in compost, though it should be noted this was believed to be due to the compact physical structure of the sample, as a powdered version of the crystalline sample achieved higher mineralization (80%) than the amorphous (70%). While the crystallinity level of the polymer was important, the particle size reduction of the polymer was a more impactful factor.

1.4.3 Effect of environment pH on PLA degradation

The pH of the compost medium also influences PLA degradation. For PLA under acidic conditions (pH < 4) the hydrolysis proceeds via chain-end scission, whereas under neutral to alkaline conditions PLA hydrolysis may take place via backbiting (de Jong et al., 2001). Backbiting refers to a mechanism in which the terminal hydroxyl group attacks the polymer backbone to form cyclic intermediates that are subsequently cleaved (de Jong et al., 2001). At either extreme, degradation proceeds faster than at neutral pH conditions (Göpferich, 1996). However, the optimal pH for enzyme production and PLA biodegradation varies among different bacterial strains. The production of PLA-degrading enzymes and the biodegradation rate of PLA are significantly influenced by the pH of the environment, with each bacterial strain having a specific pH range where enzyme activity is maximized (Bubpachat et al., 2018).

1.5 Microbial and Enzymatic Degradation of PLA

1.5.1 Enzymatic Approaches

Hydrolytic enzymes, such as protease, esterase, and lipase, are the first step in the microbial degradation of PLA. Proteinase K from *Tritirachium album* is specifically identified as a PLA-degrading enzyme. Numerous reports have indicated that PLA-degrading enzymes belong to the protease group (Mistry et al., 2022). Tsuji and Ikarashi (2004) reported no catalytic degradation of crystalline PLA by Proteinase K, indicating that crystalline regions are highly resistant to protease degradation compared to amorphous regions. Esterases are responsible for catalyzing the cleavage of ester linkages in the PLA polymer chain, and lipases, which are a significant group of esterases, have been reported to hydrolyze low molecular weight PLA and copolymers of PLA. Myburgh et al. (2023) suggest that enzyme-based processes could enhance PLA waste management and recycling systems, though substantial amounts of the appropriate enzyme(s) are required. Their study demonstrated the production of fungal PLA hydrolases in the yeast *Saccharomyces cerevisiae*, showing the efficacy of crude supernatants towards degradation of commercial PLA. The supernatant from the top-performing recombinant Y294[CLEns] strain released 9.44 g/L lactic acid from 10 g/L PLA films and resulted in approximately 40% film weight loss after 10 days.

1.5.2 Inducers

Inducers such as gelatin, elastin, silk fibroin, and some amino acids and peptides have been found to stimulate extracellular depolymerases to break down PLA (Jarerat et al., 2004). For example, the production of protease and PLA-degrading enzymes is induced by adding gelatin (0.3% w/v), resulting in greatly increased PLA biodegradation (Bubpachat et al., 2018).

Mayekar and Auras (2024) conducted a study evaluating the effects of different inducers on PLA degradation in compost under mesophilic conditions (37 °C). Each biostimulant tested (skim milk, gelatin, and ethyl lactate) was added to the compost at a 2% w/w concentration at the start of the experiment with no additional/repeated application. Gelatin was the most effective biostimulant, reducing the time required to achieve a PLA number-average molecular weight (Mn) of $\lesssim$10,000 $g \cdot mol^{-1}$ by 25%, followed by ethyl lactate (22%) and skim milk (15%). This accelerated biodegradation was attributed to enzymatic activity stimulation, in particular protease production in the case of gelatin and skim milk. Along with inducing protease production, the degradation of gelatin also generates ammonia, further increasing degradation through the alkaline hydrolysis of the polymer.

Yeast extract stimulates the production of various polymer-degrading enzymes, such as esterases and lipases (Mistry et al., 2022). Da Silva et al., (2020) also found that yeast extract at a concentration of 0.3 w/w added to soil increased biodegradation rate of PLA at 58 °C compared to that reported in literature. Quantitatively, gelatin generally appeared to be the most effective method of enhancing PLA biodegradation rates via inducers, added at the beginning of the composting process. It achieves this by triggering microbial production of extracellular proteases and depolymerases through structural similarity to PLA monomers.

1.5.3 Bacteria

The usage of bacterial consortia has shown great potential for enhanced PLA degradation in compost systems compared to native microbes. A defined bacterial consortium, designated EAc by the authors, comprised of *Nocardioides zeae* EA12, *Stenotrophomonas pavanii* EA33, *Gordonia desulfuricans* EA63, and *Chitinophaga jiangningensis* EA02 improved PLA degradation rates (measured via CO_2 evolution) 20-50% compared to PLA composted with only indigenous microbes (Mistry et al., 2023). Ester bond cleavage was more pronounced in PLA composted with EAc bioaugmentation. In contrast, for PLA composted with only native microbes, the degree of ester bond cleavage decreased as the initial concentration of PLA films increased.

Other studies have also demonstrated the effectiveness of bioaugmentation approaches in accelerating PLA degradation. Castro-Aguirre et al. (2018) reported accelerated biodegradation in compost at 58 °C through bioaugmentation with *Geobacillus* strains, increasing CO_2 evolution and reducing the biodegradation lag phase. After 45 days, biodegradation reached approximately 80% for PLA films with bioaugmentation compared to only 60% without. Satti et al. (2017) showed enhanced mineralization rates of PLA films in soil (30 °C) by bioaugmenting with *Sphingobacterium* sp. strain S2 and *Pseudomonas aeruginosa* strain S3, combined with biostimulation of the native microbial community using sodium lactate at 0.2%.

One area of future interest in finding PLA degraders will be the identification and screening of potential PLA degraders from natural environments where PLA waste is found. For example, a study by Stojanovski et al. (2025) screened and isolated 23 PLA-degrading strains, 14 of which came from industrial compost soils. This suggests that prior environmental exposure to bioplastics

had fostered the development of specialized microbial communities. Repeated isolation of the same strain (*Brevibacillus agri*) across multiple samples further supports the idea of adaptation, indicating the prevalence of plastic-degrading capabilities in environments with chronic PLA exposure. Critically, the study identified three PLA-degrading enzymes through a computational pipeline screening of the isolated strains. One purified and biochemically characterized enzyme was capable of fully solubilizing low-molecular-weight PLA powder with 43-65% conversion to lactic acid, within 18 hours at 30 °C. This work demonstrates the potential for enzyme-based approaches to PLA waste management.

1.6 Pretreatment of PLA

One potential way to accelerate PLA biodegradation is through pretreatment methods that alter its surface or molecular structure before composting. While most research has focused on thermal, chemical, or microbial strategies, ultraviolet (UV) irradiation may offer a non-chemical, energy-based approach that can induce chain scission and surface modifications in PLA. Collectively, the literature suggests that UV exposure, particularly at lower wavelengths, significantly alters the physical and chemical properties of PLA, notably reducing molecular weight, and increasing brittleness and fragmentation. Most existing studies have focused on UV-induced aging or fragmentation of PLA for durability or environmental fate assessments, rather than composting outcomes. Furthermore, these effects are amplified when combined with elevated temperature and humidity.

For example, Copinet et al. (2004) found that 315 nm UV exposure resulted in noticeable decreases in molecular weight (up to a 96% drop) and mechanical integrity of PLA when combined

with elevated temperature and humidity. Similarly, Lesaffre et al. (2017) demonstrated that combined UV irradiation, heat, and humidity reduced molecular weight by up to 91% over 125 days. Wang et al. (2024) observed fragmentation of PLA in water under UV irradiation, with 45-70% of PLA particles reduced to sizes below 100 μm in 7 days. Janorkar et al. (2007) reported a decrease in Mn from 110,000 to 4,000 g/mol after 12 hours of UV exposure.

Fewer studies have directly linked UV-induced modifications to enhanced biological degradation. Jeon and Kim (2013) evaluated the biodegradability of UV-C (245 nm)-irradiated PLA using a mesophilic bacterium (*Stenotrophomonas maltophilia*). Their results indicated the highest biodegradation (~27% after 40 days at 37 °C) occurred after 8 hours of UV exposure, compared to 10% biodegradation for non-treated samples after the same duration. Interestingly, samples exposed for more than 12 hours exhibited decreased biodegradability and increased brittleness. The authors theorized that instead of generating bioavailable intermediates, the increased exposure may have produced toxic, unstable, or unusable fragments that were less readily consumable by microorganisms. Brown et al. (2024) showed that prior UV exposure increases the extent of enzymatic hydrolysis of PLA, indicating that photodegradation can enhance subsequent biological degradation processes. Their results suggest that this effect is largely associated with reductions in molecular weight caused by UV irradiation, demonstrating a link between UV exposure and biotic degradation.

1.7 Rotary Drum Compost Systems

The BIOvator® (Nioex Systems Inc., Swan Lake, MB) is a Rotary Drum Composter (RDC) system designed to accelerate the decomposition of organic material, utilizing primarily aerobic microorganisms within a controlled environment. This technology provides a consistent and efficient composting process independent of external weather conditions, maintaining internal temperatures typically between 38 °C and 65 °C. Main advantages include odor containment relative to unmanaged or static systems, pest exclusion, and ease of management through automated rotation and monitoring systems.

The RDC was developed to provide an efficient and bio-secure method to dispose of organic waste and animal mortality in agriculture. As the RDC was designed for and generally used for mortality composting, sustained thermophilic temperatures are required to ensure pathogen destruction and meet regulatory requirements for safe handling of animal carcasses (Nioex Systems Inc., 2010). Designed by a livestock integrator in Manitoba, it can handle up to 680 kg of organic waste or carcasses a day. It is commonly employed on livestock farms to compost dead animals such as poultry, hogs, and cattle, as well as organic by-products from slaughterhouses, food waste from processing facilities, and other biodegradable materials like manure and bedding (Nioex Systems Inc., 2010).

The Forks Marketplace, a public gathering space and tourist destination in downtown Winnipeg, Manitoba (Canada) featuring shops, restaurants, and cultural attractions, has a RDC on site. It is used to process organic waste generated by the food vendors and facilities within the marketplace as part of their Target Zero sustainability initiative (Forks North Portage Corporation,

n.d.). The RDC represents only the active in-vessel composting stage; material exiting the RDC is placed in curing piles to complete the composting process. Within these piles thermophilic activity may continue, depending on ambient weather and compost activity. While The Forks reports successful composting of PLA items in the RDC, this degradation has not been quantified or characterized.

RDCs present a promising system for PLA degradation due to their ability to maintain the specific environmental conditions required for effective PLA composting. As highlighted in the literature, PLA degradation is significantly enhanced at temperatures above its glass transition temperature (Karamanlioglu et al., 2017), which is reliably achieved within the enclosed, thermally regulated, and actively aerated RDC system. Although there are advantages of the RDC system when it comes to maintaining environmental conditions required for PLA degradation, they have not yet been evaluated in peer-reviewed literature for assessing biodegradability, PLA or otherwise. As a result, testing methodology has not been established, and presents challenges: the RDC is a closed, high-volume, constantly mixing system, making it difficult to retrieve and assess specific PLA samples during or after degradation without disrupting the system.

Without a containment system, degraded samples may fragment and become unrecoverable from the bulk compost, preventing paired comparison of pre- and post-composted specimens for metrics such as mass loss, molecular weight, thermal properties, and surface morphology. One method to address this may be the use of mesh bags to hold samples as they travel through the RDC. That way, the same sample could be tracked throughout the entire process while still allowing interaction between the compost environment and the sample. Challenges with this

method would be selecting a mesh size that retains degrading PLA while allowing sufficient microbial and moisture exchange, maintaining bag integrity, and ensuring consistent exposure to compost conditions.

1.8 Research Questions, Hypotheses, and Objectives

1.8.1 Rationale of the Research

There is a lack of comprehensive understanding and practical methods to achieve complete biodegradation of PLA in industrial composting environments at both mesophilic and thermophilic temperatures. Specifically, there is a need to establish practical conditions under which PLA can be fully degraded, addressing its resistance to breakdown under standard composting conditions. This includes understanding the roles of microbial consortia, cost-effective pretreatment methods (UV pre-treatment), and environmental factors in enhancing the degradation process.

Additionally, realistic scale-up methods from isolated respirometer experiments to industrial composting systems are not well-explored. The thesis will evaluate PLA degradation in a RDC – a controlled, mechanized composting vessel designed for efficient waste processing – and compare it to controlled respirometer experiments. The objective is to assess the RDC's viability as an industrial-scale waste management solution, emphasizing parameters such as oxygen availability, temperature consistency, and the impacts of pretreatment.

1.8.2 Research Questions

The key research questions addressed in this thesis focus on characterizing PLA degradation in RDC systems and the factors that influence its rate and mechanisms. This was accomplished

through controlled experiments in Respirometer systems and then in RDCs, which are industrial-scale in-vessel composting systems.

The key questions addressed in the Respirometer systems were:

- Under what conditions can Forks RDC compost and its PLA-adapted microbial community consistently degrade PLA in lab-scale respirometer systems?
- How does the physical structure of the PLA, specifically crystalline versus amorphous, influence the degradation process?
- What is the impact of temperature on PLA degradation in these systems?
- Do bacterial inoculation or the use of biodegradation inducers enhance the rate or extent of PLA degradation?

The key question addressed in the RDC systems was:

- Can RDCs achieve similar biodegradation levels within 45 days as observed in controlled respirometer experiments at constant high temperature? The effects of mixing frequency and temperature uniformity on PLA degradation rates were evaluated.

Additionally, a lab-scale UV-chamber was built to evaluate the effects of UV irradiation on PLA films of the same type and origin as those used in the RDC and respirometry experiments, with the following question being addressed:

- How does UV-C irradiation at defined wavelength and irradiance conditions affect PLA molecular weight and thermal properties?

1.8.3 Hypotheses

The primary hypotheses guiding this research are as follows:

- The ability of RDCs to degrade PLA can be characterized and will be comparable to PLA degradation in respirometer experiments, if a thermophilic environment is maintained.
- The addition of PLA-degrading bacterial strains and gelatin to Forks RDC compost in respirometer experiments will enhance degradation rates compared to composting with only indigenous microbes, as measured by CO_2 evolution.
- UV-C irradiation at 254 nm, the peak emission wavelength of standard low-pressure mercury germicidal lamps, will produce measurable reductions in PLA molecular weight and alter thermal properties, with the extent of modification increasing with exposure duration.

1.8.4 Objectives

By focusing on these process-oriented questions, this thesis represents the first systematic characterization of PLA degradation in RDC composting systems and aims to bridge laboratory-scale findings with industrial-scale composting outcomes. A key feature of this work is the use of the same PLA source material across all experimental environments, allowing direct cross-experiment comparison rather than inference across studies using different PLA grades, thicknesses, and molecular weights. The specific objectives of this thesis were to: 1) establish conditions for PLA degradation using Forks RDC compost in lab-scale systems; 2) evaluate bioaugmentation and biostimulation as enhancement strategies under mesophilic conditions; 3) characterize PLA degradation in operating RDC systems; and 4) design and characterize a UV-C exposure system.

Chapter 2: Materials and Methods

This chapter outlines the general materials and methods used across the experiments presented in the following chapters. Each of those chapters includes a specific materials and methods section describing the procedures relevant to that particular study. The information presented here serves as a common foundation and will be referenced throughout the thesis where applicable.

2.1 PLA Films

The main polymer used in this study was Ingeo Biopolymer PLA 2500HP (Natureworks LLC), supplied by the National Research Council of Canada in nominally amorphous form with very low measured crystallinity (Xc = 0.16% by DSC). For clarity and consistency, this material is referred to as "amorphous PLA" throughout the thesis. The weight-average molecular weight (Mw) was reported by Kahraman et al. (2021) as 184,000 g/mol, and by Mysiukiewicz et al. (2020) as 193,250 g/mol, with a melt temperature (Tm) of 165 to 180 °C. The glass transition temperature (Tg) ranges from 55 to 60 °C (NatureWorks LLC, 2017) for its amorphous form. The tensile strength of this PLA is 64 MPa and the elongation-at-break is 3.6%. The polymer is predominantly PLLA-based, containing very low D-lactide content, as reported by the literature: 0.4 mol % D-lactide (Lee, 2016); 0.5 mol % D-lactide (Lee, 2020; Kahraman et al., 2021); and 0.25 mol % D-lactide (Eraslan et al., 2024). PLA coupons of 2 x 3 x 0.22 cm (L x W x H) were cut from rolls provided by the NRC. Annealing conditions (90 °C, 1 h) to produce crystalline films were established by NRC based on preliminary trials at varying durations (NRC, personal communication, June 26, 2024). Crystallinity of the annealed films was confirmed by DSC at 48%.

In addition to the Ingeo films, films cut from unused commercially available PLA cups were used in this study (hereafter referred to as “Forks PLA”). Sourced from Fools & Horses Coffee at The Forks (Winnipeg, MB), these cups were clear, rigid, single-use cold beverage cups marketed as compostable and supplied through The Forks’ foodservice operations. Based on supplier information publicly disclosed by Fools & Horses, the cups were sourced through Canada Green (Winnipeg, MB). The specific PLA resin grade, molecular weight, stereochemistry, and additive package were not available from the supplier and were not independently characterized in this study. The cups were cut into 2 by 3-centimeter films, and represent a commercially relevant, real-world PLA product rather than a well-characterized resin grade. The wall thickness of the commercially sourced PLA cups was measured using digital calipers (0.01 mm resolution) and had a mean thickness of 0.30 ± 0.02 mm (n = 5) at the midpoint height of the cup, which is where films were cut from.

2.2 Polymer Characterization Techniques

2.2.1 Mass Loss Analysis

Mass loss measurements provide a direct quantification of bulk material degradation and are used for assessing the extent of physical deterioration over time. Prior to composting, each film was cleaned and weighed using an analytical balance with a precision of at least 0.1 mg, and moisture content measured. After composting in respirometers/RDCs, films are retrieved, rinsed to remove compost residues, dried at ambient temperature, and reweighed with moisture content measured.

2.2.2 Differential Scanning Calorimetry (DSC)

DSC is conducted to monitor changes in the thermal properties of PLA, such as Tg, melting temperature (Tm), and crystallinity. A small section (~ 7 to 11 mg) of PLA film was cleaned, dried, and analyzed by DSC. The instrument used for DSC analysis was a TA DSC250 with hermetically sealable pans and lids. The thermal protocol consisted of equilibration at −30 °C, heating at 10 °C/min to 200 °C, cooling at 10 °C/min to −30 °C, followed by a second heating at 10 °C/min to 200 °C. All measurements were conducted under nitrogen purge (50 mL/min).

Thermograms generated from DSC analysis reveal several thermal characteristics for polymers. The first is Tg, which is the temperature at which the polymer transitions from a brittle, more glassy state to a more flexible rubbery state due to increased chain mobility. It appears as a reduction in the heat flow baseline; when the chain mobility of the polymer increases, it increases the amount of heat required to raise their temperature. The second is the cold crystallization temperature (Tcc), which is an upward (exothermic peak) that is observed in the first heating phase when amorphous polymer chains heat up and gain the chain mobility to reorganize in crystalline structures. It is called a “cold” crystallization peak because it happens prior to the melting and subsequent cooling of the polymer. The Tm is the temperature where the crystalline regions melt, resulting in a downward (endothermic) peak as the melting reaction requires energy to proceed. The crystallization temperature (Tc) is an exothermic peak that appears during cooling of the polymer as the polymer crystallizes following the melting process. This peak may be absent if the cooling rate is too fast, in which case the chains get frozen in place in an amorphous state as the temperature drops below Tg.

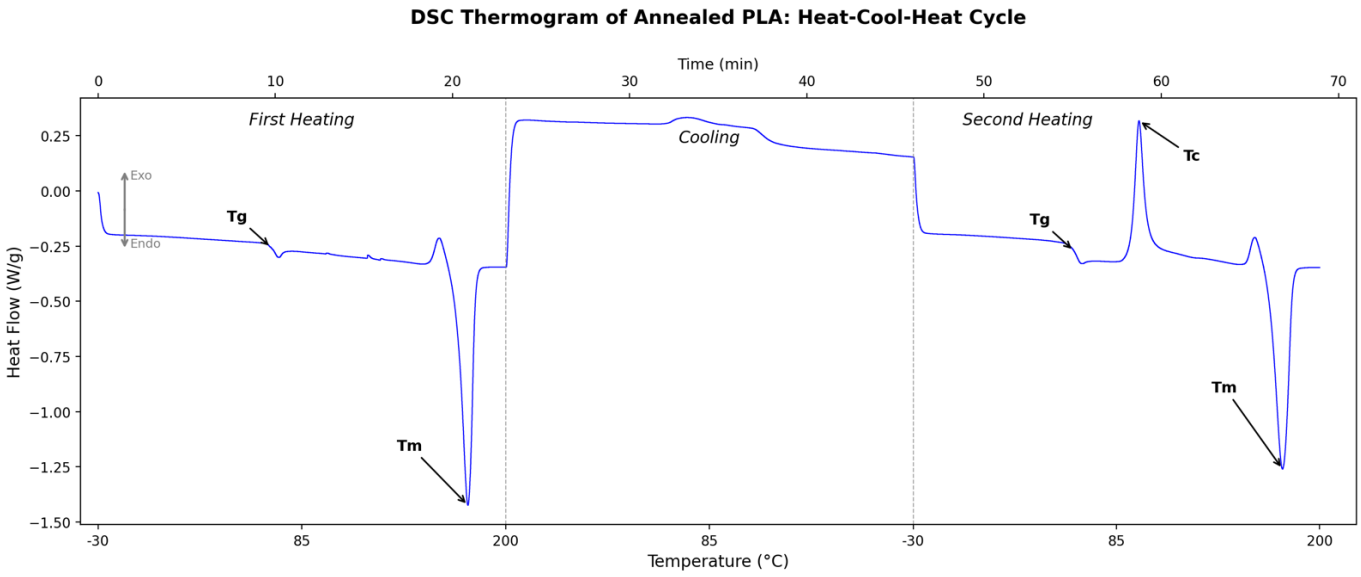

Figure 2.1 Representative DSC thermogram for annealed PLA showing a complete heat-cool-heat cycle.

During the first heating, the reduction into the lower baseline heat flow indicates the glass transition temperature for the sample (Figure 2.1). The sharp downwards peak indicates the melting temperature as the sample absorbs heat during the process.

2.2.2.1 Crystallinity Calculation

Percent crystallinity (Xc) was calculated from the first heating cycle using Equation 1 (Lim et al., 2008):

$$Xc\ (\%) = [(\Delta Hm - \Delta Hcc) / \Delta Hm^{\circ}] \times 100 \qquad \textbf{(Eq. 1)}$$

where ΔHm = enthalpy of melting (J/g), calculated by integrating the endothermic melting peak, ΔHcc = enthalpy of cold crystallization (J/g), calculated by integrating the exothermic cold crystallization peak (if present; otherwise $\Delta Hcc = 0$), and ΔHm° = enthalpy of fusion for 100%

crystalline PLA = 93.1 J/g (Fischer et al., 1973). The subtraction of ΔHcc from ΔHm accounts for crystallinity that formed during the DSC heating scan rather than being present in the original sample.

2.2.2.2 Interpretation of First vs. Second Heating

The results from the first heating cycle show the polymer thermal characteristics that reflect its previous thermal history. For example, if the sample has been annealed and had its crystallinity increased or has been composted and has had its amorphous regions degraded, that will be reflected in peaks from the first heating. The second heating cycle, following controlled cooling from the melt, reflects the intrinsic thermal properties of the polymer. All crystallinity values reported in this thesis are calculated from first heating data to capture the structural state of the polymer following experimental treatments. Tg was determined by the midpoint method from both the first and second heating scans. First heating Tg reflects the thermal state of the as-received material, while second heating Tg reflects intrinsic polymer properties after DSC first heating.

2.2.3 Intrinsic Viscosity (Viscometry) Molecular Weight Determination

Intrinsic viscosity measurements were used to estimate changes in the molecular weight of PLA as an indicator of polymer chain scission and backbone degradation. The intrinsic viscosity measurement procedure was informed by ASTM D2857-16, *Dilute Solution Viscosity of Polymers*. PLA samples were dissolved in chloroform at multiple concentrations (1, 2, 3, and 4 mg/ml). Solution flow times were measured using an Ubbelohde capillary viscometer maintained at 25 °C.

Reduced viscosity, which represents the polymer's contribution to solution viscosity normalized by concentration, was calculated at each concentration. Because polymer chain interactions inflate

reduced viscosity at higher concentrations, values were extrapolated to zero concentration to isolate the contribution of individual polymer chains, yielding a baseline intrinsic viscosity of 1.52 dL/g. This viscosity was then used to calculate the viscosity-average molecular weight using the *Mark–Houwink–Sakurada* relationship (Ravve, 2012) with literature values for PLA in chloroform (Equation 2).

For PLA samples recovered from respirometer and RDC experiments, where available material was limited to a single concentration, intrinsic viscosity was approximated using the inherent viscosity method (Equation 3) (ASTM D2857-16). Both the single-point method and multi-point extrapolation yielded comparable viscosity-average molecular weight values, supporting its use for the test samples. Example calculations are provided in Appendix D.

Viscosity-average molecular weight (Mv) was calculated using the Mark-Houwink-Sakurada equation (Equation 2):

$$M = ([\eta] / K)^{(1/a)} \qquad \textbf{(Eq. 2)}$$

where [η] is the intrinsic viscosity (dL/g), and K and a are polymer-solvent-temperature-dependent constants. For PLA in chloroform at 25 °C, K = 6.06 x 10^{-4} dL/g and a = 0.64 (Korzhikov-Vlakh et al., 2024).

Inherent viscosity was calculated using (Equation 3):

$$\eta\_inh = \ln(\eta\_r) / c \qquad \textbf{(Eq. 3)}$$

where η_r is the relative viscosity (dimensionless) and c is the polymer concentration (g/dL).

Molecular weight averages describe the distribution of chain lengths in a polymer. Mn weights all chains equally, whereas Mw assigns greater weighting toward longer chains, and tends to have

more influence over polymer properties. Mv is derived from viscosity measurements of polymer solutions, and generally falls between Mn and Mw for polymers, approaching Mw as the Mark-Houwink exponent *a* shown in Eq. 2 approaches 1 (Ravve, 2012). Size exclusion chromatography (SEC/GPC), which provides Mn and Mw directly, was not available for this study. Dilute solution viscometry was used instead; with the same Mark-Houwink constants applied to all samples. Changes in Mv between unexposed and degraded PLA are internally consistent, even though absolute Mv values may differ from Mw values reported for the same PLA grade due to differences in the measurement method and constants used. See Appendix items D19 and D20 for example calculations.

2.2.4 Scanning Electron Microscopy (SEM)

SEM provides high-resolution imaging of surface morphology to identify structural changes such as pitting, cracking, or microbial etching. PLA films were rinsed and fully dried, then mounted on aluminum stubs and sputter-coated with a 60/40 Au-Pd alloy using a Denton Vacuum Desk II Cold Sputter/Etch Unit (45 mA, 50 millitorr, 30 s) to deposit an approximately 10 nm conductive layer. Micrographs were acquired using an FEI Quanta 650 FEG Environmental SEM operated in high vacuum mode at an accelerating voltage of 5 kV, a spot size of 3.0, and a working distance of approximately 10.5 mm, using an Everhart-Thornley secondary electron detector at 2000x magnification.

Approximately 20 micrographs were captured per sample, with representative samples selected based on surface features shared by the majority of the micrographs. This meant excluding areas that had apparent mechanical damage (e.g., cuts and tears) not attributed to chemical or biotic

degradation processes. The purpose of this analysis was qualitative assessment of surface degradation features and was not intended to quantify degradation extent or infer degradation mechanisms.

Chapter 3: Influence of Temperature, Crystallinity, and Biological Enhancement on PLA Mineralization in Laboratory Composting

3.1 Introduction

Previous studies have quantified the aerobic biodegradation of PLA under controlled composting conditions using standardized respirometry methods, reporting CO_2-production during microbial degradation of PLA across thermophilic and mesophilic conditions. Table 3.1 summarizes reports in the literature, providing context for the experimental design, and interpretation of the respirometer studies presented in this chapter.

The studies in Table 3.1 show that degradation of PLA occurs under thermophilic, well-aerated composting conditions, typically at temperatures near or above the glass transition temperature of PLA (55–62 °C). Using standardized respirometry methods (ISO 14855, ASTM D5338), mineralization levels of approximately 80 to 95% are commonly reported within 45 to 145 days. In contrast, PLA shows little to no biodegradation under mesophilic conditions, even over extended periods, indicating that temperature-driven hydrolysis is the primary rate-limiting step.

Although these studies establish the importance of thermophilic conditions, most studies consider individual factors in isolation. Temperature effects are characterized without variation in polymer crystallinity, while morphology-focused studies are often completed at a single temperature. Similarly, few investigations explore whether microbial interventions can meaningfully alter PLA degradation under conditions where hydrolysis is otherwise known to be limited.

Table 3.1 Summary of published studies on aerobic biodegradation of PLA in compost respirometry systems.

Study	PLA Type	Inoculum	Temp (°C)	Duration (days)	Final Outcomes
Kunioka et al. (2006)	Commercial PLA powder	municipal solid-waste compost	58	45–90	~90–91 % degradation by ~20–35 d
Cadar et al. (2012)	Low-Mw PLA powder (Mw ≈ 15,000 g·mol^{-1})	domestic organic waste compost	50 ± 2	110	biodegradation of PLA ≈ 69–86 %
Kale et al. (2007)	NatureWorks PLA ~96% L-lactide; ~1×1 cm pieces	manure-based compost; vermiculite added	58	58	84.2 ± 0.9 % mineralization at day 58.
Kalita et al. (2021)	PLA films (NatureWorks 2003D, Mn ≈ 140,000 g·mol^{-1}, ~0.45 mm thick)	food-waste compost	58 ± 5	120–145	94.2 % biodegradation by ~120–145 d.
Kulikowska et al. (2020)	PLA disposable cups, shredded (≈2 × 2 × 0.5 mm)	municipal solid-waste compost lignocellulosic waste	58 ± 0.5	90	Complete mineralization achieved at low–moderate PLA loading (PLA:compost = 1:40–1:20, ≈70–90 d); high PLA loading (1:10) reached only ~65 % within 90 d.
Van de Perre et al. (2024)	PLA pellets, cryo-milled (<1 mm)	municipal solid-waste compost	28 ± 2	365	Negligible biodegradation (≈1–4 %) conditions.

To address these limitations, the present study examines the combined effects of initial PLA crystallinity, temperature (thermophilic versus mesophilic), and biological intervention through biostimulation and bioaugmentation. All experiments use a PLA-adapted compost inoculum obtained directly from an operating in-vessel RDC, so that lab-scale results can be better compared to real-world RDC PLA degradation results. Biodegradation is assessed through CO_2 evolution alongside molecular weight and thermal property changes.

3.2 Experimental Design and Methods

Detailed methods for respirometry setup, compost preparation, biodegradation calculations, and statistical analysis are provided in this section. Sample-specific parameters are reported within each experiment section below.

3.2.1 Respirometry Setup

Respirometers at the NRC were used for aerobic experiments. This system measures O_2, CO_2, methane (CH_4), temperature (5-70 °C), pressure, relative humidity (RH), and flow rates, with a mass flow controller accuracy of 1.5%. Vessels (2 L) were filled halfway with ~275–350 g of compost at 50% moisture content (i.e., 125–175 g dry mass), along with ~5–7 g of PLA coupons. Microcrystalline cellulose powder (20 μm particle size, derived from cotton linters; Sigma-Aldrich, catalog no. 310697) was used as a positive control substrate. Aerobic chambers were mixed twice per week for the first two weeks and then weekly for the remainder of the experiment.

3.2.2 Compost Source and Preparation

Two (2)-week-old compost that had been through the RDC once was collected from the end of the Forks RDC. This compost was then sieved with a 6 mm sieve and left in an open-air bin

overnight at 30 °C prior to use the next day in respirometer experiments. It was collected each time prior to each experiment. Directly prior to use in respirometer systems, compost pH and moisture content were measured. The moisture content was then raised to 50% using distilled water.

3.2.3 Calculation of Biodegradation via CO_2 Evolution

The extent of biodegradation was calculated using the ASTM D5338-based formula (Equation 4):

$$\%\ biodegradation = \frac{C\ mass_{avg.\ sample\ with\ compost} - C\ mass_{avg.\ only\ compost}}{TOC\ mass_{sample}}$$

$$= \frac{(\%C\ in\ CO2) * (CO2(g)_{avg.\ sample\ with\ compost} - CO2(g)_{avg.\ only\ compost})}{TOC\ value * Sample\ mass\ (g)_{initial} * \%\ dry\ weight} \qquad \textbf{(Eq. 4)}$$

where, $\%\ dry\ weight = (1 - \frac{Moisture\ Content\ \%}{100})$, TOC value = 0.5 for PLA, 0.444 for cellulose, and %C mass in CO_2 = 0.2729. TOC values were theoretical as they were not measured for each sample but based on the calculated carbon content of the PLA/cellulose chemical structures. The TOC values are expressed on a mass basis (g C g^{-1} material).

Average CO_2 values for both test (with sample) and negative control compost conditions were calculated. These values were converted into carbon mass using the %C in CO_2. The net carbon evolved from the sample was obtained by subtracting the negative control average from the test average.

To assess variability, the standard error was calculated as follows (Equation 5):

$$S_e = SQRT\left[\left(\frac{s_{test}^2}{n1}\right) + \left(\frac{s_{blank}^2}{n2}\right)\right] * \frac{100}{C_i} \qquad \textbf{(Eq. 5)}$$

where, n1 and n2 are the number of replicate test and control digesters respectively, s is the standard deviation of the total gaseous carbon produced, and Ci was theoretical carbon content of the added sample (mg). See Appendix item D18 for an example calculation of biodegradation.

ASTM D5338 quantifies biodegradation based on CO_2 evolved to the gas phase relative to theoretical carbon conversion and does not explicitly close the carbon balance. As a result, it does not directly account for additional carbon sinks such as conversion of carbon to microbial biomass, or bicarbonate formation, which occurs primarily at neutral pH. In gelatin-amended conditions, ammonia released during its degradation may increase pH, which could increase the proportion of CO_2 retained as bicarbonate. One specification of ASTM D5338 is that the system is continuously aerated, which maintains aerobic conditions and also promotes stripping of dissolved CO_2 to the gaseous phase, and so minimizes the effect of bicarbonate retention on mineralization numbers. Any bicarbonate retention would result in slight underestimation of true mineralization, as would carbon conversion into biomass.

PLA/cellulose sample mass varied between experiments depending on the amount needed to form the 25 to 1 ratio of compost to PLA/cellulose, but was always between 5 and 7 grams, and consistent within the experiments themselves (all conditions within an experiment had the same mass of added material).

3.2.4 Statistical Analyses

All statistical analyses were performed using GraphPad Prism (version 10.6.1). Data are presented as mean ± standard deviation (SD). Population standard deviation (dividing by n) was used rather than sample standard deviation (dividing by n−1) to maintain consistency with the

reporting method used by the analytical facility where the CO_2 measurements were recorded. Sample sizes were n = 3 per group unless otherwise noted; the 30 °C experiment without gelatin had n = 2 for negative control and amorphous PLA groups due to instrument channel failures.

For the 58 °C respirometer experiment, a two-way analysis of variance (ANOVA) was used to evaluate the effects of material type (cellulose, annealed PLA, amorphous PLA) and gelatin supplementation (with/without) on biodegradation. For the 30°C experiments, one-way ANOVA was performed on raw cumulative CO_2 production (mg) across all eight conditions (cellulose, negative control, annealed PLA, amorphous PLA, each with and without gelatin), to avoid error propagation inherent in the subtraction-based biodegradation calculation. Tukey's honestly significant difference (HSD) post-hoc test was used for multiple comparisons between all group means, with a family-wise significance level of $\alpha = 0.05$. The null hypothesis was that there was no difference in biodegradation among conditions regardless of material type and gelatin supplementation.

For the inoculated experiment at 30 °C, no measurable biodegradation was observed at 30 °C and so biodegradation percentages could not serve as a meaningful dependent variable. Accordingly, a one-way ANOVA was used to compare cumulative CO_2 production (mg) across all treatments (negative control, uninoculated control, Consortium 1, CA4, CA1, 3.7, 2.5, 2.3; n = 3 per group). Tukey's HSD post-hoc test was used for pairwise comparisons between all strains and Dunnett's test was used to compare each inoculated treatment to the uninoculated control ($\alpha = 0.05$). The null hypothesis was that there was no difference in cumulative CO_2 production among conditions.

For the 30 °C base experiment, a two-way ANOVA (crystallinity x gelatin) was also performed on Mv to determine whether Mv reduction was influenced by crystallinity or gelatin supplementation. For the 30 °C inoculation experiment, a one-way ANOVA was performed on Mv across treatments. Tukey HSD post-hoc comparisons were used in both cases (alpha = 0.05). Full ANOVA and Tukey results for Mv analyses are presented in Appendix D (Tables D7-D9).

3.2.5 Thermophilic Degradation

This experiment included eight respirometer conditions, each conducted in triplicate, designed to evaluate the effects of PLA crystallinity and biostimulation on aerobic biodegradation at 58 °C (Table 3.2). Gelatin was selected as the biostimulant based on its demonstrated capacity to induce microbial protease production and enhance PLA hydrolysis (Bubpachat et al., 2018; Mayekar and Auras, 2024).

Table 3.2 Summary of respirometer conditions for Experiment 1, evaluating the effects of PLA crystallinity and biostimulation on aerobic biodegradation at 58 °C. Each condition was conducted in triplicate.

Compost Treatment	**Condition**	**Purpose**
Untreated	Negative control (no PLA)	Quantifies background CO_2 evolution from the compost matrix
Untreated	Positive control (cellulose)	Confirms microbial activity and respirometer performance under untreated conditions
Untreated	Annealed PLA films	Assesses biodegradation of semi-crystalline PLA in the absence of added nutrients
Untreated	Amorphous PLA films	Provides a low-crystallinity comparison under native compost conditions
Biostimulated (0.5% w/v gelatin)	Negative control (no PLA)	Accounts for increased endogenous respiration due to additional carbon addition
Biostimulated (0.5% w/v gelatin)	Positive control (cellulose)	Verifies microbial activity under biostimulated conditions
Biostimulated (0.5% w/v gelatin)	Annealed PLA films	Evaluates whether biostimulation accelerates degradation of semi-crystalline PLA
Biostimulated (0.5% w/v gelatin)	Amorphous PLA films	Tests whether nutrient addition further enhances degradation of low-crystallinity PLA

3.2.6 Mesophilic Degradation

The experimental conditions used in Experiment 2 were identical to those described for Experiment 1, except all respirometers were operated under mesophilic temperature conditions (30 °C) and the experiment duration was 81 days instead of 45. The experiment duration was intended to be 90 days, but sensors failed near the end of the experiment and cut the experiment short. The same untreated and biostimulated compost treatments, control substrates, and PLA film types were tested. This was done to allow direct comparison of biodegradation behavior between thermophilic and mesophilic conditions. Over the course of the experiment, two replicates had measurement

instrument failure, resulting in negative control and amorphous untreated conditions having two replicates as opposed to three.

3.2.7 Mesophilic Degradation with Bacterial Inoculation

For Experiment 3, the respirometers were operated under mesophilic conditions (30 °C) and ran for 90 days. The experiment contained eight different conditions, all conducted in triplicate, designed to evaluate the impact of mesophilic PLA-degrading bacteria on amorphous PLA mineralization rates in the Forks RDC compost. The negative control, which was compost without PLA or inoculant, was intended to show the background CO_2 evolution from the indigenous compost microbial community. The "no inoculant" control, which contained compost and PLA with no inoculant, was to establish how much PLA degrades under composting conditions *without* added strains and was expected to be consistent with Experiment 2. The remaining six conditions were each of the 5 strains individually tested, and one consortium condition which was a combination of each strain added in equal volumes. A limitation of this experimental design is that no compost-plus-inoculum negative control without PLA was included, and so differences in CO_2 evolution in inoculated conditions cannot be attributed solely to effects on PLA degradation; the added strains may have altered overall compost respiration independently of PLA.

3.2.7.1 Bacteria used as inocula

The following mesophilic bacterial strains were used as inocula for selected test conditions:

- CA1 and CA4 – *Streptomyces* sp., isolated from single-household backyard compost
- 2.5 – *Cellulomonas* sp., isolated from a mixture of university garden waste and restaurant organic waste

- 3.7 – *Microbacterium* sp., isolated from Winnipeg residential organic waste
- 2.3 – *Mycolicibacterium* sp., isolated from a mixture of university garden waste and restaurant organic waste

All strains were previously isolated and identified within the laboratory by Dr. Sarita Shrestha, who completed the following: strains were isolated by incubating 1 gram of the compost sources with three pieces of PLA and 25 mL of mineral salts medium (MSM) containing 1 % (w/v) PLA powder for eight weeks. Following enrichment, isolates were obtained using PLA emulsion agar plates. Genus-level identification was determined by via 16S rRNA gene sequencing.

3.2.7.2 Inoculation protocol

Individual strains were revived from glycerol stocks stored at -80 °C, and sub-cultured in LB broth at 30 °C with shaking at 150 rpm for 24 hours. Cell concentrations were determined by plate counts on LB agar at the time of inoculation, and cultures were confirmed to be approximately 1 × 10^9 CFU/mL. This was done rather than optical density as plate counts provide a direct measure of viable cell concentration, which was more relevant for determining the inoculation dose. Cultures were harvested by centrifugation and washed once with phosphate-buffered saline (PBS) to remove residual medium, and resuspended in 45 mL PBS. Cell suspensions were added directly to the compost test conditions at two time points: at the start of the experiment (day 0) and again midway through the incubation period (day 45). Equivalent CFU were applied across all inoculated treatments at each inoculation event at 10% v/w (45 ml of 1 × 10^9 CFU/mL culture). Reinoculation at day 45 was performed to account for the possibility that the initial inoculum did not survive or

maintain population levels in the compost environment over the 90-day experiment. Sterile PBS was added to all non-inoculated conditions to control for potential effects of PBS; if phosphorus was rate-limiting for microbial activity in any condition, the PBS addition could have influenced respiration independently of the inoculated bacteria. The manual adjustment of the moisture content of the compost to 50% considered the addition of PBS as a source of moisture.

3.3 Results

3.3.1 Thermophilic Degradation

The objective of Experiment 1 was to characterize the aerobic biodegradation of amorphous and annealed PLA under thermophilic respirometer composting conditions. The main parameters of interest were the effect of initial PLA crystallinity and gelatin-based biostimulation on CO_2 evolution, biodegradation extent, and degradation kinetics in PLA-adapted compost.

3.3.1.1 CO_2 Evolution Data

Two forms of PLA, amorphous and annealed, were tested alongside a cellulose positive control to assess the degree and rate of PLA mineralization under thermophilic composting conditions, and whether initial polymer crystallinity influenced this degradation. Both amorphous and annealed PLA exhibited higher CO_2 evolution than the negative control compost (no added polymer), with final values of 80,402 ± 1,114 mg and 78,483 ± 476 mg, respectively, compared to 70,619 ± 1,803 mg for the negative control (Figure 3.1). Biodegradation was calculated according to ASTM D5338 by subtracting the CO_2 evolved from the negative control (compost without added polymer) from each treatment condition. Each vessel contained approximately 5 g of PLA, corresponding to approximately 2,400 mg of carbon, which would produce roughly 9,000 mg of

CO_2 if fully mineralized. The negative control produced 70,619 ± 1,803 mg CO_2, while the PLA conditions produced 78,483 to 80,402 mg, yielding a net difference of approximately 8,000 to 10,000 mg CO_2. This is consistent with complete mineralization of the added PLA carbon. For cellulose, the same equivalent amount of carbon was added (2400 mg), and so the same amount of CO_2 produced (~9000 mg) was to be expected if fully mineralized.

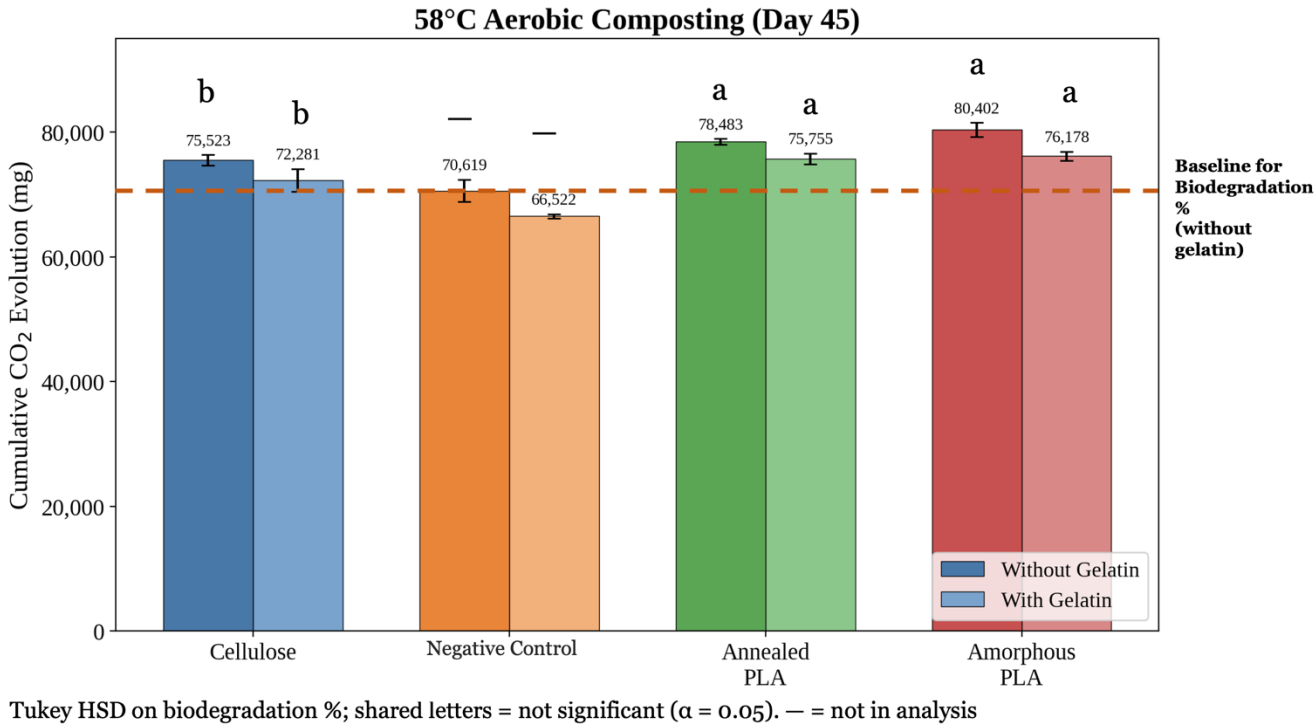

Figure 3.1 Cumulative CO_2 evolution from different compost conditions after aerobic composting at 58 °C for 45 days.

This elevated CO_2 production putatively indicates that the added PLA was actively degraded, contributing additional carbon beyond the background microbial respiration of the compost alone (Table 3.3). The low variability within replicates further supports consistent and reliable mineralization across both PLA types. These results demonstrate that under thermophilic

composting conditions exceeding the glass transition temperature, PLA is biodegradable, and that initial crystallinity has no significant influence on the final extent of cumulative CO_2 production.

Table 3.3 End-point CO_2 values & calculated percentage of biodegradation for aerobic composting at 58 °C.

Sample	**Mean ± Std Dev (mg)**	**Biodegradation (%)**
Cellulose	75,523 ± 857	63 ± 11.1
Negative Control	70,619 ± 1,803	NA
Annealed PLA	78,483 ± 476	90 ± 5.5
Amorphous PLA	80,402 ± 1,114	112 ± 12.8
Cellulose + Gelatin	72,281 ± 1,819	74 ± 23.5
Negative Control + Gelatin	66,522 ± 334	NA
Annealed PLA + Gelatin	75,755 ± 872	106 ± 10.0
Amorphous PLA + Gelatin	76,178 ± 731	111 ± 8.4

Under thermophilic conditions, both amorphous and annealed PLA films putatively underwent near-complete degradation, as evidenced by high CO_2 evolution values ranging from 90% to 112% of theoretical maximums, with moderate standard deviations (± 5 to 23%). These results were consistent across both untreated and biostimulated compost and aligned with visual disappearance of the PLA films (Figure 3.2). In contrast, cellulose, used as a positive control, showed more moderate degradation percentages (63–74%).

Figure 3.2 Compost recovered from thermophilic respirometer vessels (58 °C) following complete PLA mineralization. White deposits on wood chip surfaces were observed equally across all conditions, including negative controls without PLA, and are attributed to mineral precipitates.

Two-way ANOVA and Tukey post-hoc revealed a significant effect of material type (cellulose vs PLA) on biodegradation at 58°C ($p = 0.002$), but no significant effect of gelatin supplementation ($p = 0.29$) or interaction ($p = 0.64$). The negative control was excluded from this analysis as it does not contain a test substrate and cannot be assigned to a material type factor. Full ANOVA results are presented in Appendix D.

Biodegradation values exceeding 100% for PLA materials may be a consequence of the propagation of variance from both test and negative control conditions through the subtraction-based calculation. The net CO_2 (test condition CO_2 minus the negative control CO_2) carries the

propagated error from both measurements, resulting in even small variance in the raw CO_2 data being amplified when expressed as a percentage of theoretical yield. It could also reflect priming effects, where the presence of readily degradable polymer stimulated additional microbial activity and decomposition of native compost organic matter (Castro-Aguirre et al., 2017).

3.3.1.2 Degradation Kinetics

The biodegradation data derived from cumulative CO_2 evolution in the previous section (Section 3.3.1.1) was fit using a first-order kinetic model. Degradation kinetics were analyzed to quantify the rate of PLA mineralization, and for comparison to literature values. The model used was a first-order kinetic model with a lag-phase, created by Komilis (2006) and adapted for PLA degradation by Leejarkpai et al. (2011) (Equation 6):

$$C(t)=Cmax\times(1-e-k(t-\lambda)) \text{ for } t>\lambda \qquad \textbf{(Eq. 6)}$$

where C(t) is the cumulative biodegradation (%) at time t, calculated from CO_2 evolution relative to the theoretical carbon content of the sample, C_max is the maximum achievable biodegradation (%), k is the first-order mineralization rate constant (day^{-1}), and λ is the lag phase duration (days) (Table 3.4).

This model was chosen as it fit the observed phases of CO_2 evolution, which consisted of an initial lag phase followed by a steep curve with the active mineralization phase. The rate constant k provides a measure of degradation speed that can be compared across treatments. Parameters were estimated using nonlinear least-squares regression with both constrained and unconstrained C_max values to assess parameter sensitivity.

Table 3.4 Kinetic parameters for PLA biodegradation during aerobic composting at 58 °C over 45 days, based on first-order kinetic model.

Condition	**Sample**	**Cmax Uncon (%)**	**k Uncon (day^{-1})**	**Cmax Con (%)**	**k Con (day^{-1})**	**λ (days)**	**R^2**
Untreated	Cellulose	62.6	0.099	62.6	0.099	10.9	0.984
Untreated	Annealed PLA	97.6	0.119	97.6	0.119	21.7	0.965
Untreated	Amorphous PLA	138.7	0.069	100.0	0.141	20.9	0.974
Inducer	Cellulose	205.9	0.0094	205.9	0.0094	-3.24	0.949
Inducer	Annealed PLA	125.0	0.087	100.0	0.161	20.7	0.959
Inducer	Amorphous PLA	122.6	0.109	100.0	0.112	18.8	0.892

For PLA samples (Figures 3.3 and 3.4 on the next page), and the untreated cellulose condition (Figure 3.5 on page 64), the model generally fit well, with R-squared values above 0.95. There was an exception to this, which was the amorphous PLA with inducer added condition, which had a reduced fit of 0.892. The inducer cellulose condition did not fit the model at all, due to the lack of a significant lag phase, as can be seen in Figure 3.5 on page 64. In general, the addition of the inducer reduced the presence of a lag phase, reducing the model's fit compared to the untreated conditions.

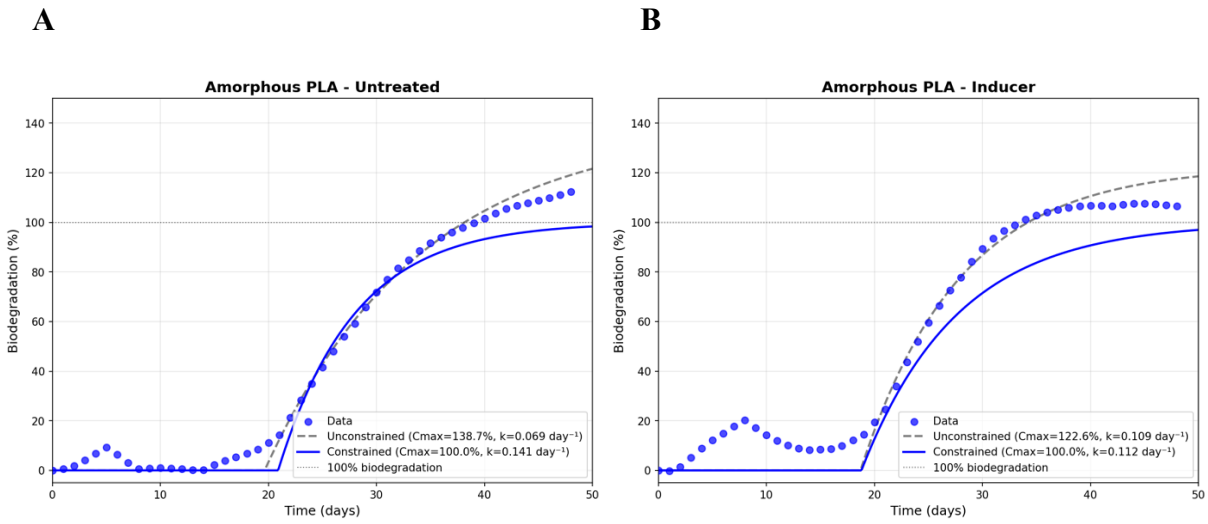

Figure 3.3 First-order kinetic model fits for A) Untreated Amorphous PLA biodegradation at 58 °C, and B) Inducer-included Amorphous PLA biodegradation at 58 °C.

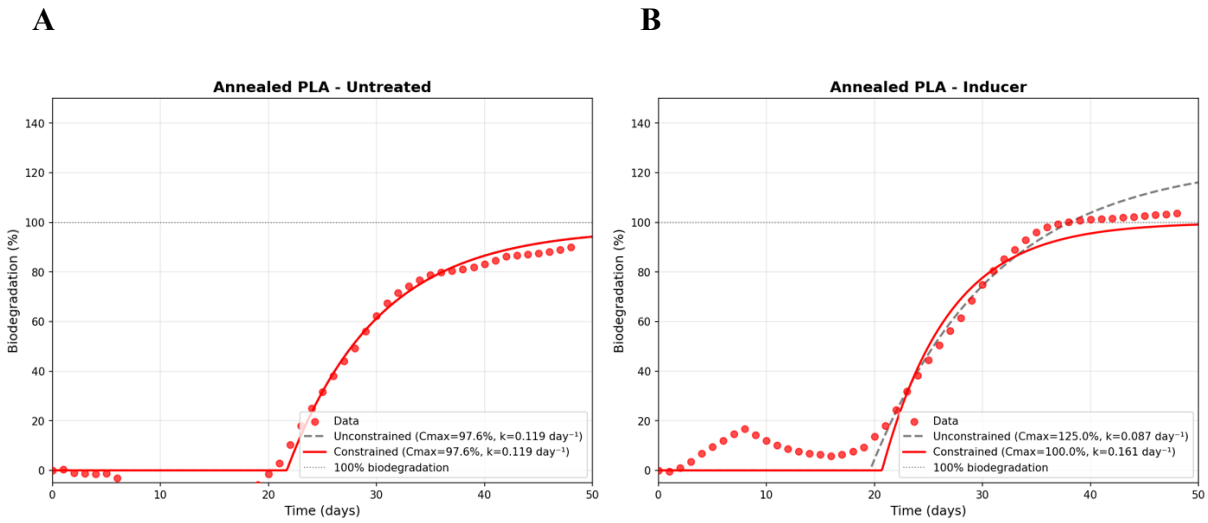

Figure 3.4 First-order kinetic model fits for A) Untreated annealed PLA biodegradation and B) Inducer conditions at 58 °C.

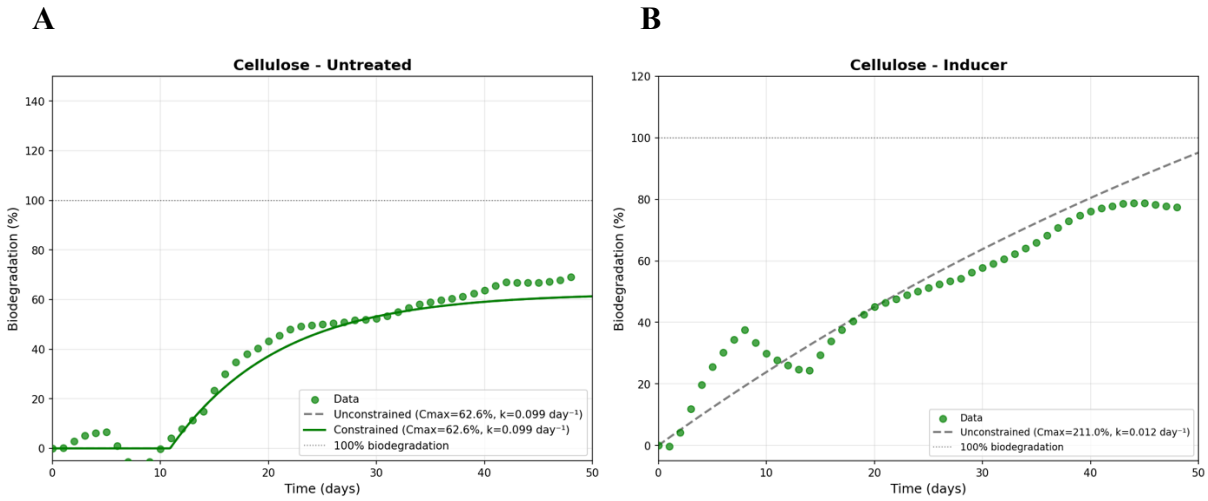

Figure 3.5 First-order kinetic model fits for A) Untreated cellulose biodegradation and B) Inducer conditions at 58 °C.

A constrained fit was applied to conditions where the reported % biodegradation reached higher than 100%. Unconstrained fitting of such data yields inflated Cmax values (123-139%) with correspondingly depressed rate constants as it accounts for more PLA than was actually present and is an artifact of biodegradation values being reported higher than 100%. For conditions where the observed biodegradation remained below 100% (Cellulose Untreated, Annealed PLA Untreated), the unconstrained and constrained fits resulted in identical parameters as the constraint only affects cases where calculated biodegradation was above the real, physical limit.

The application of the kinetics model showed that PLA samples exhibited a consistent lag phase between 19 and 22 days, while cellulose had a shorter lag phase of 11 days. This likely reflects the time required for abiotic hydrolysis to reduce molecular weight sufficiently for microbial attack. Cellulose had a shorter lag phase as it requires no prior abiotic hydrolysis before microbial attack.

The model fit well for untreated cellulose (Cmax = 62.6%, k = 0.099 day^{-1}, R^2 = 0.984) but did not adequately fit inducer conditions, which showed no lag phase and as a result yielded unrealistic parameters (Cmax = 211%). The first-order kinetics observed imply that PLA mineralization was controlled by the availability of hydrolysis products rather than by microbial biomass growth. The unconstrained PLA rate constants obtained (0.069-0.119 day^{-1}) are approximately 2.75-4.75× higher than literature values (Leejarkpai et al., 2011: k = 0.025 day^{-1}).

3.3.1.3 Compost pH

All samples maintained a pH in a range of 7.5 to 8 from start to end. The lack of acidification suggests lactic acid consumption by the microbial community, which is in line with the mineralization data.

3.3.2 Mesophilic Degradation

The objective of Experiment 2 was to characterize the aerobic biodegradation of amorphous and annealed PLA under mesophilic respirometer composting conditions. Like in Experiment 1, the main parameters of interest were the effect of initial PLA crystallinity and gelatin-based biostimulation on CO_2 evolution and biodegradation extent under reduced temperatures.

3.3.2.1 CO_2 Evolution Data

The results indicate that at 30 °C, neither annealed nor amorphous PLA produced CO_2 levels above the negative control (114,396 ± 3,442 mg and 108,538 ± 4,273 mg vs. 111,843 ± 382 mg), suggesting little to no biodegradation of PLA occurred under mesophilic conditions over the test period (Figure 3.6). In contrast, cellulose yielded more CO_2 (122,976 ± 911 mg), confirming its biodegradation (Table 3.5). The negative control and cellulose treatments showed much lower

variability compared to the PLA-containing conditions, suggesting that the presence of non-metabolized PLA may have influenced microbial community activity.

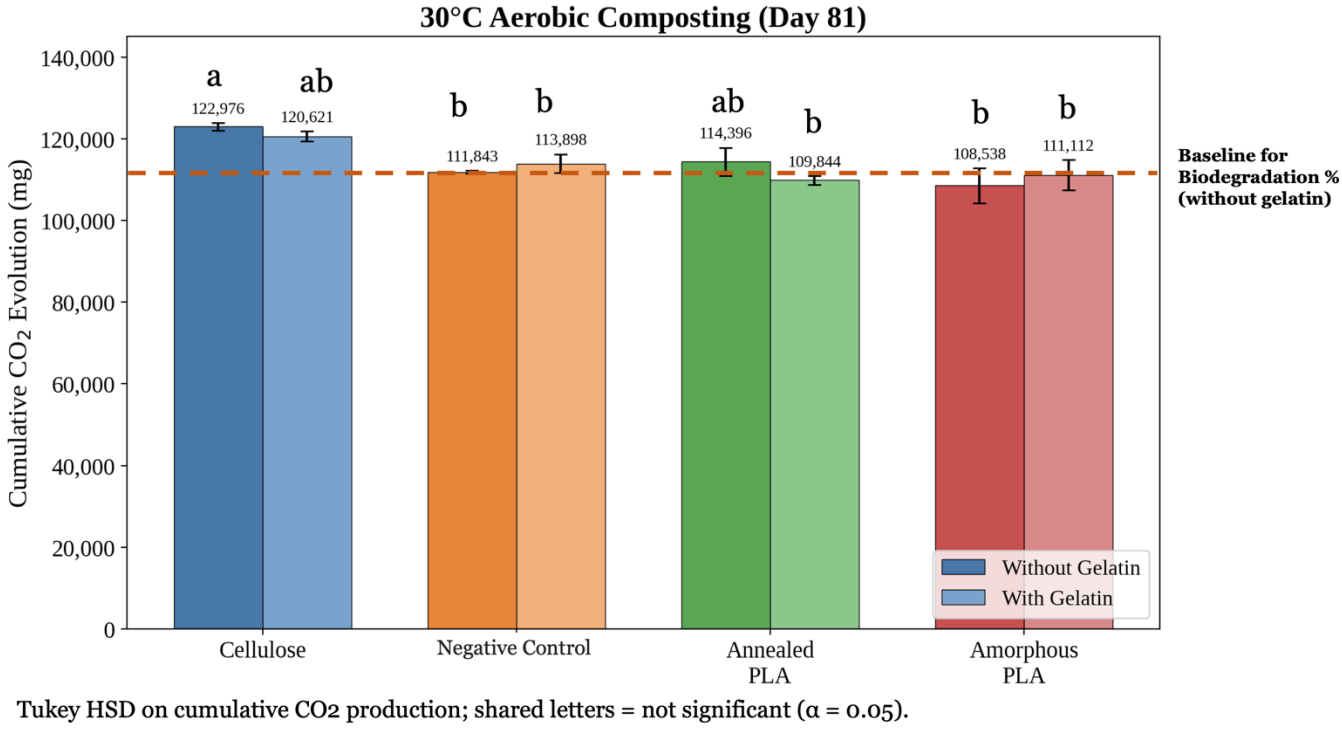

Figure 3.6 Cumulative CO_2 evolution from different compost conditions after aerobic composting at 30 °C for 81 days.

At 30 °C with gelatin added as a biostimulant, CO_2 evolution remained similar to the non-induced condition in all cases. Final CO_2 levels for PLA treatments (109,844 ± 1,071 mg for annealed and 111,112 ± 3,726 mg for amorphous) were nearly equivalent to the negative control (113,898 ± 2,290 mg), indicating no significant enhancement of PLA mineralization. Cellulose again showed elevated CO_2 production (120,621 ± 1,185 mg). As with the non-induced 30 °C condition, standard deviation was higher in PLA treatments. Both annealed and amorphous PLA

produced similar CO_2 levels, continuing the trend from the non-inducer 30 °C test. The initial PLA crystallinity had no significant effect on biodegradation under mesophilic conditions, where neither form was effectively degraded.

Table 3.5 End-point CO_2 values & calculated percentage of biodegradation for aerobic composting at 30 °C.

Sample	**Mean ± Std Dev (mg)**	**Biodegradation (%)**
Cellulose	122,976 ± 911	102 ± 8.4
Negative Control	111,843 ± 382	NA
Annealed PLA	114,396 ± 3,442	20 ± 27.0
Amorphous PLA	108,538 ± 4,273	0*
Cellulose + Gelatin	120,621 ± 1,185	62 ± 10.9
Negative Control + Gelatin	113,898 ± 2,290	NA
Annealed PLA + Gelatin	109,844 ± 1,071	0*
Amorphous PLA + Gelatin	111,112 ± 3,726	0*

*CO_2 evolution was below the compost-only negative control, indicating no observable biodegradation.

Under mesophilic conditions (30 °C, Experiment 2), neither annealed nor amorphous PLA showed consistent signs of biodegradation. Net CO_2 evolution was low or even negative relative to the negative control, and the inclusion of gelatin did not lead to significant improvement (Table 3.5). These findings indicate that, within a 81-day period, mesophilic composting conditions were insufficient to initiate or sustain meaningful PLA mineralization. The degradation observed in thermophilic compost was not replicated at lower temperatures, regardless of crystallinity or nutrient availability. These results demonstrate that cellulose readily biodegraded at mesophilic

temperatures while PLA showed negligible biodegradation (reported as 0% where CO_2 evolution was below negative control levels), regardless of crystallinity or gelatin supplementation.

A one-way ANOVA was performed on raw cumulative CO_2 production across all eight conditions at 30°C. The analysis revealed a significant difference among conditions ($p = 0.0008$). Tukey post-hoc testing showed that cellulose conditions produced significantly more CO_2 than PLA conditions and the negative control, while PLA conditions were not statistically distinguishable from the negative control. No significant difference was found between gelatin-supplemented and non-supplemented conditions for any material type (Tukey HSD, all $p > 0.49$; Appendix D, Table D5).

3.3.2.2 Molecular Weight Analysis

Viscosity-average molecular weight was measured for several recovered PLA films from each condition, to determine whether some level of depolymerization occurred even with limited to negligible mineralization (Table 3.6).

Table 3.6 Viscosity-average molecular weight (Mv) of PLA films (n = 3) following mesophilic composting at 30 °C.

Condition	**Mv ($g \cdot mol^{-1}$, mean ± SD)**	**Mv reduction from initial (%)**
Amorphous PLA	173,366 ± 4,795	15.4
Amorphous PLA + Gelatin	156,099 ± 2,586	23.9
Annealed PLA	157,628 ± 4,568	23.1
Annealed PLA + Gelatin	152,848 ± 4,939	25.4

There was measurable Mv reduction across all treatments, despite the lack of mineralization. A two-way ANOVA on Mv revealed significant effects of both crystallinity ($p = 0.005$) and gelatin supplementation ($p = 0.002$), with a significant interaction ($p = 0.037$). Tukey HSD comparisons

showed that amorphous PLA without gelatin had significantly higher Mv than all other conditions (all $p < 0.01$), which did not differ significantly from each other (all $p > 0.55$). This indicates that both annealing and gelatin supplementation promoted greater Mv reduction under mesophilic conditions, despite neither producing measurable mineralization. The significant interaction reflects that gelatin had a larger effect on amorphous PLA (17,267 g/mol reduction) than on annealed PLA (4,780 g/mol reduction, not significant). Full statistical outputs are provided in Appendix D (Tables D7, D8). The degree to which this Mv reduction is driven by abiotic hydrolysis versus microbial enzymatic activity cannot be inferred from this data. Individual replicate Mv values can be found in Appendix B (Table B1).

3.3.2.3 Compost pH

All samples maintained a pH in a range of 8.2 to 8.5 from experiment start to end. The lack of acidification is in line with the observed lack of degradation, as no lactic acid is accumulated without degradation occurring.

3.3.3 Mesophilic Degradation with Bacterial Inoculation

In the third 30 °C experiment, PLA-containing compost was inoculated with strains previously screened for PLA-degrading activity on emulsion plates. The objective of this experiment was to evaluate whether inoculation with known mesophilic PLA degraders might increase PLA degradation.

3.3.3.1 CO_2 Evolution Data

The consortium and CA4 strains yielded final CO_2 values of 114,057 ± 3,548 mg and 110,750 ± 2,114 mg, respectively, marginally above the uninoculated PLA control (111,691 ± 5,468 mg) and the no-PLA negative control (107,258 ± 3,362 mg) (Figure 3.7). Additional individual strains (CA1, 3.7, 2.5, and 2.3) produced CO_2 values ranging from 99,333 ± 2,441 mg to 109,379 ± 3,224 mg, within the range of negative control variability (except for 3.7) (Table 3.7). Visual inspection confirmed PLA film fragmentation in all treatments, but no condition showed signs of actual PLA degradation. These results suggest that, despite initial screening success on emulsion plates, the tested strains were either unable to access or metabolize solid PLA under the mesophilic composting conditions, or had a preference for another substrate in the compost.

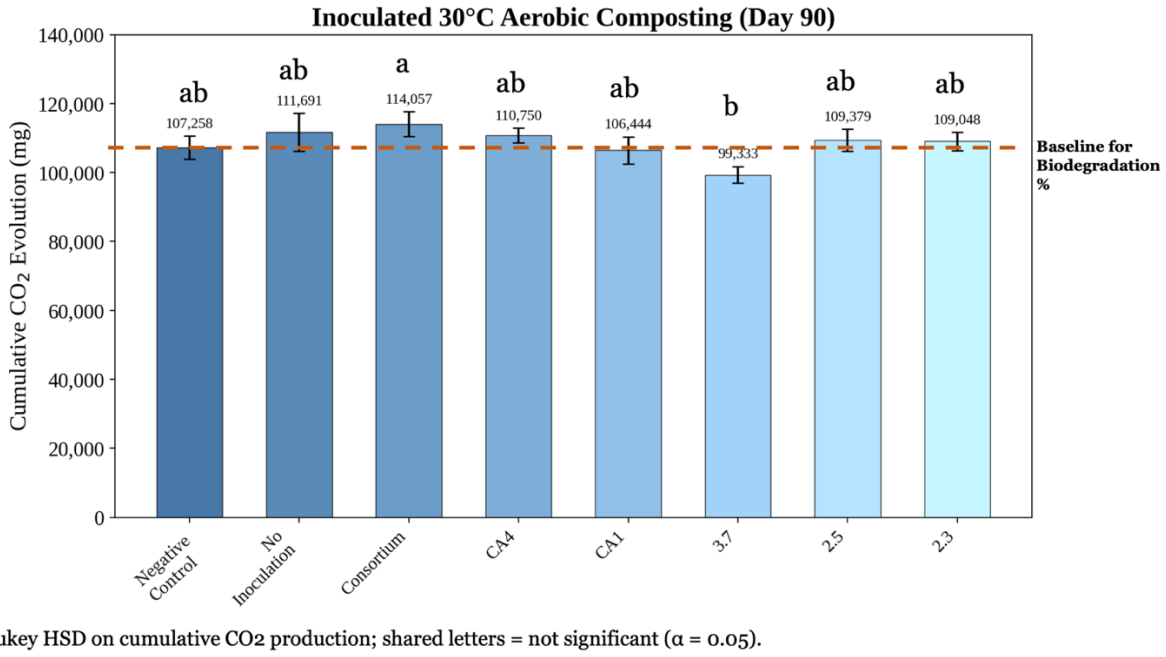

Figure 3.7 Cumulative CO_2 evolution from PLA-containing compost inoculated with different bacterial strains at 30 °C for 90 days.

Table 3.7 End-point CO_2 values & calculated biodegradation percentage for PLA-containing compost inoculated with different bacterial strains at 30 °C for 90 days.

Condition	**Mean ± Std Dev (mg)**	**Biodegradation (%)**
Negative Control	107,258 ± 3,362	NA
No Inoculum	111,691 ± 5,468	37 ± 46.2
Consortium	114,057 ± 3,548	57 ± 30.0
CA4	110,750 ± 2,114	30 ± 17.9
CA1	106,444 ± 3,940	0*
3.7	99,333 ± 2,441	0*
2.5	109,379 ± 3,224	18 ± 27.3
2.3	109,048 ± 2,666	15 ± 22.5

*CO_2 evolution was below the compost-only negative control, indicating no observable biodegradation.

A one-way ANOVA was performed on raw cumulative CO_2 production across all treatments. The analysis revealed a significant difference among treatments ($p = 0.025$). The significant result was driven by Strain 3.7 producing significantly less CO_2 than both the uninoculated control (Dunnett's test, $p = 0.015$) and Consortium 1 (Tukey HSD, $p = 0.012$), suggesting possible inhibition of microbial respiration rather than enhancement of PLA degradation. No inoculated treatment significantly increased CO_2 production relative to the uninoculated control (Dunnett's test, all $p > 0.50$).

3.3.3.2 Molecular Weight Analysis

The viscosity-average molecular weight of some of the recovered PLA films was measured to determine whether some level of depolymerization occurred even with limited to negligible mineralization. Mv measurements were performed on a subset of conditions due to limited instrument availability. The conditions shown in Table 3.7 were selected to capture the highest-

performing inoculant (consortium), the lowest-performing inoculant (Strain 3.7), and the no-inoculum control, to bracket the range of observed CO_2 responses. As can be seen in Table 3.8, Mv reductions were observed, but inoculation did not produce a significant shift in Mv relative to the no-inoculum control. The consortium condition Mv was the same as the no inoculum condition, and Strain 3.7, which showed the lowest carbon mineralization, also showed the lowest reduction in Mv. A one-way ANOVA with Tukey HSD post-hoc correction found no significant differences in Mv among treatments (all pairwise $p > 0.06$). Full statistical outputs are provided in Appendix D (Table D9). Individual replicate Mv values can be found in Appendix B (Table B1).

Table 3.8 Viscosity-average molecular weight (Mv) of PLA films following mesophilic composting with bacterial inoculation at 30 °C.

Condition	**Mv ($g \cdot mol^{-1}$, mean ± SD)**	**Mv reduction from initial (%)**
No inoculum	166,306 ± 6,596	18.9
Consortium	164,857 ± 5,752	19.6
Strain 3.7 (Microbacterium sp.*)*	186,927 ± 13,724	8.8

3.3.3.3 Compost pH

pH remained stable across all conditions, with no significant change from start to end. All samples maintained a pH in a range of 8 to 8.5. The lack of acidification may suggest the absence of lactic acid accumulation, which corroborates the lack of PLA degradation and mineralization.

3.3.3.4 SEM Observations

SEM was used to qualitatively examine surface morphology of representative PLA films before and after compost incubation under selected conditions. Prior to composting, the amorphous PLA film exhibited a smooth and uniform surface with minimal surface features at the micrometer scale, while the crystalline PLA film appeared rougher, with clear gradations along the surface (Figure 3.8). Amorphous PLA films exhibited heterogeneous surface morphologies characterized by localized roughening and the presence of discrete surface voids, both prior to and after incubation with PLA-degrading microbes (Figure 3.9). No clear qualitative differences in surface feature type or distribution were observed between the two conditions at this magnification.

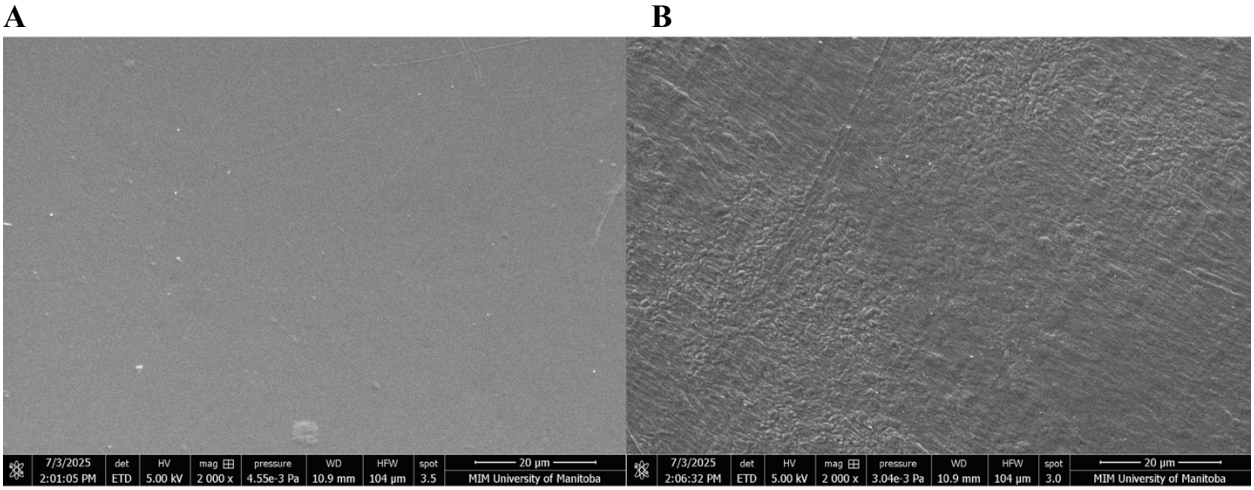

Figure 3.8 Scanning electron micrographs (2000×) of A) untreated amorphous PLA films prior to composting; B) untreated crystalline PLA film.

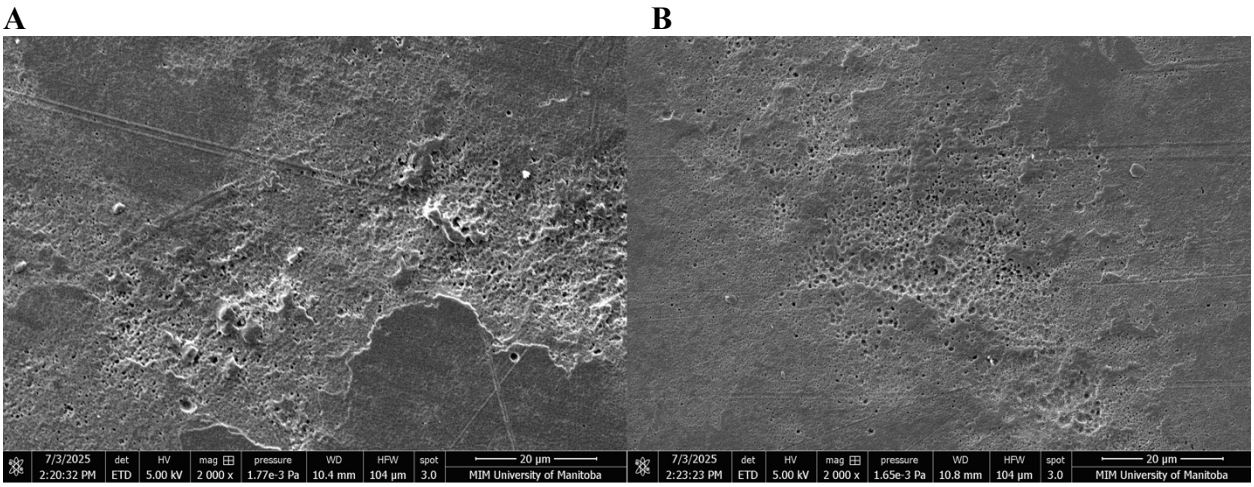

Figure 3.9 Surface morphology of amorphous PLA films pre- and post-incubation with PLA-degrading microbes. A) Amorphous PLA film prior to inoculation with PLA-degrading microbes; B) Amorphous PLA film after incubation with PLA-degrading microbes.

3.4 Discussion

3.4.1 Thermophilic Degradation of PLA

Direct comparison of PLA degradation endpoints and kinetics across studies is complicated by differences in respirometric method (CMR titration, DMR-NDIR, GC-TCD, gravimetric), sample form and thickness, sample-to-compost ratio, PLA grade and molecular weight, and compost source and activity. Broad trends in degradation rate and lag phase duration can still be compared.

Concerning PLA degradation, these results are consistent with the published literature at 58 °C. Kale et al. (2007) achieved 77–84% for PLA bottle pieces over 58 days, while Kalita et al. (2021) required 120–145 days to reach 94% biodegradation of PLA films using online GC monitoring (ASTM D5338-15) with 50 g of film (450 um thickness, Mn = 140 kDa) in 700 g compost at 58 °C, and Stloukal et al. (2015) observed 71% mineralization of PLA after 90 days. Kalita et al. (2021) and Stloukal et al. (2015) both used thicker PLA samples than those tested in this study,

which may explain the faster rate of degradation observed in this study. However, this does not necessarily explain the full extent of the faster degradation. For example, Kunioka et al. (2006) reported 90–91 % mineralization of PLA powders (125–250 μm particle size) within 20–35 days using CMR titration (ISO 14855-1) with 16.5 g of powder in 210 g compost at 58 °C. Although faster than the present study, this reflects the substantially higher surface-area-to-volume ratio of powdered materials relative to intact films. To achieve comparable results (35 vs 45 days) with considerably less surface area, may indicate genuinely favorable composting conditions in the present study. Castro-Aguirre et al. (2017) reported that films of similar thickness (Ingeo 4032D, 255 μm, Mn = 75,000 g/mol) reached ~80–100% mineralization by 60 days, broadly comparable to the present study despite differences in PLA grade and crystallinity.

Cellulose degradation ranging from 64 –74% under these conditions was consistent with the lower-end of reported cellulose degradation in the literature. Leejarkpai et al. (2011) reported 94% cellulose biodegradation over 90 days using CMR titration respirometry (ISO 14855-1) with 30 g of sample in 360 g inoculum at 58 °C, while Castro-Aguirre et al. (2017), using DMR-NDIR respirometry with 8 g of sample in 400 g compost at 58 °C, found highly variable cellulose mineralization ranging from 62–101% depending on test conditions.

Similar to degradation endpoints, kinetics of degradation at 58 °C were much faster than the reported literature. Constrained fits yielded rate constants of 0.141 day^{-1} for amorphous PLA and 0.119 day^{-1} for annealed PLA under untreated conditions, which were 5–6 times higher than those reported in other kinetic studies that used the same first-order kinetic model. Leejarkpai et al. (2011), testing thermophilic degradation of PLA film of a thickness of 300 μm, reported a rate

constant of 0.025 day^{-1} for PLA sheets at 58 °C, and Stloukal et al. (2015) found similar values of 0.0263 day^{-1} for pure PLA. Lag phases were consistent with the above-mentioned literature, with reported lag times varying between 20 and 30 days (Leejarkpai et al., 2011; Stloukal et al., 2015).

3.4.2 Mesophilic Conditions and Biostimulation/Bioaugmentation

High variability was a consistent feature across mesophilic PLA conditions, with standard deviations often exceeding or nearing the means (20-30%). In contrast, negative control degradation exhibited much lower variability, on-par with other CO_2 evolution compost studies (± 5-10%). This disparity is attributable to the signal-to-noise characteristics of the measurement rather than to process inconsistency. At 30 °C, PLA produced little to no net CO_2 above the negative control, meaning that the biodegradation calculation required subtracting two large, similar values (test and negative control CO_2, both >100,000 mg) to obtain a small net difference. Minor absolute fluctuations in either measurement, which would be negligible in the context of overall CO_2 production, were therefore amplified when expressed as a percentage of theoretical carbon content. Cellulose conditions did not exhibit this variability because the net CO_2 signal was large relative to the measurement noise. The small sample size (n = 3, and n = 2 for two conditions due to instrument failure) further limited the ability to resolve a true mean from this noise. Since there is a narrow net measurement different between treatment and control, small variation between replicates has a large effect on calculated biodegradation. Increasing the number of replicates would reduce this uncertainty and improve confidence in the mean.

Neither nutrient supplementation nor microbial inoculation at 30 °C produced results that consistently exceeded negative control respiration. While the data does not support statistically

significant claims about gains from biostimulation or inoculation, it does provide evidence that mesophilic composting alone is insufficient for PLA mineralization in the conditions tested. Gelatin has been used successfully in the past to enhance degradation as its own degradation involves proteases and esterases that are active in PLA hydrolysis (Bubpachat et al., 2018). In this case it may have provided a preferential carbon/nitrogen source, reducing selective pressure for PLA degradation. It may have also shifted microbial community toward gelatin-degraders rather than PLA-degraders and created competition for oxygen or nutrients.

None of the inoculation strategies proved effective, though there was variance in the performance between strains. *Microbacterium*, *Cellulomonas*, and *Streptomyces* are all actinobacteria, which is a phylum many identified PLA-degraders belong to. Commonly found in soil, they are known as prolific enzyme producers, often capable of producing proteases and esterases that can cleave the ester bonds holding PLA chains together. A clear zone on an emulsified-PLA agar plate, as these bacteria were identified from, indicates secretion of such enzymes, though activity in a complex compost matrix may differ from activity on emulsified PLA in pure culture.

3.4.3 Crystallinity

Kinetic analysis revealed that amorphous PLA degraded faster ($k = 0.141$ vs 0.119 day^{-1}) than crystalline PLA under thermophilic conditions, although the final level of degradation was similar. Overall polymer morphology and mechanical properties likely play into this as well – Pantani and Sorrentino (2013) found that although crystalline films degraded slower than amorphous ones at 58 °C, crystalline powder degraded faster than both of them, indicating that although crystallinity

increased time to degrade, surface area was a much more important factor overall. For industrial composting, this indicates that crystallinity is a minor concern if temperature is maintained around 58 °C, or if particle size is sufficiently small.

3.5 Conclusions

Respirometry analysis across three experiments demonstrated foremost that PLA degradation was highly temperature-dependent. Under thermophilic conditions (58 °C, Experiment 1), both annealed and amorphous PLA films exhibited biodegradation, with CO_2 evolution indicating complete or nearly-complete mineralization within 45 days. These results were consistent across untreated and biostimulated compost, and supported by visual disappearance of PLA fragments, suggesting that high temperatures alone are sufficient to support microbial breakdown of PLA in compost environments. The rapid PLA degradation paired with moderate cellulose degradation suggests that the compost conditions in this study particularly favored hydrolytic polyester degradation, and the specific mechanisms driving this selectivity warrant further investigation. Even with the presence of putative degraders, under the tested conditions the mesophilic (30 °C) environment appeared insufficient for initiating the hydrolytic and enzymatic processes required for PLA mineralization, unlike the complete breakdown observed at 58 °C. These results reinforce the temperature-dependence of PLA biodegradation.

Under the conditions tested, there was no observed appreciable degradation of PLA at mesophilic conditions. At thermophilic temperatures, substantial degradation was observed. As implemented in this chapter, neither biostimulation with gelatin nor bioaugmentation with mesophilic PLA-degrading bacteria proved capable of overcoming the temperature limitation. The

faster-than-literature degradation kinetics observed with the compost source being the Forks RDC suggest that facilities regularly processing PLA may develop enhanced degradation capacity over time. This hypothesis requires further investigation however with the isolation and identification of responsible microbes.

3.6 Recommendations for Experimental Refinement

3.6.1 Controls and Baseline Characterization

There are several different controls that would strengthen the observations made during the respirometry experiments. One control would be a lactate control, which would be compost with the addition of lactate carbon-equivalent to the amount found in the PLA conditions. This would allow better discernment of the effect of PLA's structure and how its hydrolysis affected the rate of compost respiration. If the control showed faster CO_2 accumulation, that would indicate that PLA's structure was preventing its consumption by the bacteria. This is already inferred by the curve of the biodegradation kinetic data but would be strengthened by this control.

In the inoculation experiments, any CO_2 from inoculated conditions could reflect the added bacteria metabolizing organic matter, not PLA. A compost with inoculum without PLA control would separate contributions (or inhibitions) that come from the strain's presence itself versus the strain's presence with PLA present.

The compost was collected fresh from the Forks RDC prior to each experiment. Although it was confirmed that inputs into the Forks RDC were kept consistent throughout the duration of these experiments, they are still ultimately different batches – their composition, microbial community, and nutrient status may have varied. Pre-digestion of the compost matrix prior to PLA

addition may reduce background heterotrophic activity and encourage microbial communities to shift toward PLA as a carbon source. Further characterization beyond pH and moisture content, such as C:N ratio, volatile solids, and microbial biomass, would provide additional insights.

3.6.2 Replication, Sampling, and Analytical Gaps

Across all respirometer experiments, a minimum of five samples should be used. It was found there was significant variability between replicates, especially in the cases where PLA did not degrade, and more replicates would improve statistical confidence. Additionally, higher PLA loading in each respirometer likely would improve biodegradation calculations. The 5 grams of PLA in 250 grams of compost meant that the net CO_2 difference between the negative control and test conditions was very small and amplified by large standard deviations due to low replicates. Increasing PLA loading while staying within ASTM D5338 loading ratios would improve this signal.

Through each experiment, only endpoint Mv was tracked. In the 58 °C experiment, where PLA was fully mineralized, there were no samples to measure Mv for. Mv measurement of samples at intermediate stages would provide another rate of PLA degradation and inform the lag-phase interpretation. It could be shown whether molecular weight drops during the lag phase and whether it correlates with increased CO_2 evolution at a specific Mv threshold. If this was implemented, it would require another control, sterile compost with PLA present. This would allow for the impact of abiotic thermal hydrolysis to be separated from microbial presence and activity.

Tracking soluble lactic acid concentration over time would confirm whether the lag phase corresponds to lactic acid accumulation and consumption. Measuring dissolved inorganic carbon across all conditions would correct for underestimations in CO_2 produced, and indicate whether PLA presence results in different retention of dissolved inorganic carbon relative to compost-derived carbon compared to cellulose and base compost organic matter.

In the RDCs, temperatures were often in the 40-50 °C range, between the two temperatures tested in the respirometers. The outcomes at both extremes were very different – little to no degradation versus complete mineralization. Repeating the experiments at an intermediate temperature, 45 °C, would help define whether an incremental increase in temperature also results in an increase in degradation.

3.6.3 Bioaugmentation Validation

The inoculation bacteria were revived from frozen stocks and not screened again on PLA plates to confirm PLA-degrading activity prior to inoculation. Confirming this functional activity prior to inoculation, and ideally with PLA films instead of emulsified PLA, in a full respirometer run would make for a more rigorous screening process. Additionally, the cultures should be grown on PLA prior to inoculation to prime them for PLA degradation. In the case that the bacteria were found to degrade PLA films, there should still be verification that the inoculated organisms survived or maintained population levels. This would differentiate between whether the strains failed because they were unable to degrade PLA, or whether they failed due to competitive exclusion by indigenous organisms. Furthermore, testing for the presence of the strains at the end

of the experiment would also be informative as to their population's survival throughout the course of the experiment.

As the indigenous microbes in the 58 °C compost appeared to be potentially PLA-adapted, shotgun metagenomics and metaproteomics of the compost before and after degradation would aid in identifying the responsible microbes and their active degradation enzymes. This two-fold approach accounts for the fact that only a subset of organisms carrying polymer-degrading genes are functionally active during polyester biodegradation (Meyer-Cifuentes et al., 2020).

Chapter 4: PLA Degradation and Thermal Variability in Rotary Drum Composting Systems

4.1 Introduction

A RDC is a fully enclosed, insulated, continuous-flow in-vessel composting system designed primarily for the aerobic decomposition of livestock carcasses. Unlike static or aerated composting systems, the RDC operates as a rotating drum bioreactor, in which material is repeatedly lifted, mixed, and transported along the vessel (Nioex Systems Inc. 2010). Its aeration comes from the turning of the material and not from forced air. A survey of the recent literature indicated that PLA degradation under industrial composting occurs at both laboratory and full-scale conditions when temperatures exceed Tg, with the rate depending on material thickness and residence time in the thermophilic environment (Table 4.1). However, no published work has evaluated PLA degradation within a rotating in-vessel mortality composter, a system type that differs fundamentally from both laboratory reactors and industrial windrows.

Table 4.1 Summary of published studies on PLA degradation under industrially relevant composting conditions.

Study	PLA Type	Degradation Environment	Temperature (°C)	Duration (Days)	Final Outcomes
Musioł et al. (2016)	Commercial PLA (Ingeo 2002D); extruded film & tray (~0.30 mm)	Industrial composting (open pile; closed container)	~60	7–70	Rapid Mw reduction (~50% in 14 d); faster degradation in closed container
Maragkaki et al. (2023)	Pure PLLA (PLLAB2B)	Lab composting and windrow simulation	Lab: 58 Windrow: ~50–70	Lab: ~90; Windrow: ~49	Pure PLLA reached 100% biodegradation and disintegration
Kawashima et al. (2021)	PLA-coated paper plates (40 µm PLA film)	Pilot-scale composting (180 L reactors)	Self-heating; ≥65 °C (≥48 h)	~50–60	~95% disintegration; no impact on compost process or quality
Fogašová et al. (2022)	PLA/PHB and PLA/PHB/TPS blends (PLA 30–70 wt%)	Lab and municipal composting	Lab: 58; Municipal: ~60–63	Lab: ≤90 ; Municipal: 84	100% mineralization under industrial composting; performance ≥ cellulose
Chong et al. (2024)	PLA-based rigid blend (~1 mm; Ca-silicate filled); PBS blend	Lab and full-scale in-vessel composting	Lab: 58; Full-scale: ~40–80	Lab: 28–84; Full-scale: 21	~44% mass loss in lab (12 wk) vs. ~98% remaining at full scale (3 wk); residence time limiting
Gastaldi et al. (2024)	PLA packaging (mixed rigid/flexible items)	Full-scale turned windrows	69.7 °C average for active thermophilic phase (49 days)	133	~98% mass loss for compostable plastics; PLA degradation confirmed by fragment recovery and thermal changes

Because of these unique environmental and operational characteristics, it cannot be assumed that PLA will degrade in a RDC in a manner comparable to the previously studied composting systems mentioned above (Table 4.1). This work will focus on understanding the biodegradation of PLA within RDC systems and comparing performance to that observed in controlled respirometer conditions. The goal is to evaluate the effectiveness of RDCs as real-world PLA waste management systems, with a particular emphasis on process parameters such as oxygen availability, temperature stability, and pretreatment effects.

Two RDC systems were evaluated: one at the "Forks" located in Winnipeg, Manitoba, and the other located at the University of Manitoba (U of M), Winnipeg, Manitoba. The primary difference between the Forks and the U of M RDC systems lies in their size and compost sources. The Forks RDC is roughly 13 meters long, with a residence time of 18 to 21 days for material to travel from inlet to outlet. This time represents only the active in-vessel phase; the compost is often re-inserted back into the RDC at least one more time, and then is placed in curing piles before the composting process is considered complete. The U of M RDC is roughly 5 meters, and so has a much shorter time for the compost to go through the vessel, at roughly 4 to 5 days.

The Forks processes and composts their food waste (including PLA materials) in their RDC, but this degradation of the PLA materials has not been quantified or characterized. Experiments assessed the degradation of PLA under controlled composting conditions at both Forks and U of M sites.

4.2 Experimental Design and Methods

4.2.1 RDC System and Operating Conditions

All composting trials in this chapter were conducted using a RDC in-vessel composting system (Nioex Systems Inc., Canada). The work in this study used RDC units operated at The Forks and the University of Manitoba Sustainability in Action Facility (SIAF).

4.2.1.1 System Design and Construction

The RDC consists of a stainless-steel cylindrical drum mounted on support frames with nylon roller casters and driven by an electric motor via chains, belts, and a gearbox assembly (Figure 4.1). Model capacities range from approximately 27-227 kg of organic material per day, with drum lengths between approximately 4.9 and 12.8 m and diameters of 0.9-1.2 m. Material is introduced through front loading doors, and on the larger units, internal conditions can be visually assessed through inspection windows equipped with thermometers. Compost exits the vessel through a 45 cm discharge opening at the rear.

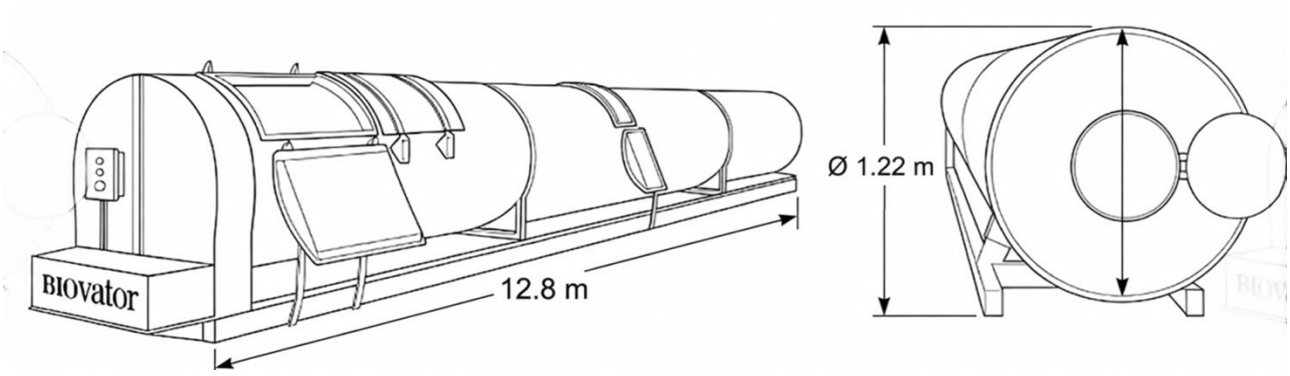

Figure 4.1 Schematic of Forks RDC, showing the inlet and outlet with unit length and diameter.

4.2.1.2 Insulation and Thermal Environment

The drum is enclosed in R8-rated foam insulation, which helps to prevent heat loss and allows thermophilic composting to be attempted during winter, though this is not always successful depending on the severity of the cold. The limits to its cold weather capability are dependent on both ambient temperature and the rate at which compost can be poured into the RDC. Regular feeding of new material into the RDC allows continued heat generation due to microbial activity; if feeding of the RDC stops, temperatures can drop low enough for the compost in the RDC to freeze, rendering it inoperable until warmer temperatures melt the material. Due to the material consistently entering and leaving the RDC, there tends to be a thermal gradient that forms along the vessel, with the highest temperatures in the midsection (which is the majority of the vessel) and cooler temperatures near the loading and discharge zones (Nioex Systems Inc., 2010).

4.2.1.3 Rotation, Aeration, and Material Movement

The RDC operates as a rotating bioreactor, with rotation frequencies, depending on loading rate and management schedule. A full rotation lasts approximately 20 minutes. Internal stainless-steel paddles lift and tumble the material during rotation, providing aeration, mixing, and conveyance. Material typically moves 15-30 centimeters per full revolution, generating a distributed residence time rather than a fixed retention period. Organic material decomposition generally occurs over 7–21 days, depending on feedstock, moisture, season, and loading density. The experiments assessed the degradation of three PLA types (Amorphous, Crystalline, Forks PLA) across 14, 28, and 42-day intervals, with five replicates per treatment, totaling 45 samples per site. The time intervals

were chosen based on the time it takes for the compost to complete a full cycle in a standard 13 m RDC, which is two weeks long.

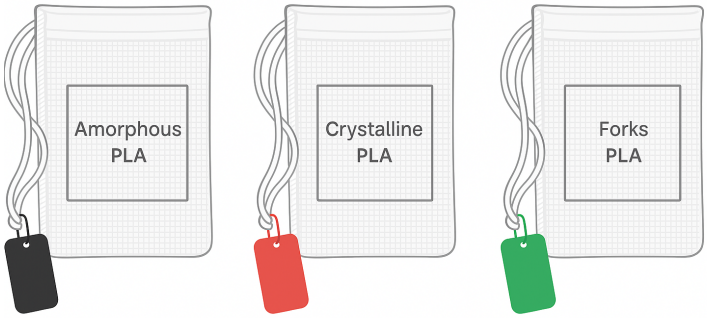

Figure 4.2 Diagram showing PLA within mesh bags along with identity tags.

The mesh bags used to contain PLA samples during these trials are ALEGI nylon media filter bags, measuring approximately 19 × 9 centimeters with a fine 180-micron nylon mesh. The objective of using these bags is to retain PLA films/fragments while allowing compost moisture and microbial communities to interact with the contents. For identification, aluminum tags are looped into the drawstring and color-coded and marked based on the retrieval timepoint and sample type.

4.2.1.4 PLA Loading Relative to Substrate Mass

In the respirometer experiments, PLA sample mass was ~5 g dry weight and was combined with approximately 175 g of dry compost for a compost-to-plastic ratio of 25:1. This ratio was based on the mass of PLA available for the experiments, and is above the minimum 6:1 dry weight ratio specified by ASTM D5338. In the SIAF RDC, PLA mass loading was much more dilute; PLA test samples in the SIAF RDC totaled no more than 5 g at any time, compared to roughly 80 kg of added dry compost a week. The Forks RDC operates with much higher PLA loading, with a 2:1 ratio of wood chips to PLA/food waste. Based on visual observation, PLA and foodwaste were present in approximately equal proportions, yielding an estimated substrate-to-plastic ratio of roughly 5:1 which is much higher plastic loading than either the respirometer experiments or the ASTM D5338 standard.

4.2.1.5 Mass Loss Analysis

Mass loss measurements provide a direct quantification of bulk material degradation and are used for assessing the extent of physical deterioration over time. Prior to composting, each film was cleaned and weighed using an analytical balance with a precision of at least 0.1 mg, and moisture content measured. After compost exposure, films were retrieved, rinsed to remove compost residues, dried at ambient temperature and reweighed with moisture content measured. To recover sample bags, compost was discharged from the RDC outlet and sorted manually. Bags designated for later timepoints, along with loose compost, were recycled back into the RDC inlet, while bags corresponding to the current retrieval timepoint were removed for analysis.

To interpret and display the film recovery data, the data was standardized into four outcome categories. These threshold values were defined empirically based on observed patterns in the recovery data. Films recovering less than 30% of their initial mass were consistently recovered as powder rather than discrete fragments, and so that was chosen as the threshold between fragmented and powderized. This classification distinguishes between outcomes caused primarily by fragmentation and incomplete recovery versus degradation (complete disappearance of visible plastic).

- Intact: ≥ 90% mass recovery. The film remained largely intact as a single piece or a small number of large fragments, with no meaningful loss of material.
- Fragmented: 30 to < 90% mass recovery. The film was present as multiple fragments, with visible plastic remaining. Material loss in this category is attributed primarily to fragmentation and recovery limitations rather than complete disappearance.
- Powderized: >0 to < 30% mass recovery. The film was present only as very fine fragments or powder that was visible but not practically recoverable as discrete pieces, indicating severe physical breakdown.
- Not Recovered: 0% mass recovery. No visible plastic residue was observed upon close inspection, indicating complete loss of recoverable material.

This approach was chosen to provide an objective and reproducible framework for interpreting mass recovery outcomes. While percent mass recovery alone captures overall losses, it does not distinguish whether missing mass reflects mechanical disintegration and incomplete recovery or true biodegradation. It is important to note, however, that while complete non-recovery of material

is consistent with extensive degradation, these measurements still reflect disintegration and physical disappearance rather than confirming direct mineralization. Images of recovered PLA samples are provided in Appendix A.

4.2.2 SIAF RDC Experiment 1 Operating Conditions

Figure 4.3 Exterior view of the SIAF RDC (Winnipeg, MB), an 18-foot rotating in-vessel composting unit used in experiments.

The SIAF RDC (Figure 4.3) was configured to operate similarly to the one in active use at the Forks, which rotates on an intermittent schedule. One difference, however, is the outlet of the RDC, which in SIAF's case was restricted to limit airflow. This was done as it had been previously found by SIAF staff that limiting the outlet size helped the smaller RDC to maintain higher temperatures, an issue more pronounced in the smaller vessel due to its lower volume of heat-generating material (J. Ackerman, University of Manitoba, 2025). For this study, a HOBOware sensor was put into the

RDC about a third of the length of the RDC to record temperature, along with the RDC's built-in temperature monitor. Gas measurements were also taken within the vessel using a syringe and analyzed on a microGC system (Agilent 490 Micro GC). This was done to identify any potential oxygen-limited scenarios that could arise in the RDC, especially given the constriction of the outlet.

For the first SIAF RDC Experiment, the drum was rotated once every 2 hours, with one revolution taking 20 minutes. The outlet was 80% restricted to retain material and limit heat loss. Carbon and nitrogen sources were fed into the RDC weekly, with 40 kg of carbon, and 40 kg dry chicken manure mixed with 150 L of water to form a slurry, maintaining a moisture content of 65% wet basis and a C:N ratio of ~35:1. The carbon source was initially dry leaves, before switching to barley straw in week 3; the reason for the switch in carbon material was that barley straw was readily available while sources of dry leaves had run out. Internal temperatures generally remained between 40 and 50 °C, with a brief decline in week 3 due to a feed interruption during the transition from dry leaves to straw. The relationship between internal and ambient temperatures is discussed in Section 4.3.1.3.

4.2.3 SIAF RDC Experiment 2 Operating Conditions

For this second experiment, conditions were identical to the first experiment except the RDC was rotated continuously as opposed to every 2 hours. Additionally, barley straw and dry leaves were used as the carbon source from the start of the experiment through to the end, as opposed to the first experiment where barley straw was only incorporated starting at week 3. Daily temperature readings for this experiment can be found in Appendix C (Table C2).

4.2.4 SIAF RDC Experiment 3 Operating Conditions

The RDC was operated identically to Experiment 2, rotating continuously. The primary objective was to characterize thermal heterogeneity within the RDC by placing temperature sensors inside individual mesh bags. The experiment ran for one week before a power interruption and subsequent freezing of the vessel contents prevented further operation within the thesis timeline. 7 of the 20 temperature sensors were recovered, and temperature data from the initial week, during which the RDC was operating under thermophilic conditions comparable to those observed in Experiments 1 and 2, were successfully retained. This data provides individual-bag thermal tracking within the RDC, a design improvement informed by Experiment 2, and contributes directly to the characterization of thermal heterogeneity experienced by individual PLA samples within the vessel.

4.2.5 Forks RDC Operating Conditions

Figure 4.4 Exterior view of the Forks Market RDC (Winnipeg, MB), a 42-foot rotating in-vessel composting unit used in experiments.

For the first experiment, the bags were placed individually into the RDC (Figure 4.4), consistent with the SIAF experiments. This resulted in no successful recoveries, as the constant and high-volume compost output made identification and retrieval of individual bags not possible.

For the second experiment, the sample bags were placed into larger mesh bags of the same material, with compost added inside the larger bags. They were grouped according to their retrieval timepoints of 3 and 6 weeks, with three weeks being the amount of time it took material to move

completely through the RDC. Even with this method, some bags fell out of the larger mesh one and were not recovered, leading to lower replicate numbers (between 3 and 5) for each condition. The Forks RDC maintained temperatures between approximately 40 and 60 °C for the duration of the experiment (Section 4.3.4.3) and rotated on an intermittent schedule (20 minutes every 2 hours). Daily temperature readings for this experiment can be found in Appendix C (Table C3).

4.3 Results

4.3.1 SIAF RDC Experiment 1

The objective of the first experiment at the SIAF RDC site was to characterize PLA degradation over a six-week period under standard RDC operating conditions.

4.3.1.1 Mass Recovery Data

For each experiment, a single summary table reports the percentage of samples within each outcome category (described in the methods section) at each timepoint, along with the total number of replicates (n). This approach aimed to improve interpretability while maintaining transparency regarding variation between replicates, as this was not as well captured by mean values for each replicate set. Full replicate-level mass recovery data, including individual sample masses, percent recovery values, and qualitative notes, are provided in the Appendix (Appendix A). Not all bags were successfully recovered at every timepoint as they would get lost in the mass of compost exiting the RDC; reported sample sizes reflect the number of bags retrieved.

As shown in Table 4.2, all films recovered after week 2 were partially intact (51–100% recovery), with crystalline films showing the earliest fragmentation. By week 4, some films had begun to completely disappear, with crystalline PLA having the highest proportion of

gone/powderized films and amorphous the least. For both the amorphous and Forks conditions there were films that were still entirely intact. By week 6, 77% of films were fully or nearly fully degraded, with the remaining 23% intact or fragmented across all films types.

Table 4.2 Distribution of PLA film recovery outcomes for SIAF Experiment 1 at 2, 4 and 6 weeks.

Time (weeks)	**PLA Type**	**n**	**Intact (%)**	**Fragmented (%)**	**Powderized (%)**	**Gone (%)**
2	Amorphous	5	60	20	20	0
2	Crystalline	5	20	80	0	0
2	Forks PLA	5	60	40	0	0
4	Amorphous	5	40	20	20	20
4	Crystalline	5	0	40	40	20
4	Forks PLA	5	40	0	40	20
6	Amorphous	4	25	0	25	50
6	Crystalline	4	0	25	50	25
6	Forks PLA	5	20	0	20	60

This binary outcome, with most films degraded or completely intact by 6 weeks, suggests a difference in exposure conditions inside the RDC. The literature, as well as previous respirometer trials, suggest a critical temperature threshold must be reached (> 55 °C). It is possible some films did not experience this threshold within the RDC as they did not degrade, despite the temperature on the sensors reaching and maintaining temperatures higher than the threshold repeatedly over the trial. Most films degrading suggests a temperature above 55 °C must be reached, but not necessarily maintained, to achieve degradation over similar timespans to the respirometer studies. The temperature within the RDC fluctuated from 40 to 60 °C, as can be seen in Figure 4.5 in Section 4.3.1.3, while in the respirometer experiments the temperature was an unwavering 58 °C;

despite these fluctuating temperatures in the RDC, complete disappearance of some samples was observed. Daily temperature readings for this experiment can be found in Appendix C (Table C1).

Crystalline PLA showed earlier and/or more extensive loss of recoverable mass in several replicates relative to amorphous PLA in this experiment. This can be attributed to the brittle nature of the crystalline samples, which led to earlier fragmentation. This fragmentation increased the surface area for degradation, and so is a likely factor in the higher disappearance of the crystalline samples compared to the others. Intermittent rotation allowed localized persistence of favorable or unfavorable degradation environments, leading to uneven outcomes among nominally identical samples. For the next study, the RDC was rotated constantly, to observe whether that improved film degradation outcome homogeneity.

4.3.1.2 Molecular Weight Data

Viscosity-average molecular weight (Mv) measurements were used to assess molecular-level degradation of PLA films recovered from the SIAF RDC. They were not completed for every individual film, but from a recoverable representative from each condition, as in most cases that was all that was available. As a result, they serve as complementary observations rather than to establish any statistically significant trend. The Mv reduction column is reporting the % reduction from the measured initial Mv of the polymer source, which was 205,000 $g \cdot mol^{-1}$ for the amorphous/crystalline PLA and 217,000 $g \cdot mol^{-1}$ for the Forks PLA. Mv data for all SIAF RDC experiments can be found in Appendix B (Table B2).

Table 4.3 Viscosity-average molecular weight of PLA recovered from SIAF RDC Experiment 1.

PLA Type / Source	**Exposure time**	**Mv (g·mol^{-1})**	**Mv reduction (%)**
Crystalline PLA (fragments)	2 weeks	47,300	76.9
Crystalline PLA (fragments)	2 weeks	32,893	84
Crystalline PLA (fragments)	4 weeks	30,414	85.2
Amorphous PLA (intact)	2 weeks	99,374	51.5
Amorphous PLA (intact)	4 weeks	95,826	53.2
Amorphous PLA (intact)	6 weeks	97,325	52.5
Forks PLA (intact)	2 weeks	82,668	61.9
Forks PLA (intact)	4 weeks	70,354	67.6
Forks PLA (fragmented strands)	6 weeks	31,663	85.4

For all films, there was substantial molecular weight reduction within two weeks (≥ 51%). Crystalline samples were fragmented, which corresponded with reduced molecular weight. This was also true for the 6-week Forks PLA sample, which fragmented into long strands and had a heavy Mv reduction (85.4%). The reason hypothesized for the faster molecular degradation of the crystalline PLA is that it fragmented quicker, and into smaller pieces than the other conditions – increasing the surface area available for hydrolytic attack, which has been shown to be a more impactful factor than crystallinity in PLA degradation (Pantani and Sorrentino, 2013).

4.3.1.3 Ambient Temperature Comparison

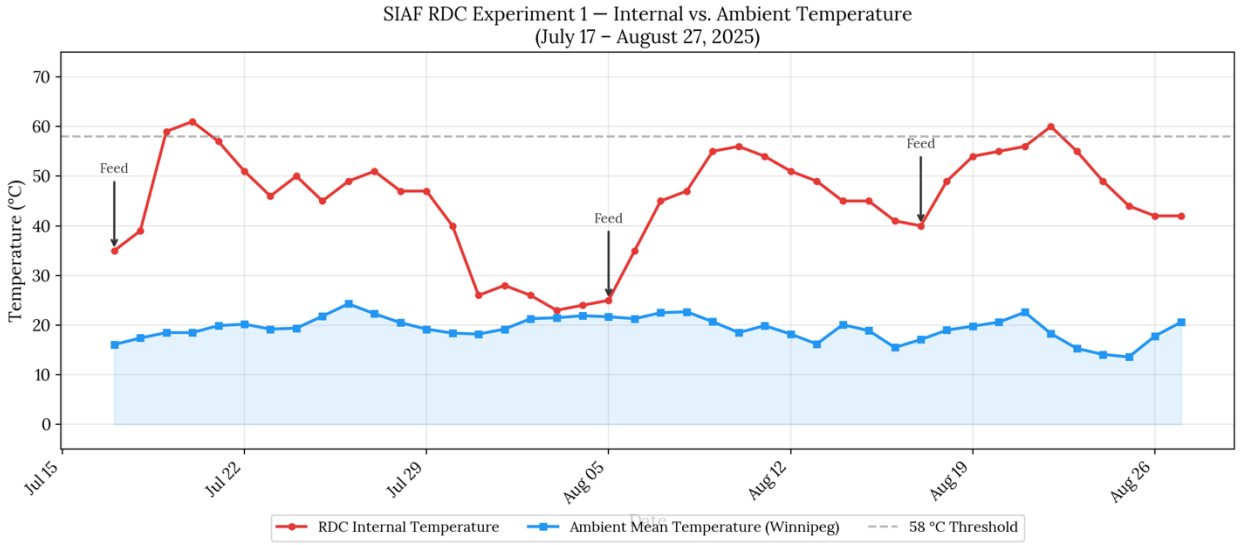

Figure 4.5 Internal temperature profile of the SIAF RDC compared to ambient temperature during Experiment 1.

During weeks 1 and 2, RDC internal temperatures reached approximately 60 °C, followed by a brief decline to around 30 °C in week 3 due to a delay in feeding during the transition from dry leaves to straw, before recovering to 40-60 °C during weeks 4 through 6 (Figure 4.5). The overall RDC temperature range remained between 40 and 60 °C for the majority of the trial. Throughout the trial, ambient mean daily temperatures remained stable at ~19 °C. The mid-trial crash of RDC internal temperatures was due to feed interruption, and did not correlate with the ambient weather. All three internal temperature cycles (rise/crash/recovery) were driven by feeding and microbial activity, with no correlation to ambient temperatures. Each trough in internal temperature represents the decline of a heating cycle as microbial activity decreased.

4.3.2 SIAF RDC Experiment 2

The objective of this experiment was to observe the effect continuous rotation would have on the degradation outcomes of the PLA film samples, over the same time durations (2 weeks, 4 weeks, 6 weeks) as observed in the first experiment. Continuous rotation was expected to improve homogeneity of environmental conditions within the RDC, and potentially improve aeration, while reducing temperature because of the increased aeration.

4.3.2.1 Mass Recovery Data

At 2 weeks, crystalline PLA already exhibited substantially lower mass recovery compared to Experiment 1, including multiple samples with no recoverable material (Table 4.4). In contrast to Experiment 1, where no samples were completely gone until week 4, this experiment showed accelerated degradation due to continuous rotation. By 4 weeks, all crystalline PLA samples had completely degraded (100% gone), while amorphous samples were largely powderized and Forks PLA remained mostly intact. At 6 weeks, one amorphous film was recovered completely intact, with the rest being entirely gone. For the Forks PLA samples, one film was intact while the remaining three were heavily powderized and non-recoverable, though powder was visible within the bags. All crystalline films were gone by week 6.

Table 4.4 Distribution of PLA film recovery outcomes for Experiment 2 at 2, 4 and 6 weeks.

Time (weeks)	**PLA Type**	**n**	**Intact (%)**	**Fragmented (%)**	**Powderized (%)**	**Gone (%)**
2	Amorphous	5	60	20	0	20
2	Crystalline	5	0	40	20	40
2	Forks PLA	5	20	80	0	0
4	Amorphous	5	0	0	80	20
4	Crystalline	5	0	0	0	100
4	Forks PLA	5	80	0	0	20
6	Amorphous	4	25	0	0	75
6	Crystalline	3	0	0	0	100
6	Forks PLA	4	25	0	75	0

Continuous rotation dramatically reduced replicate variability for amorphous and crystalline PLA, producing more uniform endpoints. Loss of recoverable mass occurred earlier and more synchronously than in Experiment 1. However, given the existence of intact samples for both amorphous and Forks samples, there did still appear to be a difference in RDC environmental conditions that affected the degradation outcomes. The trend of crystalline films fragmenting and degrading quicker from Experiment 1 was also observed in this second experiment.

4.3.2.2 Molecular Weight Data

Viscosity-average Mv measurements were used to characterize degradation of PLA films recovered from SIAF RDC Experiment 2, providing comparative context to Experiment 1 under continuous rotation.

Table 4.5 Viscosity-average molecular weight of PLA recovered from SIAF RDC Experiment 2.

PLA Type / Source	**Exposure Time**	**Mv (g·mol^{-1})**	**Mv reduction (%)**
Crystalline PLA	2 weeks	22,983	88.8
Amorphous PLA	4 weeks	9,024	95.6
Amorphous PLA	6 weeks	7,614	96.3
Forks PLA	2 weeks	11,776	94.6
Forks PLA	4 weeks	14,914	93.1
Forks PLA	6 weeks	10,976	94.9

In this experiment, much more severe molecular degradation was seen than in Experiment 1. All samples showed at least 89% reduction in molecular weight by 2 weeks, which aligns with the complete disappearance of some PLA films that was observed in the mass recovery analysis for that same timepoint. By 6 weeks, Mv values had decreased by 95%, values associated with complete loss of mechanical integrity and general film persistence.

4.3.2.3 Ambient Temperature Comparison

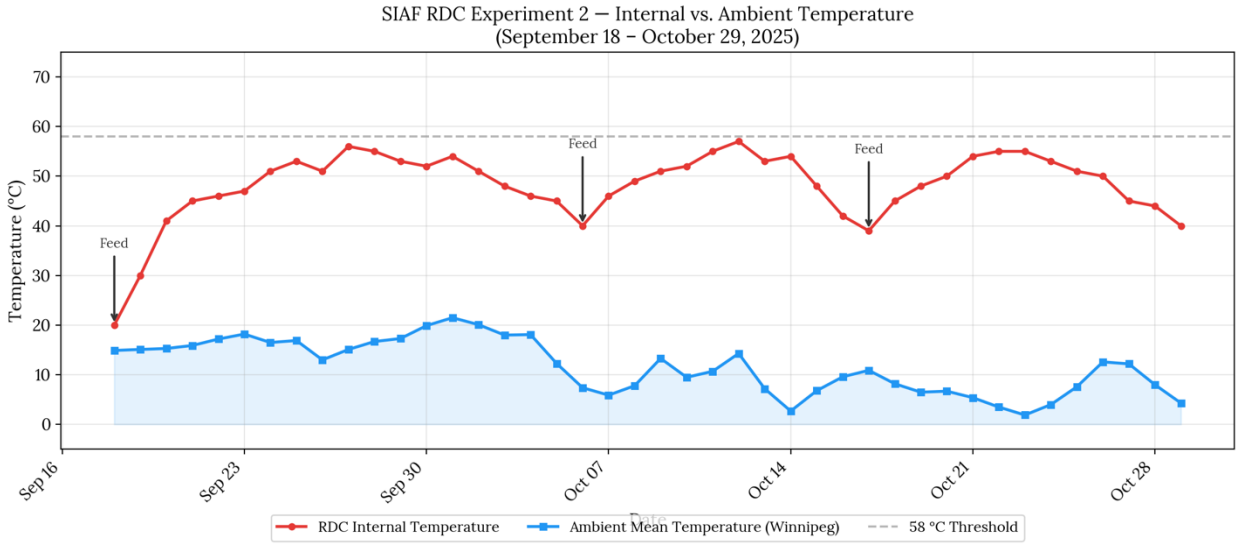

Figure 4.6 Internal temperature profile of the SIAF RDC compared to ambient temperature during Experiment 2.

For the second RDC trial, ambient temperatures were stable or increasing between September 18 and October 4, then declined over the two subsequent feeding cycles (Figure 4.6). Yet the internal RDC temperature remained within the 40 to 60 °C range throughout, regardless of ambient temperature trends. The differential between internal and ambient temperatures grew from 31 °C to 42 °C, over the duration of the experiment. Periodic troughs in internal temperature reflect the natural decline of each heating cycle. Additional feedstock was added at these points (Figure 4.6, arrows), renewing microbial activity and driving the next heating cycle.

4.3.3 SIAF RDC Experiment 3

The objective of Experiment 3 was to characterize thermal heterogeneity within the RDC using per-bag temperature sensors.

4.3.3.1 Temperature Sensor Data

Temperature sensor data was used to quantify the spatial and temporal variability in thermal conditions within the SIAF RDC during Experiment 3. As the sensors were free-moving and redistributed by the rotation of the RDC, the temperature records show variability in sensor exposure rather than showing specific temperatures at fixed points in the RDC.

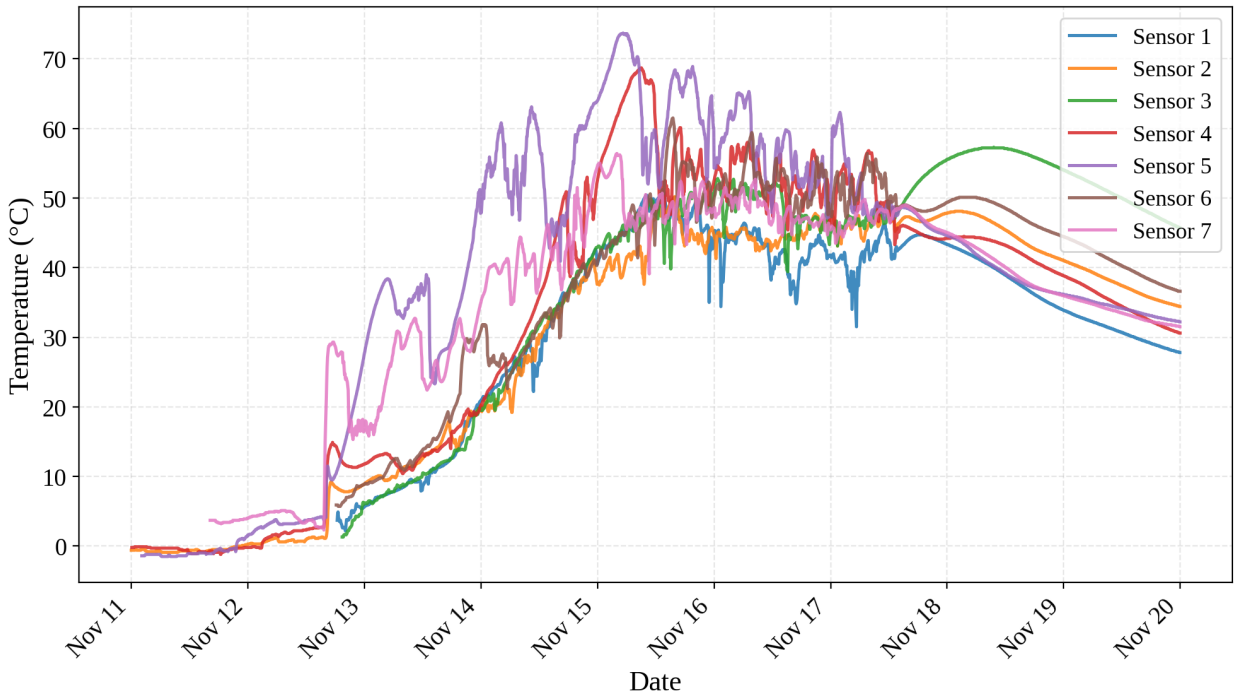

Figure 4.7 Temperature-time profiles for seven sensors in the SIAF RDC during Experiment 3.

Figure 4.7 shows the temperature-time profiles for the sensors, while Table 4.6 summarizes the key thermal metrics for each sensor over the experiment. From the sensor data it is clear to see that

thermal exposure varied substantially by sensor, with some sensors never reaching 55 °C or greater, while others reached max temperatures near 70 °C.

Table 4.6 Summary of thermal exposure metrics by sensor for SIAF RDC Experiment 3.

Sensor ID	**Max temp (°C)**	**Mean temp (°C)**	**Time ≥ 40 °C (hours)**	**Time ≥ 55 °C (hours)**
Sensor 1	50.9	34.13	77.5	0.0
Sensor 2	50.2	28.13	93.2	0.0
Sensor 3	57.3	39.35	98.8	22.5
Sensor 4	68.7	32.13	102.3	25.0
Sensor 5	73.7	38.69	108.9	49.8
Sensor 6	61.5	39.93	98.1	6.7
Sensor 7	56.4	36.23	101.0	1.9

This variability is further reflected in cumulative thermal exposure metrics (Table 4.6). Total time above 40 °C ranged from 77.5 to 108.9 h across sensors, while time above 55 °C varied from 0 to 49.8 h. Sensor 5 accumulated 49.8 h above 55 °C; Sensors 1 and 2 accumulated zero. This contrast in thermal exposure occurred within the same vessel, under continuous rotation, over identical residence times. Mean temperatures also differed by sensor, spanning from 28.1 °C (Sensor 2) to 39.9 °C (Sensor 6). After one week of exposure under these conditions, recovered PLA film samples were opaque and somewhat fragmented but remained mostly intact. No fragmentation or macroscopic material failure was observed at this stage, which was expected due to the short duration of exposure.

Even having been operated with continuous rotation, the sensor data demonstrated that thermal exposure was highly variable for the individual films. This is despite the compost appearing visibly homogenized, mixed thoroughly through the turning of the RDC upon entry. Heat generation is

driven by microbial activity, which is dependent on oxygen availability, moisture content, and nutrient distribution.

This heterogeneity would explain why identical residence times yield different outcomes even with continuous rotation in the RDC. From the past experiments as well as the literature, it is well established that degradation greatly accelerates above PLA's Tg (Karamanlioglu et al., 2017), and so films that experience little or no time ≥ 55 °C would therefore be expected to undergo limited molecular weight reduction. Films that had sustained thermophilic exposure in the RDC could have experienced substantial degradation, explaining why some films had completely disappeared by 2 weeks in some cases, with others persisting almost entirely after 6 weeks. These results reinforce the concept of specific thermal exposure being a more meaningful predictor of PLA degradation than residence time or maximum temperature in degradation cases driven by microbial activity. Residence time is often implicitly assumed to represent time spent at elevated temperature; for industrial, compost-driven processes where there is greater inherent environmental variability, it may not be as useful a metric for degradation unless environmental homogeneity is assured. Seo et al. (2024) observed a temperature gradient of ~28°C between layers within an enclosed pilot-scale vertical composting reactor, even under continuous mechanical stirring. In full-scale RDCs, where ambient conditions are variable and mixing is less controlled, such thermal heterogeneity is plausibly more pronounced.

4.3.3.2 Molecular Weight Data

Viscosity-average molecular weight was measured for the recovered films associated with each sensor to quantify Mv reduction. Recovered sensors 3 through 5 were placed in mesh bags without films (20 total sensors deployed, 15 in bags with films, 5 extra without films) and so lacked Mv data to go along with the temperature data.

Table 4.7 Summary of thermal exposure and viscosity-average molecular weight loss by sensor for SIAF RDC Experiment 3.

Sensor ID	**Mean (°C)**	**Hours ≥40°C**	**Hours ≥55°C**	**Mv (g·mol⁻¹)**	**Mv reduction (%)**
Sensor 1	34.1	77.5	0	144419	29.6
Sensor 2	28.1	93.2	0	154656	24.6
Sensor 6	39.9	98.1	6.7	147176	28.2
Sensor 7	36.2	101	1.9	136326	33.5

Molecular weight reduction varied from 24.6% to 33.5% across sensors. Sensor 2 (coolest conditions) showed the lowest molecular weight loss (24.6%). Sensor 7 showed the highest molecular weight reduction (33.5%) despite moderate mean temperature. Due to the small sample size, these observations are qualitative in nature. Statistical analysis to determine significance was not appropriate given the limited number of data points and absence of replicate measurements.

4.3.3.3 Ambient Temperature Comparison

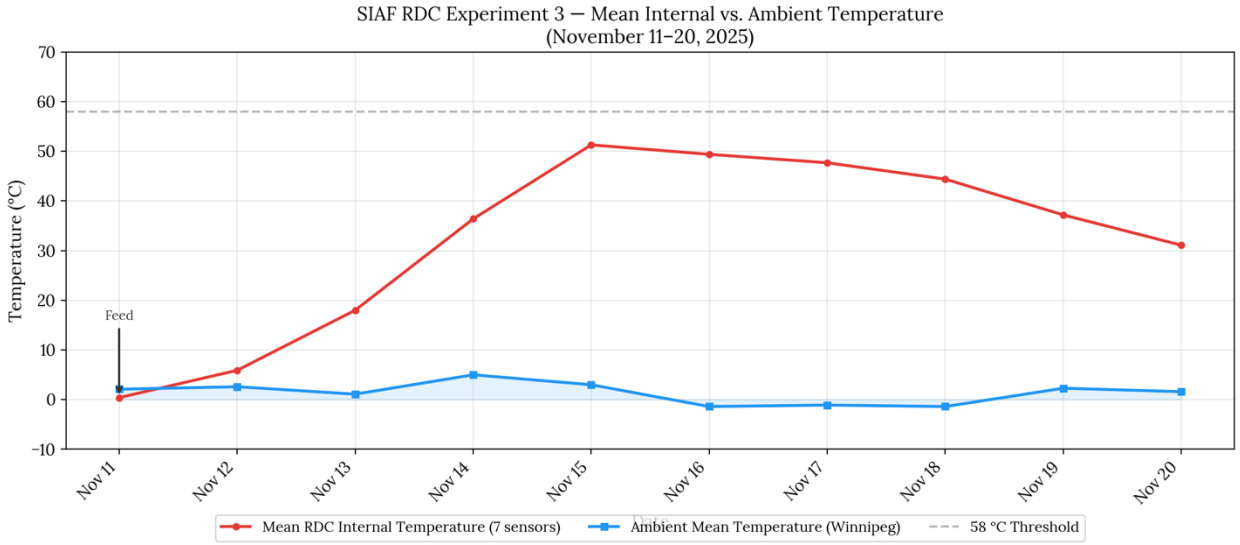

Figure 4.8 Mean internal temperature of the SIAF RDC (seven sensors) compared to ambient temperature during Experiment 3.

In the third RDC trial the temperature sensors took ~4 days to reach peak temperatures (Figure 4.8). Ambient mean temperature was between -1.4 °C and 5 °C for the entire period, meaning the RDC had to generate a 50 °C differential to reach thermophilic conditions. The decline from Nov 18-20 corresponds to the power interruption described in Section 4.2.4, after which the system could not recover.

4.3.4 The Forks RDC Experiments

The objective of these experiments was to evaluate PLA degradation in the Forks RDC, and to compare performance to the SIAF RDC and respirometer trials. The Forks RDC is a different size than the SIAF RDC and has much higher PLA loading; these experiments aimed to characterize these distinct conditions and observe degradation within them, using the mesh bag method.

4.3.4.1 Mass Recovery Data

For the first Forks RDC experiment, no bags were recovered as they were lost in the large mass of compost exiting the RDC, and so were not included in the mass-recovery comparisons. For the second Forks RDC experiment, the lab-prepared PLA films showed substantial fragmentation at three weeks, while Forks PLA remained mostly intact. At 6 weeks, amorphous and crystalline PLA films were powderized and unrecoverable (visible but not separable), whereas Forks PLA still exhibited high mass recovery, often as elongated or partially deformed fragments (Table 4.8).

Table 4.8 Distribution of PLA film recovery outcomes following Forks RDC composting at 3 and 6 weeks.

Time (weeks)	**PLA Type**	**n**	**Intact (%)**	**Fragmented (%)**	**Powderized (%)**	**Gone (%)**
3	Amorphous	5	60	40	0	0
3	Crystalline	3	0	33	67	0
3	Forks PLA	4	75	25	0	0
6	Amorphous	4	0	0	100	0
6	Crystalline	3	0	0	100	0
6	Forks PLA	3	100	0	0	0

Lab-prepared PLA reached highly degraded states more slowly at the Forks RDC than at the SIAF RDC, despite similar reported temperature ranges. Forks PLA consistently showed greater

persistence across timepoints compared to lab-prepared films. The Forks RDC environment was less effective at driving commercial PLA beyond the recoverable-fragment stage within the examined residence times. One potential reason for this is that the Forks RDC rotates intermittently (like SIAF RDC Experiment 1, which had less degradation observed than in continuously-rotating Experiment 2), and so may also contain more thermal heterogeneity. It also may be due to much higher overall PLA loading; a much larger ratio of PLA to compost (compared to SIAF) would provide greater competition for microbial activity. The lower degradation may also be due to the placement of sample bags within a larger mesh bag rather than as individual units. This could have reduced the surface area for thermal and microbial degradation to occur. The addition of compost into the larger bags, along with the smaller ones, was done to mitigate this potential effect, but may not have been effective.

4.3.4.2 Molecular Weight Data

Viscosity-average Mv measurements were used to assess molecular degradation of PLA films recovered from the Forks RDC, with replicate measurements for Forks PLA enabling comparison between exposure times (Table 4.9).

Table 4.9 Viscosity-average molecular weight of PLA recovered from Forks RDC experiment.

PLA Type / Source	**Exposure Time**	**Mv (g·mol⁻¹)**	**Mv reduction (%)**
Forks PLA	3 weeks (replicate 1)	107,215	50.6
Forks PLA	3 weeks (replicate 2)	110,439	49.1
Forks PLA	3 weeks (replicate 3)	111,092	48.8
Forks PLA	6 weeks (replicate 1)	31,614	85.4
Forks PLA	6 weeks (replicate 2)	22,483	89.6
Forks PLA	6 weeks (replicate 3)	32,457	85
Amorphous PLA	3 weeks	94,049	54.1
Crystalline PLA	3 weeks	95,642	53.4

Forks PLA experienced a meaningful reduction in Mv between 3 and 6 weeks, with mean Mv decreasing from approximately 110,000 to 29,000 g·mol^{-1}. At three weeks, the Forks PLA had higher Mv values than the amorphous and crystalline PLA, which was consistent with the trends seen for Forks PLA in both the preceding Mv and mass loss analyses. An unpaired t-test confirmed that Mv reduction between 3 and 6 weeks was statistically significant ($p < 0.0001$) (Appendix D, Table D10).

4.3.4.3 Ambient Temperature Comparison

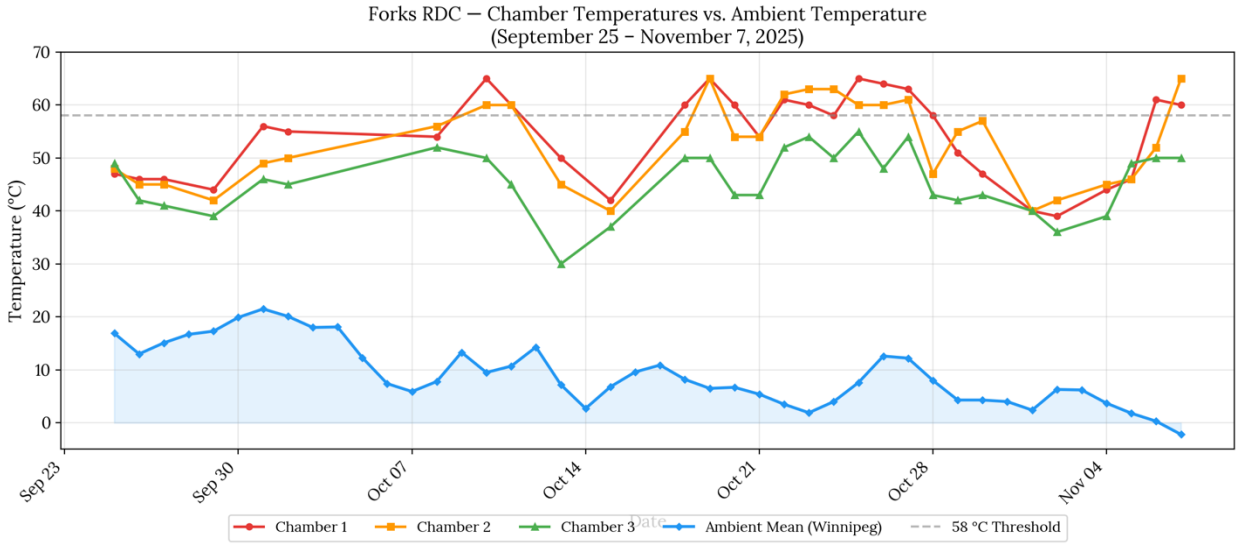

Figure 4.9 Chamber temperature profiles of the Forks RDC compared to ambient temperature.

Mean temperature increased in all chambers over the duration of the experiment, with the overall differential growing from ~35 °C to ~48 °C (Figure 4.9). Chamber 3 reached ≥ 55 °C on only 1 of 30 days and never hit 58 °C, which mirrors the sensor-level heterogeneity from SIAF Experiment 3 but at a vessel-scale spatial level. Chamber 3, the last chamber before the RDC outlet, never reached PLA's Tg (58 °C), while Chambers 1 and 2 spend 11 and 12 days respectively above it. Internal temperature troughs correspond to feeding events, consistent with the pattern observed in the SIAF experiments, though exact feed times were not recorded as the Forks RDC was operated by facility staff.

4.3.5 Thermal and Crystalline Changes in PLA Recovered from RDC Composting

Differential scanning calorimetry (DSC) was used to assess changes in PLA crystallinity and thermal behavior following exposure in RDC composting systems. Crystallinity (Xc) was calculated from the measured melting enthalpy assuming a heat of fusion for 100% crystalline PLA of 93 J g^{-1}. DSC outputs and thermograms can be found in Appendix B.

Table 4.10 Differential scanning calorimetry (DSC) results for PLA samples recovered from RDC composting experiments.

Sample	**Description**	**Tg, 1st heating (°C)**	**Tg, 2nd heating (°C)**	**Tm (°C)**	**Tcc (°C)**	**Crystallinity, Xc (%)**
Forks Untreated	Initial Forks PLA	64.9	58.4	149.72	—	40.41
FBE2 3w	Forks RDC, 3 weeks	69.6	55.9	150.61	—	20.47
FBE2 6w	Forks RDC, 6 weeks	67.6	49.7	153.44	—	49.76
SBE1 4w A	SIAF RDC, amorphous	67.1	49.5	171.56	—	42.05
SBE1 4w C	SIAF RDC, crystalline	62.7	54.4	171.79	—	67.00
SBE1 4w F	SIAF RDC, Forks PLA	63.8	51.5	153.18	—	38.00

For the Forks sample, the 3-week sample had a 50% reduction in crystallinity, while the 6-week sample had increased crystallinity compared to the untreated sample. It is important to note that these are different samples, and so it cannot be assumed that these results would be consistently observed for any given sample, or that this is a consistent time-dependent trend. Instead, this behavior is consistent with variability in cumulative thermal exposure within the RDC. Samples

experiencing limited thermophilic exposure may undergo partial chain scission without sufficient chain mobility or time for secondary crystallization, resulting in reduced crystallinity. In contrast, samples exposed to higher cumulative thermal exposures may progress further into hydrolysis-driven degradation, allowing shortened polymer chains to reorganize into crystalline domains and increasing measured crystallinity.

The amorphous sample saw greatly increased crystallinity, from essentially 0% to 42%, which is consistent with preferential degradation of amorphous regions through hydrolysis under thermophilic composting conditions, which increases the relative fraction of the polymer remaining in a crystalline state. This was also observed for the crystalline sample, which saw crystallinity increase from 47% to 67%.

Tg values from the DSC thermograms are presented in Table 4.10. First heating Tg values for composted samples (63-70°C) remained similar to or slightly higher than the untreated Forks PLA (65°C), consistent with physical aging and annealing during thermophilic exposure. In contrast, second heating Tg values for composted samples (49-55°C) were lower than untreated PLA (58-59°C), consistent with the molecular weight reduction observed in these samples (Section 4.3.4.2). A lowered intrinsic Tg suggests partially degraded PLA recovered from composting may be more susceptible to continued degradation at lower temperatures than the original untreated material.

Overall, the DSC results align with the observed molecular weight reduction and following physical disappearance of PLA in RDC systems, and that secondary crystallization occurs only when sufficient cumulative thermophilic exposure is achieved. The observed variability in

crystallinity across recovered samples is indicative of their heterogeneous thermal exposures and provides insight into their varying degradation outcomes.

4.4 Discussion

4.4.1 Mesh Bag Recovery Method

The mesh-bag recovery method was effective for recovering samples, and quantifying degradation of the polymer. However, mass-recovery outcomes quantify disintegration and loss of recoverable material, not direct mineralization, and the effectiveness of the mesh-bag method is dependent on the volume of material that moves through the RDC; the more compost there is compared to the number of bags, the harder the bags are to find leaving the RDC. This occasionally resulted in bags not being recovered at later timepoints when the ratio of bags to compost volume was at its lowest. This resulted in reduced replicate numbers at later timepoints which could limit statistical inference.

4.4.2 PLA Degradation

There were several consistent patterns across the SIAF experiments, the primary one being that significant physical degradation of PLA is achievable in RDC systems within weeks, though complete mineralization was not confirmed in these experiments. Outcomes are bimodal, with most films fully degraded and occasional samples remaining largely intact. This bimodal pattern is consistent with the Tg threshold observation often reported in PLA degradation literature (Karamanlioglu et al., 2017); once hydrolysis proceeds past a critical point brought on by high temperature (heavy fragmentation, loss of molecular weight), greater degradation and

mineralization can proceed. Films that never reached sufficient thermal exposure would never have crossed that threshold.

Continuous rotation improved mixing and reduced the number of intact samples at the end of 6 weeks, but still did not guarantee uniform exposure. Experiment 3 demonstrated that equal residence time can correspond to widely different thermal exposures, which can explain variability in degradation outcomes more effectively than residence time or peak temperature alone. Crystalline PLA consistently showed earlier fragmentation and loss of recoverable mass in the RDC, hypothesized to be from the steel paddles breaking the brittle films into fragments, increasing surface area and accelerating overall disappearance. In the respirometer experiments, where manual mixing exerted less mechanical force, amorphous PLA mineralized faster ($k = 0.141$ vs. 0.119 day^{-1}), suggesting hydrolysis susceptibility was the dominant factor rather than mechanical fragmentation.

Molecular weight analysis revealed that reduction in Mv consistently preceded physical disappearance of the polymer. Even when the films appeared visually intact, they showed Mv reduction greater than 50%, confirming Mv as an early indicator of PLA degradation. Material-dependent differences in Mv reduction were evident at early timepoints, but diminished the longer the exposure period.

The experiments showed that repeated exposure to thermophilic temperature windows (even when the average temperature remains below typical PLA Tg values) was sufficient to induce significant or full degradation. This contrasts with the respirometer experiments, where exposure occurred at either 58 °C (resulting in complete mineralization) or 30 °C (fragmentation without

mineralization) for the entire duration of the experiments. For example, a film sample in the 58 °C respirometer experienced 168 hours per week above 55 °C, whereas in the RDC the maximum duration recorded in Experiment 3 for any sensor above 55 °C was approximately 50 hours - less than one-third of the respirometer exposure. This highlights that achieving complete degradation of PLA may not require sustained temperatures above 55 °C but can occur through intermittent thermophilic exposure while the system operates at a lower average temperature. No prior study has examined the effect of intermittent or repeated thermophilic exposure on PLA degradation in compost; existing studies have evaluated PLA degradation under either sustained thermophilic conditions, or in compost where activity is initially thermophilic and progresses to mesophilic with a reduction in compost activity (Table 4.1).

4.4.3 RDC Scale

The SIAF RDC demonstrated a greater capacity to reduce PLA films beyond the recoverable stage within 4 to 6 weeks. The Forks RDC, despite its larger size, showed reduced effectiveness for commercial PLA degradation, potentially due to intermittent rotation, higher plastic loading, different matrix structure, compost microbial community, and thermal distributions. That said, smaller RDC systems are more sensitive to ambient temperature, feed interruptions, and heat loss, with operation during cold winters not feasible for those reasons. The larger RDC can maintain temperatures between 40 °C and 60 °C during the winter, due to the larger mass of material that can be fed into them.

4.5 Conclusions

RDC composting systems are capable of degrading PLA materials under industrially relevant conditions when thermophilic conditions are sustained. This is possible through continuous feed and adequate moisture and aeration; performance degrades under inconsistent loading and operational interruptions that result in lowered temperatures due to colder ambient temperatures. Rotation improves degradation consistency but does not completely eliminate the variability in sample thermal exposure. Cumulative thermal exposure, not residence time, predicts PLA degradation in heterogeneous composting environments like the RDC. The non-uniform thermal, aerobic, and moisture microenvironments are not exclusive to the RDC; they have also been reported for windrow, pile, and in-vessel composting systems (Seo et al., 2024; Gastaldi et al., 2024; Yang et al., 2023; Warmadewanthi et al., 2022).

These findings demonstrate the need to evaluate compostable plastics within real operational systems, where heterogeneous thermal exposure, distributed residence times, mechanical forces, and material loading constraints, which were all observed in the RDC experiments, differ from laboratory reactors.

4.6 Recommendations for Experimental Refinement

4.6.1 Recovery Method Validation

One of the key limitations of the RDC experiments was that the mesh bag retrieval method allows for PLA fragments smaller than 180 μm to pass through. One potential method to test this would be to run a substantially higher PLA loading test in the RDC, with all the plastic in mesh bags, and then perform microplastics analysis of the outgoing compost. Mass-based polymer

quantification of the finished compost could be performed using thermal extraction desorption-gas chromatography/mass spectrometry (TED-GC/MS), which has been validated for compost matrices and can identify and quantify PLA (Wiesner et al., 2023). Then, when the PLA is "gone" as was described as an outcome category, it could be determined whether "gone" means mineralized or just fragmented below detection. This would be helpful as the compost that leaves the RDC goes back into use – but not before sitting in curing piles. Analysis of the compost leaving the Forks RDC, and then of the curing piles, would inform operators of whether compost leaving the RDC has a high microplastic load, and whether the curing piles result in reduction of that load.

Additional mesh bag controls would also help address the 180 μm mesh limitation. A material that is known to not degrade, but has similar brittleness and thermal properties to PLA, could be placed into mesh bags and then into the RDC. This would directly quantify losses due to mechanical fragmentation versus actual biodegradation.

4.6.2 Environmental Monitoring

One of the largest pieces of evidence for the RDC heterogeneous environment was the data gained from the per-bag temperature sensors in Experiment 3. Unfortunately, this data was short in duration, only gathered for one of the planned six weeks of observation. Re-running full-length RDC PLA degradation experiments with temperature sensors in each bag would allow for statements of correlation as to why some bags did not degrade and others appeared to degrade completely. Including per-bag humidity and oxygen concentration in these experiments would

provide a clearer picture of co-varying factors in RDC micro-environments. Continuous oxygen monitoring would also allow for confirmation of anaerobic pocket formation.

4.6.3 Forks PLA Characterization

In the Forks RDC, the Forks PLA showed greater persistence than lab-prepared PLA, but reasons for this could not be determined as the characterization of the PLA was limited. More information on its processing history, molecular weight distribution, and grade would strengthen its comparison to the Ingeo polymers.

Chapter 5: Molecular Weight Reduction of PLA Following UV-C Treatment

5.1 Introduction

If PLA degradation in composting systems is limited by the rate of hydrolysis, a pretreatment step that reduces molecular weight prior to composting could accelerate the process. UV-C irradiation has been shown to induce chain scission in PLA, which makes it a potential PLA degradation pretreatment approach. Studies of photo-oxidation of PLA mediated by UV-irradiation vary widely in their experimental conditions and outcomes. The PLA materials also differed, varying from thin films, thick-walled cups, microplastics, blends, and flame-retarded formulations, each with different optical penetration depths and degradation kinetics. Environmental conditions varied across the studies. Some studies were conducted in air (both dry and humid), while others were conducted in water and compost of different temperatures, all of which can strongly influence hydrolytic and oxidative pathways. While this diversity of experimental approaches is expected, it makes direct comparisons between studies difficult; nevertheless, consistent patterns in PLA photo-oxidative behavior can still be identified (Jeon and Kim, 2013; Janorkar et al., 2007; Copinet et al., 2004; Lesaffre et al., 2017).

UV-irradiation consistently lowered PLA molecular weight, increased brittleness, and produced surface oxidation regardless of wavelength or polymer morphology. Additionally, higher temperature and humidity accelerated degradation through UV-assisted hydrolysis. The wavelength of UV light the polymer was exposed to dictated the speed and manner of degradation: UV-C irradiation produced chain scission and fragmentation in hours to days, whereas lower-

intensity UV-A/UV-B exposures required weeks to months to produce similar results (Jeon and Kim, 2013; Wang et al., 2024; Copinet et al., 2004).

Sample thickness is a critical factor governing UV-induced degradation of PLA. UV penetration depth in PLA is limited by strong absorption of the radiation by ester functional groups. The thinner the film is, the more uniform the chain scission will be throughout the material. This effect is evident when comparing studies using thin films versus thicker films or bulk materials. Janorkar et al. (2007) reported a reduction in number-average molecular weight from 110,000 $g \cdot mol^{-1}$ to ~ 4000 $g \cdot mol^{-1}$ after 12 h under 254 nm UV exposure for 125 μm films, while and Kim (2013) observed significant embrittlement and molecular weight reduction (188,000 $g \cdot mol^{-1}$ to 41,000 $g \cdot mol^{-1}$ after 24 h) in 300 μm PLA films exposed to 245nm light. Thin commercial packaging films showed significant molecular weight loss and discoloration within minutes to hours under UV-C irradiation (Zhang et al., 2013). These results suggest that thicker samples may retain an undegraded core even as surface degradation occurs, leading to mechanical failure without proportional bulk mineralization.

Prior literature demonstrates that UV exposure results in molecular weight loss, brittleness, and thermal transitions, but inconsistent reporting of irradiance, polymer morphology, and exposure time prevents meaningful cross-study interpretation (Jeon and Kim, 2013; Janorkar et al., 2007; Copinet et al., 2004). A UV-C exposure chamber was designed and constructed to provide a controlled, reproducible platform for characterization of UV–PLA interactions. By fixing the wavelength and using spatial intensity variation within the chamber as a proxy for different irradiance levels, this study evaluates PLA films under defined conditions, establishing a

methodological baseline for future pretreatment studies and providing the lab with a functional tool for ongoing UV research. 254 nm was selected as it is the peak emission wavelength of standard low-pressure mercury germicidal lamps, which are relatively inexpensive, commercially available, and scalable; the envisioned application is a pretreatment step in which PLA waste would be exposed to UV-C irradiation prior to entering the RDC, reducing molecular weight and increasing brittleness to accelerate biodegradation in the composting environment.

5.2 Experimental Design and Methods

A custom chamber housing an 18 W UV-C lamp was built to test the effect of UV pretreatment on PLA films (Figure 5.1). The chamber was built using a sealed NEMA 4x steel electrical enclosure, with a 120 mm DC cooling fan installed to maintain stable internal temperatures and ensure any effects on the polymer were due to irradiation and not heat. The internal temperature was monitored using a digital probe thermometer inserted through an access port on top of the chamber and was consistently at ambient room temperature (22 °C) throughout operation. Humidity was not measured or controlled but was assumed to remain at ambient laboratory conditions throughout. As the chamber was sealed and maintained at room temperature, conditions were dry relative to the elevated temperature and humidity used in some published UV-PLA studies (e.g., Copinet et al., 2004; Lesaffre et al., 2017). UV-C output was verified using an AquaHorti AH-UVCBA UV light meter, which provides UV irradiance measurements for UV-A, UV-B, and UV-C light sources in units of $\mu W/cm^2$. This instrument was used to measure UV-C irradiance at film height at different positions within the chamber.

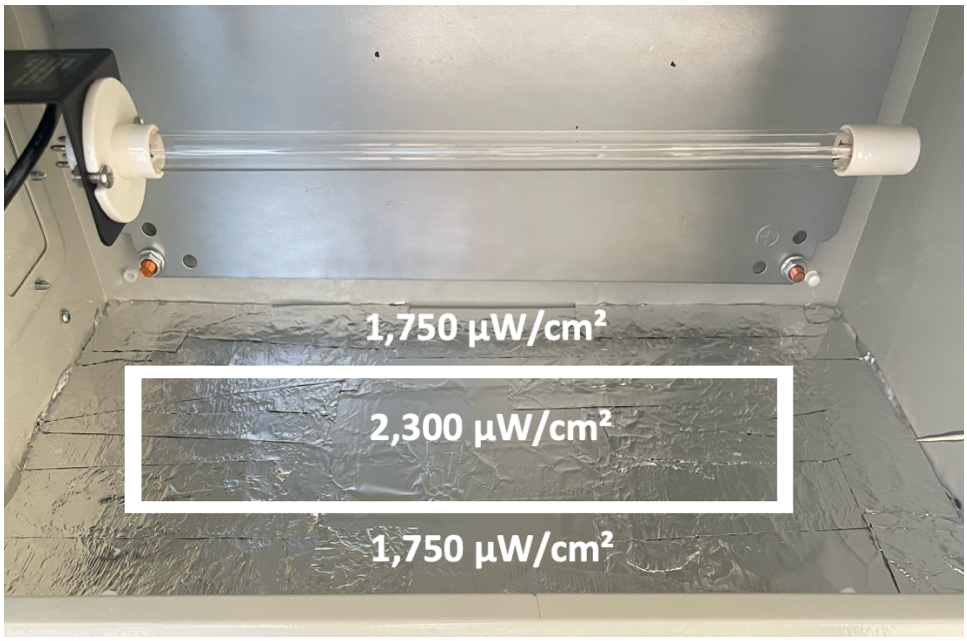

Figure 5.1 Inside of UV Chamber.

Irradiance varied spatially within the chamber, and so samples were assigned to two irradiance groups based on their column position relative to the lamp. (Table 5.1):

Table 5.1 Mean irradiance relative to the UV-lamp position in the chamber.

Irradiance Level	Position in Chamber	Mean Irradiance (µW cm^{-2})
Lower (L)	Left or right column	1750
Higher (H)	Center column (directly under lamp)	2300

The PLA types tested were the amorphous, crystalline, and Forks films, the irradiances tested were 1750 and 2300 µW cm^{-2}, and the exposure durations were 1, 2, 8, and 24 hours. Samples were irradiated on a single side only. At longer exposure times, films fragmented into many small pieces during handling, making flipping infeasible. The implications of this brittleness for pretreatment applications are discussed below.

5.3 Results

5.3.1 Mass loss

No measurable mass loss was observed for any PLA type at any exposure time under either irradiance condition (1–24 h), as measured after very gentle rinsing with distilled water, patting dry with Kim wipes, and drying overnight at room temperature. The UV treatment caused molecular-level changes without detectable bulk material loss.

5.3.2 Molecular-weight (Mv) response to UV-C exposure

UV-C exposure produced large, rapid reductions in Mv for all PLA types under both irradiance conditions (Figure 5.2; Tables 5.2 and 5.3). By 1 h, Mv reductions were already ~69 to 73% across all materials. By 8 h, all materials were less than 20,000 $g \cdot mol^{-1}$, and by 24 h, all materials were around 9000 to 13,000 $g \cdot mol^{-1}$ ($\geq$ 93% reduction). Individual replicate Mv values for UV-C conditions can be found in Appendix B (Table B4).

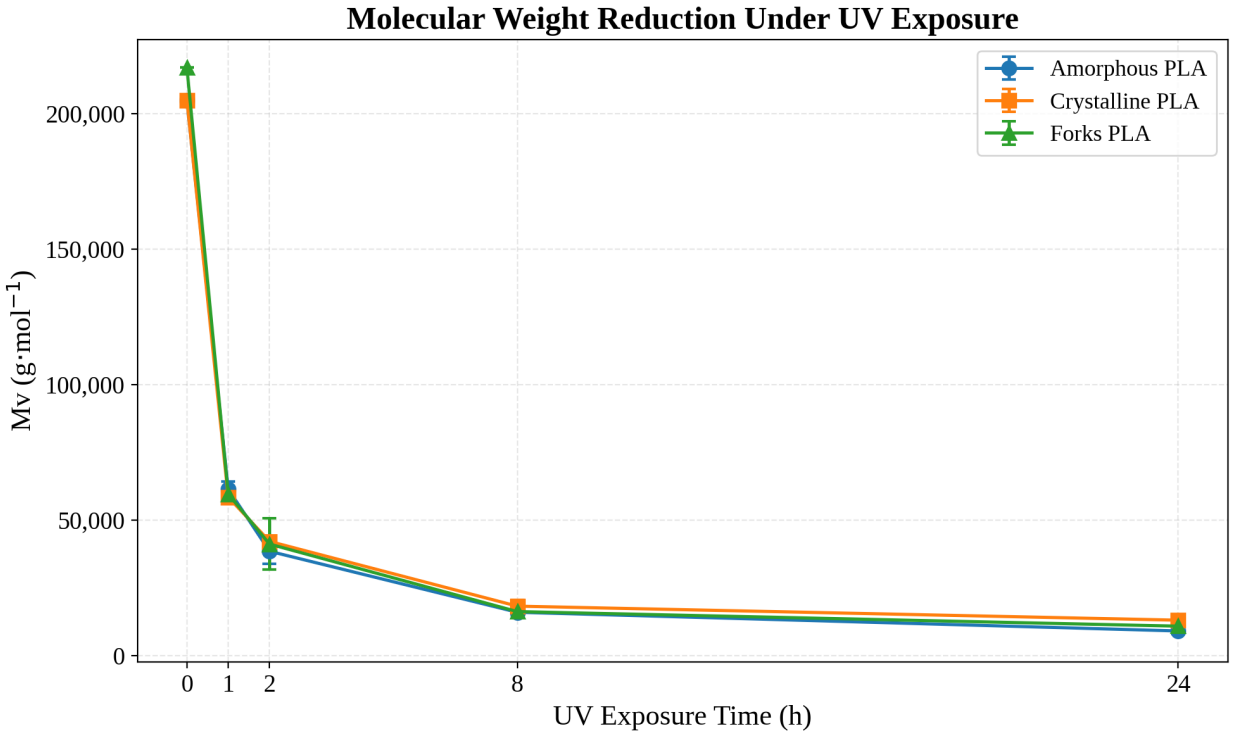

Figure 5.2 Kinetics of viscosity-average molecular weight (Mv) reduction of amorphous, crystalline, and field-recovered (Forks) PLA films during high-irradiance UV exposure.

Most of the changes in polymer Mv were evident within the first hour of UV irradiation, after which, the reduction in Mv slowed as the polymers reached extremely low Mv (Figure 5.2). Interestingly, there was little difference between Mv reduction at the different irradiance levels. At every time point, the difference was not significant. The tested irradiance contrast was small (2300 vs 1750 $\mu W \cdot cm^{-2}$; ~1.3×), which makes it difficult to resolve dose-rate effects. However, within this range, it does suggest the speed of reduction does not necessarily increase with increasing irradiance. Similarly, there was little difference in Mv reduction between amorphous, crystalline, and Forks PLA films.

Table 5.2 Molecular weight reduction of PLA films under 2300 μW cm^{-2} UV exposure. Replicate N = 3 for all conditions.

Time (h)	Sample type	Mv (g·mol^{-1}, mean ± SD)	Mv reduction (%)
0	Amorphous PLA	205,011 ± 177	NA*
0	Crystalline PLA	205,100 ± 202	NA*
0	Forks PLA	217,128 ± 232	NA*
1	Amorphous PLA	61,484 ± 2,842	70
1	Crystalline PLA	58,541 ± 2,428	71.4
1	Forks PLA	59,643 ± 612	72.5
2	Amorphous PLA	38,533 ± 4,679	81.2
2	Crystalline PLA	42,180 ± 510	79.4
2	Forks PLA	41,180 ± 9,428	81
8	Amorphous PLA	16,023 ± 822	92.2
8	Crystalline PLA	18,278 ± 2,370	91.1
8	Forks PLA	16,270 ± 1,958	92.5
24	Amorphous PLA	9,120 ± 983	95.6
24	Crystalline PLA	13,105 ± 1,117	93.6
24	Forks PLA	10,894 ± 2,581	95

***t0 samples (first three sample rows) are the source of comparison for the later timepoints Mv reduction %.**

Table 5.3 Molecular weight reduction of PLA films under 1750 µW cm^{-2} UV exposure. Replicate N = 3 for all conditions.

Time (h)	Sample type	Mv (g·mol^{-1}, mean ± SD)	Mv reduction (%)
0	Amorphous PLA	205,011 ± 177	NA
0	Crystalline PLA	205,100 ± 202	NA
0	Forks PLA	217,128 ± 232	NA
1	Amorphous PLA	59,899 ± 1,379	70.8
1	Crystalline PLA	62,662 ± 3,934	69.4
1	Forks PLA	63,172 ± 2,207	70.9
2	Amorphous PLA	39,053 ± 1,641	80.9
2	Crystalline PLA	45,701 ± 1,897	77.7
2	Forks PLA	56,996 ± 7,980	73.7
8	Amorphous PLA	14,188 ± 1,338	93.1
8	Crystalline PLA	16,196 ± 3,327	92.1
8	Forks PLA	20,148 ± 1,327	90.7
24	Amorphous PLA	10,608 ± 663	94.8
24	Crystalline PLA	13,448 ± 1,675	93.4
24	Forks PLA	13,177 ± 980	93.9

Two-way ANOVA (material x irradiance) was performed on Mv at each exposure timepoint. Irradiance had no significant effect at any timepoint after Bonferroni correction. Material type was significant only at 24 hours ($p = 0.006$), with crystalline PLA retaining higher Mv than amorphous PLA (Tukey $p = 0.005$). Overall, irradiance had no consistent effect on Mv reduction, while material type differences emerged only at the 24-hour timepoint. Full ANOVA tables are provided in Appendix D (Tables D11-D15).

5.3.3 Thermal and Crystalline Changes in PLA Following UV-C Exposure (DSC Analysis)

Differential scanning calorimetry (DSC) was used to assess changes in PLA crystallinity and thermal behavior following UV-C exposure (Table 5.4). Crystallinity (Xc) was calculated from the measured melting enthalpy assuming a heat of fusion for 100% crystalline PLA of 93 J g^{-1}. DSC outputs and thermograms can be found in Appendix B.

UV-C exposure induced polymer changes are distinct from those seen from aerobic thermophilic degradation. UV-C irradiation reduced Mv of PLA polymers and generally induced an increase in the percentage of crystallinity; the exception was crystalline PLA, where crystallinity peaked at 8 h (63%) before decreasing at 24 h (49.6%). One possible reason for this is that while UV exposure initially promotes secondary crystallization following chain scission, prolonged exposure progressively disrupts crystalline order due to photochemical damage.

For all samples, melting temperatures decreased substantially at longer exposure durations (Table 5.4). This indicates increasing structural disorder and is consistent with photochemical damage and not just pure hydrolytic degradation. At UV-C wavelengths, PLA photodegradation is expected to proceed primarily via a Norrish II mechanism, involving chain scission with C=C bond formation (Tertyshnaya & Podzorova 2020), though photolysis of the C–O backbone bond and photooxidation via hydroperoxide intermediates have also been proposed as alternative pathways (Janorkar et al., 2007). Both composting and UV-C exposure decreased melting temperature relative to the original polymer. The UV-treated films showed stronger evidence of disrupted crystalline order. The appearance of cold crystallization peaks in the amorphous UV-treated samples also suggests disruption of the original crystalline structure and formation of

mobile amorphous fractions. For the amorphous PLA sample after 8 h of UV exposure, the calculated DSC crystallinity was −2.74% and is therefore reported as ~0%, as the cold crystallization enthalpy exceeding the melting enthalpy means the sample was essentially amorphous with some experimental noise. The appearance of cold crystallization peaks were observed in some but not all UV-treated samples; the limited number of DSC measurements precludes determination of whether cold crystallization peaks were a systematic pattern or sample-level variability. Tg values from the DSC thermograms are presented in Table 5.4. Both first and second heating Tg decreased progressively with UV-C exposure duration across all PLA types. For crystalline PLA, second heating Tg decreased from 59°C (untreated) to 44°C (24 hr); for Forks PLA, from 58°C to 44°C; and for amorphous PLA, from 49°C (8 hr) to 39°C (24 hr).

Table 5.4 Differential scanning calorimetry (DSC) results for PLA films following UV-C exposure at varying durations.

Sample ID	**Tg, 1st heating (°C)**	**Tg, 2nd heating (°C)**	**PLA Type**	**UV Exposure Time (h)**	**Tm (°C)**	**Tcc (°C)**	**Crystallinity, Xc (%)**
APLA 8 h	51.5	48.8	Amorphous PLA	8	157.47	100.13	~0
APLA 24 h	45.7	39.3	Amorphous PLA	24	139.79	100.79	8.53
CPLA 1 h	55.6	56.6	Crystalline PLA	1	173.12	—	49.27
CPLA 2 h	54.8	55.8	Crystalline PLA	2	171.79	—	51.02
CPLA 8 h	47.9	49.9	Crystalline PLA	8	161.70	—	63.03
CPLA 24 h	43.4	43.8	Crystalline PLA	24	153.43	—	49.58
FPLA 8 h	50.5	51.6	Forks PLA	8	146.38	—	50.49
FPLA 24 h	45.8	44.1	Forks PLA	24	139.65	—	51.25

Note: All DSC measurements represent single replicates (n = 1).

5.4 Discussion

5.4.1 Comparison to prior UV degradation studies

Table 5.5 summarizes the experimental conditions and key outcomes of published UV degradation studies on PLA, alongside the present results, to facilitate direct comparison across wavelength, irradiance, film thickness, and molecular weight reduction.

Table 5.5 Summary of published studies investigating UV-induced degradation of polylactic acid (PLA) under varying wavelengths, irradiance levels, and material forms.

Study	**UV Wavelength(s)**	**Irradiance (µW/cm²)**	**PLA Form**	**Key Results**
Present study	254 nm	1750–2300	220-300 µm films	Mv 205,000/217,000 → 9,000–13,000 after 24 h.
Jeon and Kim (2013)	245 nm	245 nm lamp: 3,220	PLA Polymer 2003D, 300 µm thick	Mw 188,000→41,000 after 24 h.
Janorkar et al. (2007)	232–500 nm (photografting), 254 nm (sterilization lamp)	Photografting lamp: 25,000 @ 365 nm Sterilization lamp: Not reported (30W power, 60cm from film)	PLA 125 µm thick	Photografting lamp: Mn 110,000→4000 in 12 h. Sterilization lamp: Mn 110,000→40,000 in 12 h.
Wang et al. (2024)	254 nm	400	PLA-3033D powder	PLA microplastics fragmented heavily (45–70% <100 µm after 7 days).
Zhang et al. (2013)	254 nm	28,000–32,000 measured at 3–5 mm from the lamp	NatureWorks PLA bag	Mw 113,500→~10,000 after 60–90 min. Mass loss 4–9%. Severe brittleness & discoloration.
Copinet et al. (2004)	315 nm	Not reported	PLA film 180-200 µm thick	Up to 96% Mw drop at 60 °C & 100% RH in 15 weeks.
Lesaffre et al. (2017)	351 nm (UVA-351)	76 (0.76 W/m²)	NatureWorks LLC PLA, 3000 µm plates w/ additives	Mn decreased 54–91% over 90-125 days.

Results from this study were comparable to Zhang et al. (2013) who reported a reduction in Mw from 113,500 to 10,000 g·mol^{-1} (90% reduction) in 1.5 hours, while the present study observed an Mv drop from 205,000 g·mol^{-1} to 40,000 g·mol^{-1} (80% reduction) in 2 hours. A difference is that Zhang et al. (2013) also observed mass loss, which was not seen in the present study. Their faster Mw reduction and mass loss may be attributed to the use of thinner films (~60 µm compared to 220 µm) or a higher irradiance level (irradiance level not stated in the study).

The present study can also be compared to Jeon and Kim (2013), which was one of the only studies that also reported irradiance level. Using a 245 nm lamp with an irradiance of 3220 µW/cm², and 300 µm PLA films, Jeon and Kim (2013) reported a 78.2% Mw reduction from 188,000 g·mol^{-1} to 41,000 g·mol^{-1} after 24 hours. Despite using a slightly lower wavelength and higher irradiance, they reported less of a drop after 24 hours than the present study. This may be attributed to the thickness of the films, which plays a substantial role in UV degradation capacity, though it could also be other factors such as PLA grade or exposure geometry.

Janorkar et al. (2007) used two different lamps, which each provided very different results. Using a photografting lamp, which produced variable wavelengths between 232-500 nm (with an average of 365 nm), and a very high irradiance of 25,000 µW/cm², Janorkar et al. (2007) reported a 96% reduction in Mw, from 110,000 g·mol^{-1} to 4000 g·mol^{-1} in 12 hours. Using a 254 nm sterilization lamp, they observed a 63% reduction in Mw, from 110,000 g·mol^{-1} to 40,000 g·mol^{-1}, though the irradiance was not reported. The Mw decreased further to 20,000 g·mol^{-1} after 36 h exposure, confirming that even when the overall degree of reduction is not as severe, most of the reduction happens within the first hours of exposure. Compared to the present study, their results

highlight that irradiance may be as important as the wavelength of the light. Along with the present results, these studies highlight the importance of wavelength, irradiance, and also film thickness in predicting the extent of bulk molecular-weight reduction.

5.4.2 Context within composting-based degradation

When compared to the other Mv values observed for films tested in other chapters, UV-irradiation induced reductions in molecular weight occurred on timescales orders of magnitude shorter than any composting condition tested. Mesophilic composting produced only ~9 to 25 % Mv reduction over the tested timeframe of 81 days, and thermophilic composting required weeks to reach comparable Mv values to the UV-irradiated samples. Despite this molecular weight reduction, no mass loss was observed during UV exposure, indicating that UV pretreatment on the timescale tested alters polymer structure without causing direct disintegration. Morphology also had no apparent role in Mv reduction under UV exposure, which differed from composting conditions, where initial polymer morphology played a larger role in film persistence. The reduction of Tg observed has practical implications: if UV-pretreated PLA has a lower effective glass transition temperature, hydrolysis and subsequent biodegradation may proceed at composting temperatures below the Tg of untreated PLA (55-60°C). This would expand the range of composting conditions under which UV-pretreated PLA could degrade, which is relevant for systems that do not consistently reach thermophilic temperatures. Under composting conditions, PLA is exposed to elevated temperature and humidity, which impact the rate of degradation; in the present experiment, both temperature and humidity were not controlled and remained at ambient

room conditions. Increased temperature and humidity would be expected to have substantial additive effects on UV-driven PLA degradation, as observed by Copinet et al. (2004) (Table 5.5).

5.5 Conclusions

This work established a functional UV-C exposure chamber with defined and reproducible irradiance conditions, providing the laboratory with a reusable platform for future UV pretreatment studies across a range of conditions. UV-C pre-treatment caused rapid and extensive alterations in the molecular structure of PLA films, reducing viscosity-average molecular weight by more than 70% within 1 hour and more than 90% within 8 hours, and reaching ~9000 to 13,000 $g \cdot mol^{-1}$ after 24 h. This occurred and was consistent for all film types. Within the irradiance range test, differences in UV intensity had no impact on Mv reduction. These results demonstrate that UV-C pretreatment may serve as a very effective means of reducing PLA molecular weight without inducing mass loss, with molecular weight end-points comparable to those achieved by weeks-long durations of optimized thermophilic composting. The increased brittleness of the samples is also an effective outcome for PLA pretreatment, as increased brittleness was associated with faster loss of recoverable mass in the RDC trials. In comparison with prior studies (Table 5.5), the results highlight that film thickness, exposure geometry, and reported irradiance are critical variables that must be consistently defined in future UV–PLA studies to enable meaningful comparison of degradation kinetics and endpoints. This study evaluated the effect of a single-defined UV wavelength with stated irradiance on PLA materials identical to those used in the composting chapters. This allowed direct comparison of UV-induced molecular weight reduction to

composting-induced degradation on the same materials. This side-by-side characterization has not been reported previously.

5.6 Recommendations for Experimental Refinement

5.6.1 Validation of UV Pretreatment Effects

The specific degradation mechanism of the UV degradation of PLA observed in Chapter 5 was not investigated. FTIR spectroscopy would help to confirm the literature-suggested mechanisms, such as Norrish II chain scission with associated C=C bond formation, carbonyl group changes, and photo-oxidation products from hydroperoxide intermediates. UV-treated films should be placed in water to determine whether UV-induced structural changes lead to direct physical disintegration in the absence of microbial activity.

The UV-C exposure reduced Mv to levels comparable to the heavily degraded compost samples (~9,000-13,000 g/mol), but it was not actually tested in compost. The products generated from UV degradation may be different from those produced during compost-condition-driven hydrolysis. Until it is tested, Mv reduction via UV-C exposure cannot be assumed to be a working pretreatment method for increasing PLA degradation in RDC systems.

5.6.2 Refinement of Exposure Parameters

During the UV-C experiments, the 70% drop in MV occurred during the first hour. Sampling every 15 minutes during this first hour would better characterize the degradation kinetics. The cost of a pretreatment method is important to its feasibility, so it is critical to be able to understand the optimal trade-off between treatment cost and desired outcome. For example, if 15 minutes of UV

exposure results in 90% of the Mv reduction that an hour of UV exposure provides, the 15-minute option might be more desirable if it costs significantly less.

Along with temperature and UV wavelength, humidity is an important factor in PLA degradation due to UV exposure (Copinet et al., 2004). For this study, humidity was assumed to be ambient but was not measured. Measuring humidity and potentially controlling it as a variable would improve the study. Similarly, measuring a larger irradiance difference of the UV source would be informative. In this study irradiance was not deliberately varied, as it was primarily tested to see if placing PLA at different positions within the constructed chamber would result in different degradation outcomes. Given that there was no difference in outcome between the two tested irradiances, a larger difference between them is required to establish a dose-response relationship. This could be achieved with the use of neutral density filters, which reduce light intensity uniformly across wavelengths.

Chapter 6: Synthesis and Engineering Significance

6.1 Cross-Chapter Synthesis

The objectives of this thesis were to: 1) establish conditions for consistent PLA degradation using RDC compost in lab-scale systems; 2) evaluate bioaugmentation and biostimulation as enhancement strategies; 3) characterize PLA degradation in operating RDC systems; and 4) design and characterize a UV-C exposure system. As the same Ingeo PLA source material was used across respirometry, RDC composting, and UV-C exposure experiments, degradation outcomes can be compared directly across chapters without the variation in polymer grade, thickness, and molecular weight that would otherwise limit cross-study comparison.

The first hypothesis was that PLA degradation performance in RDC systems could be linked to controlled respirometer experiments. This was supported as respirometer degradation outcomes aligned with RDC degradation outcomes when sufficient thermal exposure was achieved.

The second hypothesis was that bioaugmentation and biostimulation would improve biodegradation rates. Across all experiments, temperature was the most important variable. At 30 °C, there was slow hydrolysis, and no mineralization. At 58 °C in the respirometer study, there was a lag phase of 19 to 22 days where abiotic hydrolysis reduced PLA molecular weight before microbial mineralization could proceed. This lag phase was consistent with those reported in PLA degradation kinetics studies, which report lag times between 20 and 30 days (Leejarkpai et al., 2011; Stloukal et al., 2015). The rate constants observed under thermophilic conditions in this study were 3-5 times higher than those reported by Leejarkpai et al. (2011) and Stloukal et al. (2015) for PLA at 58 °C. Gelatin-amendment and inoculation were not able to shortcut around the

temperature requirement. The insufficiency of mesophilic conditions for PLA degradation is consistent with the literature. Van de Perre et al. (2024) observed negligible PLA biodegradation (1-4 %) at 28 °C over 365 days without biostimulation or bioaugmentation; in the present study these interventions did not improve outcomes at mesophilic temperatures.

The third hypothesis was that a custom-built UV-C chamber will produce measurable reductions in PLA molecular weight and alter polymer thermal properties. This was supported; UV dramatically reduced Mv rapidly, a property consistent with quick degradation in the other studies. UV-C exposure depressed Tg in both first and second heating scans, suggesting that UV-pretreated PLA may be susceptible to degradation at composting temperatures below the Tg of untreated PLA. Due to weather and time constraints, the UV-treated films were not able to be tested in the RDC or other composting conditions.

A consistent pattern observed across all degradation conditions was increased relative crystallization after exposure, whether that be due to the preferential consumption in the microbial environments or secondary crystallization after UV exposure. Across the thesis, three primary factors affected the rate-limiting hydrolysis step. The first was temperature, where cumulative thermal exposure determined whether significant degradation occurred at all within the experiment timespans. The second was surface area; in the RDC, crystalline PLA lost recoverable mass fastest due to mechanical fragmentation increasing exposed surface, while in respirometers, amorphous PLA degraded faster because gentler mixing had less impact than amorphous PLA susceptibility to hydrolysis. This observation draws on different measures of degradation: mineralization via CO_2 evolution in respirometers, and physical loss of recoverable mass in the RDC. While these are not

directly comparable, together they point to consistent patterns. Third, UV-C exposure reduced PLA molecular weight to levels associated with physical disappearance in composting, through a photochemical pathway as opposed to a biological one.

6.2 Engineering Significance

This study is the first characterization of PLA degradation in rotating in-vessel mortality composters, and the first direct comparison of lab respirometry to field RDC performance using same compost source and polymers. It demonstrated that intermittent thermophilic exposure (not sustained 58 °C) can achieve complete physical degradation in similar if not faster timepoints than sustained thermophilic conditions. However, outcomes remained probabilistic rather than guaranteed, with some films persisting intact under the same nominal residence times due to heterogeneous thermal exposure. The RDC studies quantified the observed thermal exposure variability within a single vessel and proposed it as a potential explanation for starkly differing degradation outcomes in the same vessel.

In RDC systems, cumulative thermal exposure was the primary predictor of degradation. Surface area accelerated outcomes when thermal conditions are met, with biological interventions and initial crystallinity being secondary factors. These factors operate within a system that also requires adequate moisture and oxygen availability to sustain thermophilic microbial activity. Without them, the microbial mineralization step cannot proceed even if hydrolysis is complete. Therefore, maintaining cumulative thermophilic exposure above the Tg threshold (e.g., hours ≥55 °C) is more important for PLA degradation reliability than microbial manipulation, but facility operators should also ensure adequate aeration and moisture levels are maintained.

A key engineering implication is that residence time is a poor predictor of PLA degradation in in-vessel composting systems unless they are known to be consistently homogeneous in internal environment; cumulative thermal exposure is a more defensible metric for design and monitoring. Continuous rotation improves composting outcomes, but still does not guarantee uniformity. The thermal heterogeneity observed in the RDC also has implications beyond PLA degradation; regulatory requirements for mortality composting mandate sustained temperatures above 55 °C for a minimum of five days to ensure pathogen destruction (Nioex Systems Inc., 2010), and the temperature variability documented in this study suggests that not all material within the vessel may reliably meet this threshold.

The UV chapter demonstrated that for the two irradiance conditions tested, the difference in irradiance had no effect on Mv reduction, though reporting irradiance and film characteristics (thickness) remains important for reproducibility and cross-study comparison.

6.3 Scope Limitations

RDC experiments measured physical disappearance, not CO_2 evolution. Combined with the mesh bag recovery method, which in theory could lose microplastics smaller than 180 μm, means that material that "disappeared" could include undetected microplastic fragments. As a result, disappearance outcomes cannot be interpreted as mineralization or complete carbon conversion in the RDC trials. Furthermore, the mesh bag method has recovery limitations at high compost volumes, as they can be difficult to find. Another limitation of the RDC studies is that only temperature was logged consistently; oxygen and moisture spatial distributions were not characterized and so their role in degradation outcomes is not quantified. An economic analysis of

the practical scalability of RDC systems compared to other degradation methods was not assessed. In the respirometer studies, microbial communities responsible for degradation were not identified.

6.4 Recommendations for Future Work

A re-evaluation of experimental design in light of the preliminary results obtained for each of the previous studies are detailed in Sections 3.6, 4.6, and 5.6. From these there are three main priorities, addressed in this section in summary. The first priority is that the relationship between per-bag thermal exposure and degradation outcome should be quantified over the duration of full-length RDC trial, ideally with oxygen and moisture sensors incorporated into the bag as well. Through these experiments the conclusions regarding RDC thermal heterogeneity and its relationship to PLA degradation could be better characterized and supported.

The second priority is that UV-C pretreatment should be integrated with composting trials to determine whether the severe molecular weight reduction achieved by UV exposure translates to accelerated mineralization under composting conditions above and below PLA's Tg. If possible, this should involve the testing of a scaled-up chamber appropriate for the volume of PLA plastic that is processed at the Forks RDC, and its impact on PLA degradation rates there.

Thirdly, microplastic fate and microbial community dynamics in the tested RDCs require characterization. Filtered compost analysis should be used to confirm whether physical disappearance of PLA in the RDC represents mineralization or fragmentation below the 180 μm mesh detection limit, and also to evaluate the presence of microplastics currently exiting the Forks RDC and Forks curing piles, where the degradation of PLA is most likely continuing.

Metagenomic analysis of RDC compost could identify organisms responsible for PLA degradation and clarify whether repeated PLA exposure drives community-level adaptation.

References

Ainali, N. M., Kalaronis, D., Evgenidou, E., Kyzas, G. Z., Bobori, D. C., Kaloyianni, M., Yang, X., Bikiaris, D. N., & Lambropoulou, D. A. (2022). Do poly(lactic acid) microplastics instigate a threat? A perception for their dynamic towards environmental pollution and toxicity. Science of The Total Environment, 832, 155014. https://doi.org/10.1016/j.scitotenv.2022.155014

Bher, A., Mayekar, P. C., Auras, R. A., & Schvezov, C. E. (2022). Biodegradation of Biodegradable Polymers in Mesophilic Aerobic Environments. International Journal of Molecular Sciences, 23(20), 12165. https://doi.org/10.3390/ijms232012165

Brown, M. H., Badzinski, T. D., Pardoe, E., Ehlebracht, M., & Maurer-Jones, M. A. (2024). UV Light Degradation of Polylactic Acid Kickstarts Enzymatic Hydrolysis. ACS Materials Au, 4(1), 92–98. https://doi.org/10.1021/acsmaterialsau.3c00065

Bubpachat, T., Sombatsompop, N., & Prapagdee, B. (2018). Isolation and role of polylactic acid-degrading bacteria on degrading enzymes productions and PLA biodegradability at mesophilic conditions. Polymer Degradation and Stability, 152, 75–85. https://doi.org/10.1016/j.polymdegradstab.2018.03.023

Cadar, O., Paul, M., Roman, C., Miclean, M., & Majdik, C. (2012). Biodegradation behaviour of poly(lactic acid) and (lactic acid-ethylene glycol-malonic or succinic acid) copolymers under controlled composting conditions in a laboratory test system. Polymer Degradation and Stability, 97(3), 354–357. https://doi.org/10.1016/j.polymdegradstab.2011.12.006

Castro-Aguirre, E., Auras, R., Selke, S., Rubino, M., & Marsh, T. (2017). Insights on the aerobic biodegradation of polymers by analysis of evolved carbon dioxide in simulated composting conditions. Polymer Degradation and Stability, 137, 251–271. https://doi.org/10.1016/j.polymdegradstab.2017.01.017

Castro-Aguirre, E., Auras, R., Selke, S., Rubino, M., & Marsh, T. (2018). Enhancing the biodegradation rate of poly(lactic acid) films and PLA bio-nanocomposites in simulated composting through bioaugmentation. Polymer Degradation and Stability, 154, 46–54. https://doi.org/10.1016/j.polymdegradstab.2018.05.017

Ceresana. (2023). Market study: Bioplastics (8th ed.). Ceresana Market Research. https://ceresana.com/en/produkt/market-study-bioplastics

Chong, Z. K., Hofmann, A., Haye, M., Wilson, S., Sohoo, I., Alassali, A., & Kuchta, K. (2024). Lab-scale and full-scale industrial composting of biodegradable plastic blends for packaging. Open Research Europe, 2, 101. https://doi.org/10.12688/openreseurope.14893.3

Copinet, A., Bertrand, C., Govindin, S., Coma, V., & Couturier, Y. (2004). Effects of ultraviolet light (315 nm), temperature and relative humidity on the degradation of polylactic acid plastic films. Chemosphere, 55(5), 763–773. https://doi.org/10.1016/j.chemosphere.2003.11.038

D20 Committee. (2023). Specification for Labeling of Plastics Designed to be Aerobically Composted in Municipal or Industrial Facilities. ASTM International. https://doi.org/10.1520/D6400-21

D20 Committee. (2021). Test Method for Determining Aerobic Biodegradation of Plastic Materials Under Controlled Composting Conditions, Incorporating Thermophilic Temperatures. ASTM International. https://doi.org/10.1520/D5338-15R21

D20 Committee. (2016). Test Method for Dilute Solution Viscosity of Polymers. ASTM International. https://doi.org/10.1520/D2857-16

Da Silva, S. A., Hinkel, E. W., Lisboa, T. C., Selistre, V. V., Da Silva, A. J., Da Silva, L. O. F., Faccin, D. J. L., & Cardozo, N. S. M. (2020). A biostimulation-based accelerated method for evaluating the biodegradability of polymers. Polymer Testing, 91, 106732. https://doi.org/10.1016/j.polymertesting.2020.106732

De Jong, S. J., Arias, E. R., Rijkers, D. T. S., Van Nostrum, C. F., Kettenes-van Den Bosch, J. J., & Hennink, W. E. (2001). New insights into the hydrolytic degradation of poly(lactic acid): Participation of the alcohol terminus. Polymer, 42(7), 2795–2802. https://doi.org/10.1016/S0032-3861(00)00646-7

Dhiman, V., Pant, D., & Sharma, S. D. (2022). Single-Use Plastics: An Escalating Global Environmental Problem. In N. N. Dalei & A. Gupta (Eds.), Economics and Policy of Energy and Environmental Sustainability (pp. 215–243). Springer Nature Singapore. https://doi.org/10.1007/978-981-19-5061-2_11

Elsawy, M. A., Kim, K.-H., Park, J.-W., & Deep, A. (2017). Hydrolytic degradation of polylactic acid (PLA) and its composites. Renewable and Sustainable Energy Reviews, 79, 1346–1352. https://doi.org/10.1016/j.rser.2017.05.143

Environment Canada. (2013). Technical document on municipal solid waste organics processing. Government of Canada.

Eraslan, K., Altınbay, A., & Nofar, M. (2024). In-situ self-reinforcement of amorphous polylactide (PLA) through induced crystallites network and its highly ductile and toughened PLA/poly(butylene adipate-co-terephthalate) (PBAT) blends. International Journal of Biological Macromolecules, 272, 132936. https://doi.org/10.1016/j.ijbiomac.2024.132936

Fakhrizada, H., & Dahman, Y. (2025). Degradable Alternatives to Single-Use Plastics: Mechanisms, Materials, and Strategies for Sustainable Polyolefin Replacement. Molecules, 30(21), 4301. https://doi.org/10.3390/molecules30214301

Fiori, S. (2014). CHAPTER 13. Industrial Uses of PLA. In A. Jiménez, M. Peltzer, & R. Ruseckaite (Eds.), Polymer Chemistry Series (pp. 315–333). Royal Society of Chemistry. https://doi.org/10.1039/9781782624806-00315

Fischer, E. W., Sterzel, H. J., & Wegner, G. (1973). Investigation of the structure of solution grown crystals of lactide copolymers by means of chemical reactions. Kolloid-Zeitschrift Und Zeitschrift Für Polymere, 251(11), 980–990. https://doi.org/10.1007/BF01498927

Fogašová, M., Figalla, S., Danišová, L., Medlenová, E., Hlaváčiková, S., Vanovčanová, Z., Omaníková, L., Baco, A., Horváth, V., Mikolajová, M., Feranc, J., Bočkaj, J., Plavec, R., Alexy, P., Repiská, M., Přikryl, R., Kontárová, S., Báreková, A., Sláviková, M., … Kadlečková, M. (2022). PLA/PHB-Based Materials Fully Biodegradable under Both Industrial and Home-Composting Conditions. Polymers, 14(19), 4113. https://doi.org/10.3390/polym14194113

Forks North Portage Corporation. (n.d.). Target Zero: Composting. Retrieved https://www.theforks.com/target-zero/composting

Gastaldi, E., Buendia, F., Greuet, P., Benbrahim Bouchou, Z., Benihya, A., Cesar, G., & Domenek, S. (2024). Degradation and environmental assessment of compostable

packaging mixed with biowaste in full-scale industrial composting conditions. Bioresource Technology, 400, 130670. https://doi.org/10.1016/j.biortech.2024.130670

Gautam, B. P. S., Qureshi, A., Gwasikoti, A., Kumar, V., & Gondwal, M. (2024). Global Scenario of Plastic Production, Consumption, and Waste Generation and Their Impacts on Environment and Human Health. In R. Soni, P. Debbarma, D. C. Suyal, & R. Goel (Eds.), Advanced Strategies for Biodegradation of Plastic Polymers (pp. 1–34). Springer Nature Switzerland. https://doi.org/10.1007/978-3-031-55661-6_1

Göpferich, A. (1996). Mechanisms of polymer degradation and erosion. Biomaterials, 17(2), 103–114. https://doi.org/10.1016/0142-9612(96)85755-3

Gorrasi, G., & Pantani, R. (2017). Hydrolysis and Biodegradation of Poly(lactic acid). In M. L. Di Lorenzo & R. Androsch (Eds.), Synthesis, Structure and Properties of Poly(lactic acid) (Vol. 279, pp. 119–151). Springer International Publishing. https://doi.org/10.1007/12_2016_12

Höglund, A., Odelius, K., & Albertsson, A.-C. (2012). Crucial Differences in the Hydrolytic Degradation between Industrial Polylactide and Laboratory-Scale Poly(L -lactide). ACS Applied Materials & Interfaces, 4(5), 2788–2793. https://doi.org/10.1021/am300438k

Iñiguez-Franco, F., Auras, R., Ahmed, J., Selke, S., Rubino, M., Dolan, K., & Soto-Valdez, H. (2018). Control of hydrolytic degradation of Poly(lactic acid) by incorporation of chain extender: From bulk to surface erosion. Polymer Testing, 67, 190–196. https://doi.org/10.1016/j.polymertesting.2018.02.028

Janorkar, A. V., Metters, A. T., & Hirt, D. E. (2007). Degradation of poly(L -lactide) films under ultraviolet-induced photografting and sterilization conditions. Journal of Applied Polymer Science, 106(2), 1042–1047. https://doi.org/10.1002/app.24692

Jarerat, A., Tokiwa, Y., & Tanaka, H. (2004). Microbial Poly(L-Lactide)-Degrading Enzyme Induced by Amino Acids, Peptides, and Poly(L-Amino Acids). Journal of Polymers and the Environment, 12(3), 139–146. https://doi.org/10.1023/B:JOOE.0000038545.69235.f2

Jeon, H. J., & Kim, M. N. (2013). Biodegradation of poly(l-lactide) (PLA) exposed to UV irradiation by a mesophilic bacterium. International Biodeterioration & Biodegradation, 85, 289–293. https://doi.org/10.1016/j.ibiod.2013.08.013

Kahraman, Y., Özdemir, B., Kılıç, V., Goksu, Y. A., & Nofar, M. (2021). Super toughened and highly ductile PLA / TPU blend systems by in situ reactive interfacial compatibilization using multifunctional epoxy-based chain extender. Journal of Applied Polymer Science, 138(20), 50457. https://doi.org/10.1002/app.50457

Kale, G., Auras, R., Singh, S. P., & Narayan, R. (2007). Biodegradability of polylactide bottles in real and simulated composting conditions. Polymer Testing, 26(8), 1049–1061. https://doi.org/10.1016/j.polymertesting.2007.07.006

Kalita, N. K., Sarmah, A., Bhasney, S. M., Kalamdhad, A., & Katiyar, V. (2021). Demonstrating an ideal compostable plastic using biodegradability kinetics of poly(lactic acid) (PLA) based green biocomposite films under aerobic composting conditions. Environmental Challenges, 3, 100030. https://doi.org/10.1016/j.envc.2021.100030

Karamanlioglu, M., Preziosi, R., & Robson, G. D. (2017). Abiotic and biotic environmental degradation of the bioplastic polymer poly(lactic acid): A review. Polymer Degradation and Stability, 137, 122–130. https://doi.org/10.1016/j.polymdegradstab.2017.01.009

Kawashima, N., Yagi, T., & Kojima, K. (2021). Pilot-Scale Composting Test of Polylactic Acid for Social Implementation. Sustainability, 13(4), 1654. https://doi.org/10.3390/su13041654

Komilis, D. P. (2006). A kinetic analysis of solid waste composting at optimal conditions. Waste Management, 26(1), 82–91. https://doi.org/10.1016/j.wasman.2004.12.021

Korzhikov-Vlakh, V., Sinitsyna, E., Arkhipov, K., Levit, M., Korzhikova-Vlakh, E., & Tennikova, T. (2024). Improvement in Biological Performance of Poly(Lactic Acid)-Based Materials via Single-Point Surface Modification with Glycopolymer. Surfaces, 7(4), 1008–1028. https://doi.org/10.3390/surfaces7040067

Kulikowska, D., Bernat, K., Wojnowska-Baryła, I., Pasieczna-Patkowska, S., & Jabłoński, R. (2020). Composting as a disposal route of PLA materials: Kinetics of the aerobic biodegradation. Desalination and Water Treatment, 206, 153–164. https://doi.org/10.5004/dwt.2020.26355

Kun, E., & Kálmán, M. (2013). Effect of Crystallinity on PLA's Microbiological Behaviour. Materials Science Forum, 752, 241–247. https://doi.org/10.4028/www.scientific.net/MSF.752.241

Kunioka, M., Ninomiya, F., & Funabashi, M. (2006). Biodegradation of poly(lactic acid) powders proposed as the reference test materials for the international standard of biodegradation evaluation methods. Polymer Degradation and Stability, 91(9), 1919–1928. https://doi.org/10.1016/j.polymdegradstab.2006.03.003

Lambert, S., & Wagner, M. (2017). Environmental performance of bio-based and biodegradable plastics: The road ahead. Chemical Society Reviews, 46(22), 6855–6871. https://doi.org/10.1039/C7CS00149E

Lee, R. E., Azdast, T., Wang, G., Wang, X., Lee, P. C., & Park, C. B. (2020). Highly expanded fine-cell foam of polylactide/polyhydroxyalkanoate/nano-fibrillated polytetrafluoroethylene composites blown with mold-opening injection molding. International Journal of Biological Macromolecules, 155, 286–292. https://doi.org/10.1016/j.ijbiomac.2020.03.212

Lee, R. E., Guo, Y., Tamber, H., Planeta, M., & Leung, S. N. S. (2016). Thermoforming of Polylactic Acid Foam Sheets: Crystallization Behaviors and Thermal Stability. Industrial & Engineering Chemistry Research, 55(3), 560–567. https://doi.org/10.1021/acs.iecr.5b03473

Leejarkpai, T., Suwanmanee, U., Rudeekit, Y., & Mungcharoen, T. (2011). Biodegradable kinetics of plastics under controlled composting conditions. Waste Management, 31(6), 1153–1161. https://doi.org/10.1016/j.wasman.2010.12.011

Lesaffre, N., Bellayer, S., Vezin, H., Fontaine, G., Jimenez, M., & Bourbigot, S. (2017). Recent advances on the ageing of flame retarded PLA: Effect of UV-light and/or relative humidity. Polymer Degradation and Stability, 139, 143–164. https://doi.org/10.1016/j.polymdegradstab.2017.04.007

Lim, L.-T., Auras, R., & Rubino, M. (2008). Processing technologies for poly(lactic acid). Progress in Polymer Science, 33(8), 820–852. https://doi.org/10.1016/j.progpolymsci.2008.05.004

Lizundia, E., Mateos, P., & Vilas, J. L. (2017). Tuneable hydrolytic degradation of poly(l-lactide) scaffolds triggered by ZnO nanoparticles. Materials Science and Engineering: C, 75, 714–720. https://doi.org/10.1016/j.msec.2017.02.104

Lucas, N., Bienaime, C., Belloy, C., Queneudec, M., Silvestre, F., & Nava-Saucedo, J.-E. (2008). Polymer biodegradation: Mechanisms and estimation techniques – A review. Chemosphere, 73(4), 429–442. https://doi.org/10.1016/j.chemosphere.2008.06.064

MacDonald, R. T., McCarthy, S. P., & Gross, R. A. (1996). Enzymatic Degradability of Poly(lactide): Effects of Chain Stereochemistry and Material Crystallinity. Macromolecules, 29(23), 7356–7361. https://doi.org/10.1021/ma960513j

Madhavan Nampoothiri, K., Nair, N. R., & John, R. P. (2010). An overview of the recent developments in polylactide (PLA) research. Bioresource Technology, 101(22), 8493–8501. https://doi.org/10.1016/j.biortech.2010.05.092

Maragkaki, A., Malliaros, N. G., Sampathianakis, I., Lolos, T., Tsompanidis, C., & Manios, T. (2023). Evaluation of Biodegradability of Polylactic Acid and Compostable Bags from Food Waste under Industrial Composting. Sustainability, 15(22), 15963. https://doi.org/10.3390/su152215963

Mayekar, P. C., & Auras, R. (2024). Accelerating Biodegradation: Enhancing Poly(lactic acid) Breakdown at Mesophilic Environmental Conditions with Biostimulants. Macromolecular Rapid Communications, 45(7), 2300641. https://doi.org/10.1002/marc.202300641

Meyer-Cifuentes, I.E., Werner, J., Jehmlich, N. et al. (2020). Synergistic biodegradation of aromatic-aliphatic copolyester plastic by a marine microbial consortium. Nat Commun 11, 5790. https://doi.org/10.1038/s41467-020-19583-2

Mistry, A. N., Kachenchart, B., Pinyakong, O., Assavalapsakul, W., Jitpraphai, S. M., Somwangthanaroj, A., & Luepromchai, E. (2023). Bioaugmentation with a defined bacterial consortium: A key to degrade high molecular weight polylactic acid during traditional composting. Bioresource Technology, 367, 128237. https://doi.org/10.1016/j.biortech.2022.128237

Mistry, A. N., Kachenchart, B., Wongthanaroj, A., Somwangthanaroj, A., & Luepromchai, E. (2022). Rapid biodegradation of high molecular weight semi-crystalline polylactic acid at ambient temperature via enzymatic and alkaline hydrolysis by a defined bacterial consortium. Polymer Degradation and Stability, 202, 110051. https://doi.org/10.1016/j.polymdegradstab.2022.110051

Musioł, M., Sikorska, W., Adamus, G., Janeczek, H., Richert, J., Malinowski, R., Jiang, G., & Kowalczuk, M. (2016). Forensic engineering of advanced polymeric materials. Part III - Biodegradation of thermoformed rigid PLA packaging under industrial composting conditions. Waste Management, 52, 69–76. https://doi.org/10.1016/j.wasman.2016.04.016

Myburgh, M. W., Favaro, L., Van Zyl, W. H., & Viljoen-Bloom, M. (2023). Engineered yeast for the efficient hydrolysis of polylactic acid. Bioresource Technology, 378, 129008. https://doi.org/10.1016/j.biortech.2023.129008

Mysiukiewicz, O., Barczewski, M., Skórczewska, K., & Matykiewicz, D. (2020). Correlation between Processing Parameters and Degradation of Different Polylactide Grades during Twin-Screw Extrusion. Polymers, 12(6), 1333. https://doi.org/10.3390/polym12061333

Napper, I. E., & Thompson, R. C. (2023). Plastics and the Environment. Annual Review of Environment and Resources, 48(1), 55–79. https://doi.org/10.1146/annurev-environ-112522-072642

NatureWorks LLC. (2017). Ingeo™ Biopolymer 2500HP Technical Data Sheet. NatureWorks LLC. https://www.natureworksllc.com/~/media/Files/NatureWorks/Technical-Documents/Technical-Data-Sheets/TechnicalDataSheet_2500HP_extrusion_pdf.pdf

Nioex Systems Inc. (2010). BIOvator® MANUAL. Nioex Systems Inc. https://www.nioex.com/biovator

Nizamuddin, S., & Chen, C. (2024). Biobased, biodegradable and compostable plastics: Chemical nature, biodegradation pathways and environmental strategy. Environmental Science and Pollution Research, 31(6), 8387–8399. https://doi.org/10.1007/s11356-023-31689-w

Olaya-Rincon, M., Serra-Rada, J., Silva, C. D., Barcelona, P., Dosta, J., Astals, S., & Martínez, M. (2025). Thermophilic anaerobic biodegradation of commercial polylactic acid products. Bioresource Technology, 425, 132296. https://doi.org/10.1016/j.biortech.2025.132296

Pantani, R., & Sorrentino, A. (2013). Influence of crystallinity on the biodegradation rate of injection-moulded poly(lactic acid) samples in controlled composting conditions.

Polymer Degradation and Stability, 98(5), 1089–1096. https://doi.org/10.1016/j.polymdegradstab.2013.01.005

Pitt, C. G., & Zhong-wei, G. (1987). Modification of the rates of chain cleavage of poly(ε-caprolactone) and related polyesters in the solid state. Journal of Controlled Release, 4(4), 283–292. https://doi.org/10.1016/0168-3659(87)90020-4

Quecholac-Piña, X., Hernández-Berriel, M. D. C., Mañón-Salas, M. D. C., Espinosa-Valdemar, R. M., & Vázquez-Morillas, A. (2020). Degradation of Plastics under Anaerobic Conditions: A Short Review. Polymers, 12(1), 109. https://doi.org/10.3390/polym12010109

Ranakoti, L., Gangil, B., Mishra, S. K., Singh, T., Sharma, S., Ilyas, R. A., & El-Khatib, S. (2022). Critical Review on Polylactic Acid: Properties, Structure, Processing, Biocomposites, and Nanocomposites. Materials, 15(12), 4312. https://doi.org/10.3390/ma15124312

Ravve, A. (2012). Principles of Polymer Chemistry. Springer New York. https://doi.org/10.1007/978-1-4614-2212-9

Rezvani Ghomi, E. R., Khosravi, F., Saedi Ardahaei, A. S., Dai, Y., Neisiany, R. E., Foroughi, F., Wu, M., Das, O., & Ramakrishna, S. (2021). The Life Cycle Assessment for Polylactic Acid (PLA) to Make It a Low-Carbon Material. Polymers, 13(11), 1854. https://doi.org/10.3390/polym13111854

Satti, S. M., Shah, A. A., Auras, R., & Marsh, T. L. (2017). Isolation and characterization of bacteria capable of degrading poly(lactic acid) at ambient temperature. Polymer Degradation and Stability, 144, 392–400. https://doi.org/10.1016/j.polymdegradstab.2017.08.023

Seo, H.-J., Lee, D.-H., & Seo, I.-H. (2024). Thermal Environment Monitoring and Model Development of an Enclosed Vertical-Type Composting Facility. Applied Sciences, 14(10), 4043. https://doi.org/10.3390/app14104043

Shi, B., & Palfery, D. (2012). Temperature-dependent polylactic acid (PLA) anaerobic biodegradability. International Journal of Environment and Waste Management, 10(2/3), 297. https://doi.org/10.1504/IJEWM.2012.048324

Shrestha, S., Snowdon, M., & Levin, D. B. (2025). Enzymatic Degradation of PLA: Preferential Degradation of the Amorphous Fraction. Polymers, 17(22), 3042. https://doi.org/10.3390/polym17223042

Stloukal, P., Pekařová, S., Kalendova, A., Mattausch, H., Laske, S., Holzer, C., Chitu, L., Bodner, S., Maier, G., Slouf, M., & Koutny, M. (2015). Kinetics and mechanism of the biodegradation of PLA/clay nanocomposites during thermophilic phase of composting process. Waste Management, 42, 31–40. https://doi.org/10.1016/j.wasman.2015.04.006

Stojanovski, G., Bawn, M., Locks, A., Ambrose-Dempster, E., Ward, J. M., Jeffries, J. W. E., & Hailes, H. C. (2025). Functional Enrichment and Sequence-Based Discovery Identify Promiscuous and Efficient Poly Lactic Acid Degrading Enzymes. Environmental Science & Technology, 59(17), 8602–8613. https://doi.org/10.1021/acs.est.4c07279

Swetha, T. A., Ananthi, V., Bora, A., Sengottuvelan, N., Ponnuchamy, K., Muthusamy, G., & Arun, A. (2023). A review on biodegradable polylactic acid (PLA) production from fermentative food waste—Its applications and degradation. International Journal of Biological Macromolecules, 234, 123703. https://doi.org/10.1016/j.ijbiomac.2023.123703

Tertyshnaya, Yu. V., & Podzorova, M. V. (2020). Effect of UV Irradiation on the Structural and Dynamic Characteristics of Polylactide and Its Blends with Polyethylene. Russian Journal of Physical Chemistry B, 14(1), 167–175. https://doi.org/10.1134/S1990793120010170

Tokiwa, Y., & Suzuki, T. (1977). Hydrolysis of polyesters by lipases. Nature, 270(5632), 76–78. https://doi.org/10.1038/270076a0

Tsuji, H., & Ikarashi, K. (2004). In Vitro Hydrolysis of Poly(l -lactide) Crystalline Residues as Extended-Chain Crystallites: II. Effects of Hydrolysis Temperature. Biomacromolecules, 5(3), 1021–1028. https://doi.org/10.1021/bm0345231

Tsuji, H., & Miyauchi, S. (2001). Enzymatic Hydrolysis of Poly(lactide)s: Effects of Molecular Weight, l -Lactide Content, and Enantiomeric and Diastereoisomeric Polymer Blending. Biomacromolecules, 2(2), 597–604. https://doi.org/10.1021/bm010048k

United States Environmental Protection Agency. (2025, December 29). Approaches to composting. https://www.epa.gov/sustainable-management-food/approaches-composting

Van De Perre, D., Serbruyns, L., Coltelli, M.-B., Gigante, V., Aliotta, L., Lazzeri, A., Geerinck, R., & Verstichel, S. (2024). Tuning Biodegradation of Poly (lactic acid) (PLA) at Mild Temperature by Blending with Poly (butylene succinate-co-adipate) (PBSA) or Polycaprolactone (PCL). Materials, 17(22), 5436. https://doi.org/10.3390/ma17225436

Wang, X., Chen, J., Jia, W., Huang, K., & Ma, Y. (2024). Comparing the Aging Processes of PLA and PE: The Impact of UV Irradiation and Water. Processes, 12(4), 635. https://doi.org/10.3390/pr12040635

Warmadewanthi, I., Krisnaputra, A. B., Saptarini, D., Andiya, A. M., Mahubessy, R. C., & Humaidi, F. (2022). The Distribution of Temperature on Aerobic Composting of Food Waste: Experimental studies and CFD analysis. IOP Conference Series: Earth and Environmental Science, 1095(1), 012032. https://doi.org/10.1088/1755-1315/1095/1/012032

Wiesner, Y., Bednarz, M., Braun, U., Bannick, C.G., Ricking, M., & Altmann, K. (2023). A promising approach to monitor microplastic masses in composts. Frontiers in Environmental Chemistry, 4, 1281558. https://doi.org/10.3389/fenvc.2023.1281558

Yang, Y., Kong, Y., Wang, G., Shen, Y., Tang, R., Yin, Z., Yang, J., Li, G., & Yuan, J. (2023). Temporal succession and spatial heterogeneity of humification, pathogens and bacterial community in facultative heap composting. Process Safety and Environmental Protection, 176, 734–746. https://doi.org/10.1016/j.psep.2023.06.049

Yeşiller N, Hanson JL, Yee EH. Waste heat generation: A comprehensive review. Waste Manag. 2015 Aug;42:166-79. doi: 10.1016/j.wasman.2015.04.004. Epub 2015 May 8. PMID: 25962825. 10.1016/j.wasman.2015.04.004

Zhang, C., Rathi, S., Goddard, J., Constantine, K., & Collins, P. (2013). The Effect of UV Treatment on the Degradation of Compostable Polylactic Acid. Journal of Emerging Investigators. https://doi.org/10.59720/13-023

Appendix

Appendix A – Raw mass recovery and film condition data

Table A1 – SIAF RDC Experiment 1: individual film recovery data

Two Weeks

Labeling	Condition	Film Mass (g)	Film Mass Recovered	%Mass Recovered	Observations
F3	Forks 3	0.2522	0.252	100	fully recovered sample in one piece (no mass loss), completely opaque
F4	Forks 4	0.2628	0.1944	74	very fragmented, some pieces so small they were visible but not recoverable, recovery incomplete
F1	Forks 1	0.2453	0.2453	100	fully recovered sample in one piece (no mass loss), completely opaque
F5	Forks 5	0.2422	0.2418	100	fully recovered sample in one piece (no mass loss), completely opaque
F2	Forks 2	0.2348	0.1186	51	very fragmented, some pieces so small they were visible but not recoverable, recovery incomplete
C3	Crystalline 3	0.1493	0.1484	99	fragmented into several large pieces but almost completely recovered, likely no mass loss
C2	Crystalline 2	0.1484	0.1099	74	very fragmented, some pieces so small they were visible but not recoverable, recovery incomplete
C5	Crystalline 5	0.1287	0.1034	80	fragmented into many pieces, recovery incomplete due to how small some of the fragmented pieces are, likely no mass loss
C1	Crystalline 1	0.1643	0.1174	71	very fragmented, some pieces so small they were visible but not recoverable, recovery incomplete
C4	Crystalline 4	0.1314	0.1162	88	fragmented into many pieces, recovery incomplete due to how small some of the fragmented pieces are, likely no mass loss
A4	Amorphous 4	0.1358	0.0333	25	fragmented into many pieces, recovery incomplete due to how small some of the fragmented pieces are, likely no mass loss
A1	Amorphous 1	0.1335	0.1292	97	fragmented into several large pieces but almost completely recovered, likely no mass loss
A2	Amorphous 2	0.1393	0.1407	101	fragmented into several large pieces but completely recovered, likely no mass loss
A3	Amorphous 3	0.135	0.1335	99	fragmented into several large pieces but almost completely recovered, likely no mass loss
A5	Amorphous 5	0.1362	0.0759	56	fragmented into many pieces, recovery incomplete due to how small some of the fragmented pieces are, likely no mass loss

Four Weeks

Labeling	Condition	Film Mass (g)	Film Mass Recovered	%Mass Recovered	Observations
F1	Forks 1	0.2414	0	0	no visible plastic left
F2	Forks 2	0.2616	0.263	101	fully recovered sample in one piece (no mass loss), completely opaque
F5	Forks 5	0.2578	0.2448	95	fragmented into several large pieces but almost completely recovered, likely no mass loss
F4	*Forks 4*	*0.2628*	0	0	extremely fragmented, white powder visible, but not recoverable.
F3	Forks 3	0.2395	0.0618	26	fragmented into many pieces, recovery incomplete due to how small some of the fragmented pieces are, likely no mass loss
C2	Crystalline 2	0.1522	0	0	no visible plastic left
C4	Crystalline 4	0.1693	0.0822	49	fragmented into many pieces, recovery incomplete due to how small some of the fragmented pieces are
C1	Crystalline 1	0.1429	0.046	32	fragmented into many pieces, recovery incomplete due to how small some of the fragmented pieces are, likely no mass loss
C3	Crystalline 3	0.151	0	0	extremely fragmented, very small amount of white powder visible, but not recoverable, appears almost entirely degraded
C1	Crystalline 1	0.1382	0	0	extremely fragmented, very small amount of white powder visible, but not recoverable, appears almost entirely degraded
A3	Amorphous 3	0.1493	0.136	91	fragmented into several large pieces but almost completely recovered, likely no mass loss
A5	Amorphous 5	0.1382	0	0	no visible plastic left
A4	Amorphous 4	0.1434	0.1401	98	fragmented into several large pieces but almost completely recovered, likely no mass loss
A1	Amorphous 1	0.1505	0.1227	82	somewhat fragmented, recovery incomplete, likely no mass loss
A2	Amorphous 2	0.1292	0.0338	26	fragmented into many pieces, recovery incomplete due to how small some of the fragmented pieces are, likely no mass loss

Six Weeks

Labeling	Condition	Film Mass (g)	Film Mass Recovered	%Mass Recovered	Observations
F2	Forks 2	0.2674	0	0	no visible plastic left
F4	Forks 4	0.2469	0.246	100	fully recovered sample in one piece (no mass loss), completely opaque
F1	Forks 1	0.2646	0	0	no visible plastic left
F3	Forks 3	0.2371	0.0056	2	almost entirely degraded - small amount of tiny fragments left
F2	Forks 2	0.2933	0	0	no visible plastic left
C2	Crystalline 2	0.1522	0.0041	3	almost entirely degraded - small amount of tiny fragments left
C1	Crystalline 1	0.1331	0.0299	22	mostly degraded - some fragments left
C5	Crystalline 5	0.1381	0	0	no visible plastic left
C4	Crystalline 4	0.1346	0.1115	83	fragmented into many pieces, recovery incomplete due to how small some of the fragmented pieces are
A5	Amorphous 5	0.1298	0	0	no visible plastic left
A1	Amorphous 1	0.1388	0.0363	26	mostly degraded - some fragments left
A3	Amorphous 3	0.1325	0.1311	99	fragmented into several large pieces but almost completely recovered, likely no mass loss
A2	Amorphous 2	0.1324	0	0	no visible plastic left

Table A2 – SIAF RDC Experiment 2: individual film recovery data

Two Weeks

Labeling	Condition	Film Mass (g)	Film Mass Recovered	%Mass Remaining	Observations
F1	Forks 1	0.2078	0.1501	72	entire film recovered, has lost weight
F2	Forks 2	0.1889	0.1554	82	entire film recovered, has lost weight
F3	Forks 3	0.1849	0.1417	77	entire film recovered, has lost weight
F4	Forks 4	0.1968	0.1928	98	entire film recovered, no lost weight
F5	Forks 5	0.1925	0.131	68	entire film recovered, has lost weight
C1	Crystalline 1	0.1398	0.0945	68	heavily fragmented
C2	Crystalline 2	0.1338	0.0802	60	heavily fragmented
C3	Crystalline 3	0.1396	0.0325	23	heavily fragmented
C4	Crystalline 4	0.1312	0	0	no film left to recover
C5	Crystalline 4	0.138	0	0	no film left to recover
A1	Amorphous 1	0.1326	0.132	100	fragmented, but mass recovered
A2	Amorphous 2	0.1269	0.124	98	fragmented, but mass recovered
A3	Amorphous 3	0.1311	0	0	no film left to recover
A4	Amorphous 4	0.1261	0.1221	97	fragmented, but mass recovered
A5	Amorphous 5	0.131	0.0417	32	heavily fragmented

Four Weeks

Labeling	Condition	Film Mass (g)	Film Mass Recovered	%Mass Remaining	Observations
F1	*Forks 1*	*0.1852*	0.1843	100	entire film recovered, no lost weight
F2	Forks 2	0.1701	0.1694	100	entire film recovered, no lost weight
F3	Forks 3	0.1623	0	0	no film left to recover
F4	*Forks 4*	*0.1754*	0.1704	97	entire film recovered, no lost weight
F5	Forks 5	0.1878	0.1854	99	entire film recovered, no lost weight
C1	Crystalline 1	0.1462	0	0	no film left to recover
C2	Crystalline 2	0.1373	0	0	no film left to recover
C3	*Crystalline 3*	*0.1335*	0	0	no film left to recover
C4	*Crystalline 4*	*0.1344*	0	0	no film left to recover
C5	Crystalline 5	0.1319	0	0	no film left to recover
A1	Amorphous 1	0.1321	0	0	powder visible
A2	*Amorphous 2*	*0.1287*	0	0	powder visible
A3	Amorphous 3	0.1307	0	0	powder visible
A4	*Amorphous 4*	*0.1379*	0	0	powder visible
A5	Amorphous 5	0.1442	0	0	no film left to recover

Six Weeks

Labeling	Condition	Film Mass (g)	Film Mass Recovered	%Mass Remaining	Observations
F1	Forks 1	0.1842	0		powder visible
F2	Forks 2	0.206	0		powder visible
F3	Forks 3	0.173	0.1712		entire film recovered, no lost weight
F4	*Forks 4*	*0.1779*	0		powder visible
C1	Crystalline 1	0.1467	0		no film left to recover
C2	Crystalline 3	0.1333	0		no film left to recover
C3	Crystalline 3	0.1303	0		no film left to recover
A1	*Amorphous 1*	*0.1301*	0.1292		fragmented but recovered
A2	Amorphous 2	0.1275	0		no film left to recover
A3	Amorphous 3	0.1304	0		no film left to recover
A4	Amorphous 4	0.1309	0		no film left to recover

Table A3 – Forks RDC Experiment (grouped-bag method): individual film recovery data

3 Weeks Labeling	Condition	Film Mass (g)	Film Mass Recovered	%Mass Remaining	Observations
F2	Forks 2	0.3208	0.2336	72.81795511	fragmented in long strands but recovered 70%
F3	Forks 3	0.2795	0.2856	102.1824687	almost fully intact
F4	Forks 4	0.2681	0.2628	98.0231257	almost fully intact
F5	Forks 5	0.2441	0.2441	100	almost fully intact
C1	Crystalline 1	0.1535	0	0	powderized - not recoverable but lots of them
C2	Crystalline 2	0.1546	0.0732	47.34799483	fragmented and partially recovered
C4	Crystalline 4	0.1484	0.0336	22.64150943	fragmented and partially recovered
A1	Amorphous 1	0.1427	0.1368	95.865452	fragmented but recovered
A2	Amorphous 2	0.1388		0	powderized - not recoverable but lots of them
A3	Amorphous 3	0.1236	0.0426	34.46601942	fragmented and partially recovered
A4	Amorphous 4	0.1227	0.13	105.9494703	fragmented and partially recovered
A5	Amorphous 5	0.1402	0.142	101.2838802	fragmented and partially recovered

6 Weeks

Labeling	Condition	Film Mass (g)	Film Mass Recovered	%Mass Remaining	Observations
F2	Forks 2	0.2049	0.1964	95.85163494	fragmented in long strands but recovered
F3	Forks 3	0.2101	0.2099	99.90480723	fragmented in long strands but recovered
F4	Forks 4	0.2892	0.2619	90.56016598	fragmented in long strands but recovered
C1	Crystalline 1	0.136	0	0	fragments - not recoverable but lots of them
C4	Crystalline 4	0.1394	0	0	fragments - not recoverable but lots of them
C5	Crystalline 5	0.1383	0	0	fragments - not recoverable but lots of them
A1	Amorphous 1	0.14	0	0	fragments - not recoverable but lots of them
A2	Amorphous 2	0.1186	0	0	fragments - not recoverable but lots of them
A3	Amorphous 3	0.1136	0	0	fragments - not recoverable but lots of them
A4	Amorphous 4	0.1813	0	0	fragments - not recoverable but lots of them

Figure A1 – Lightly fragmented PLA film with 100% recovery

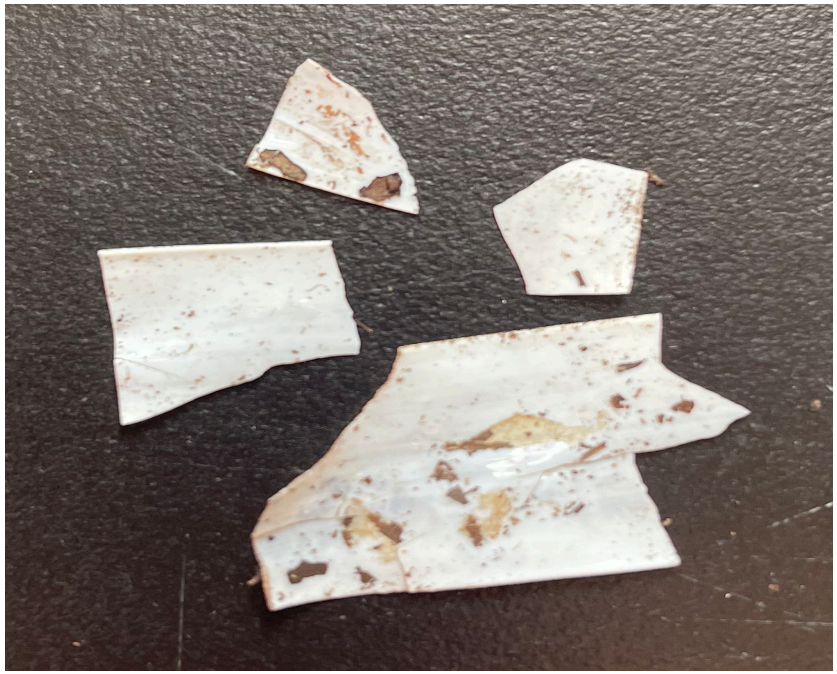

Figure A2 – Heavily fragmented/powderized PLA film with 22% recovery

Appendix B – Molecular weight and DSC raw outputs

Table B1 – Respirometer PLA Mv Data (30 °C Experiments)

30 °C Base Experiment (Crystallinity × Gelatin)

Experiment	Sample	Replicate	Mv (g·mol^{-1})
30 °C Experiment	Amorphous PLA	1	167,956
30 °C Experiment	Amorphous PLA	2	177,088
30 °C Experiment	Amorphous PLA	3	175,054
30 °C Experiment	Amorphous PLA + gelatin	1	155,099
30 °C Experiment	Amorphous PLA + gelatin	2	159,035
30 °C Experiment	Amorphous PLA + gelatin	3	154,163
30 °C Experiment	Annealed PLA	1	157,604
30 °C Experiment	Annealed PLA	2	162,209
30 °C Experiment	Annealed PLA	3	153,072
30 °C Experiment	Annealed PLA + gelatin	1	158,424
30 °C Experiment	Annealed PLA + gelatin	2	151,096
30 °C Experiment	Annealed PLA + gelatin	3	149,024

30 °C Inoculation Experiment

Experiment	Inoculum	Replicate	Mv ($g \cdot mol^{-1}$)
30 °C Inoculation Experiment	No inoculum	1	173,886
30 °C Inoculation Experiment	No inoculum	2	161,868
30 °C Inoculation Experiment	No inoculum	3	163,166
30 °C Inoculation Experiment	Consortium	1	158,326
30 °C Inoculation Experiment	Consortium	2	167,071
30 °C Inoculation Experiment	Consortium	3	169,173
30 °C Inoculation Experiment	*Microbacterium* sp. 3.7	1	202,769
30 °C Inoculation Experiment	*Microbacterium* sp. 3.7	2	178,657
30 °C Inoculation Experiment	*Microbacterium* sp. 3.7	3	179,355

Table B2 – SIAF RDC PLA Mv Data

Experiment	Material	Exposure	Condition	Mv (g·mol⁻¹)
SIAF RDC Exp. 1	Crystalline PLA	2 weeks	intact	47,300
SIAF RDC Exp. 1	Amorphous PLA	2 weeks	intact	99,374
SIAF RDC Exp. 1	Forks PLA	2 weeks	intact	82,668
SIAF RDC Exp. 1	Amorphous PLA	4 weeks	—	95,826
SIAF RDC Exp. 1	Forks PLA	4 weeks	—	70,354
SIAF RDC Exp. 1	Crystalline PLA	4 weeks	—	30,414
SIAF RDC Exp. 1	Amorphous PLA	6 weeks	intact	97,325
SIAF RDC Exp. 1	Forks PLA	6 weeks	—	31,663
SIAF RDC Exp. 1	Crystalline PLA	2 weeks	intact	32,893
SIAF RDC Exp. 2	Crystalline PLA	2 weeks	intact	22,983
SIAF RDC Exp. 2	Amorphous PLA	4 weeks	intact	9,024
SIAF RDC Exp. 2	Forks PLA	2 weeks	intact	11,776
SIAF RDC Exp. 2	Forks PLA	4 weeks	intact	14,914
SIAF RDC Exp. 2	Amorphous PLA	6 weeks	intact	7,614
SIAF RDC Exp. 2	Forks PLA	6 weeks	—	10,976
SIAF RDC Exp. 3	Sensor 1	—	—	144,419
SIAF RDC Exp. 3	Sensor 2	—	—	154,656
SIAF RDC Exp. 3	Sensor 6	—	—	147,176
SIAF RDC Exp. 3	Sensor 7	—	—	136,326

Table B3 – Forks RDC PLA Mv Data

Experiment	Material	Exposure	Replicate	Mv (g·mol^{-1})
Forks RDC Exp.	Forks PLA	3 weeks	1	107,215
Forks RDC Exp.	Forks PLA	3 weeks	2	110,439
Forks RDC Exp.	Forks PLA	3 weeks	3	111,092
Forks RDC Exp.	Forks PLA	6 weeks	1	31,614
Forks RDC Exp.	Forks PLA	6 weeks	2	22,483
Forks RDC Exp.	Forks PLA	6 weeks	3	32,457
Forks RDC Exp.	Amorphous PLA	3 weeks	—	94,049
Forks RDC Exp.	Crystalline PLA	3 weeks	—	95,642

Table B4 – UV-C Exposure PLA Mv Data

Structure is grouped by irradiance × exposure time, with replicates explicit.

1 h Exposure

Irradiance	Material	Replicate	Mv (g·mol^{-1})
High	Amorphous PLA	1	62,229
High	Amorphous PLA	2	58,344
High	Amorphous PLA	3	63,880
High	Crystalline PLA	1	57,947
High	Crystalline PLA	2	56,466
High	Crystalline PLA	3	61,211
High	Forks PLA	1	60,270
High	Forks PLA	2	59,612
High	Forks PLA	3	59,048
Low	Amorphous PLA	1	59,516
Low	Amorphous PLA	2	61,429
Low	Amorphous PLA	3	58,753
Low	Crystalline PLA	1	59,782
Low	Crystalline PLA	2	67,145
Low	Crystalline PLA	3	61,060
Low	Forks PLA	1	64,135
Low	Forks PLA	2	64,733
Low	Forks PLA	3	60,647

2 h Exposure

Irradiance	Material	Replicate	Mv (g·mol^{-1})
High	Amorphous PLA	1	42,965
High	Amorphous PLA	2	33,641
High	Amorphous PLA	3	38,992
High	Crystalline PLA	1	41,715
High	Crystalline PLA	2	42,098
High	Crystalline PLA	3	42,726
High	Forks PLA	1	40,093
High	Forks PLA	2	51,104
High	Forks PLA	3	32,343
Low	Amorphous PLA	1	38,374
Low	Amorphous PLA	2	37,861
Low	Amorphous PLA	3	40,925
Low	Crystalline PLA	1	45,537
Low	Crystalline PLA	2	43,891
Low	Crystalline PLA	3	47,675
Low	Forks PLA	1	47,957
Low	Forks PLA	2	63,068
Low	Forks PLA	3	59,962

8 h Exposure

Irradiance	Material	Replicate	Mv (g·mol^{-1})
High	Amorphous PLA	1	15,735
High	Amorphous PLA	2	15,384
High	Amorphous PLA	3	16,950
High	Crystalline PLA	1	16,248
High	Crystalline PLA	2	20,883
High	Crystalline PLA	3	17,703
High	Forks PLA	1	16,755
High	Forks PLA	2	14,115
High	Forks PLA	3	17,940
Low	Amorphous PLA	1	15,593
Low	Amorphous PLA	2	14,044
Low	Amorphous PLA	3	12,928
Low	Crystalline PLA	1	19,691
Low	Crystalline PLA	2	15,829
Low	Crystalline PLA	3	13,067
Low	Forks PLA	1	21,648
Low	Forks PLA	2	19,670
Low	Forks PLA	3	19,126

24 h Exposure

Irradiance	Material	Replicate	Mv (g·mol^{-1})
High	Amorphous PLA	1	8,534
High	Amorphous PLA	2	10,254
High	Amorphous PLA	3	8,571
High	Crystalline PLA	1	11,845
High	Crystalline PLA	2	13,496
High	Crystalline PLA	3	13,974
High	Forks PLA	1	7,914
High	Forks PLA	2	12,326
High	Forks PLA	3	12,441
Low	Amorphous PLA	1	10,918
Low	Amorphous PLA	2	9,847
Low	Amorphous PLA	3	11,060
Low	Crystalline PLA	1	12,101
Low	Crystalline PLA	2	15,323
Low	Crystalline PLA	3	12,920
Low	Forks PLA	1	12,046
Low	Forks PLA	2	13,719
Low	Forks PLA	3	13,766

Table B5 – DSC outputs for composted PLA samples

Sample	Tg, 1st heating (°C)	Tg, 2nd heating (°C)	Tm (°C)	Tcc (°C)	Net ΔH (J/g)	Xc (%)
Annealed Untreated	65	58.8	176.54	—	44.33	47.62
Forks Untreated	64.9	58.4	149.72	—	37.62	40.41
FBE2 3w	69.6	55.9	150.61	—	19.06	20.47
FBE2 6w	67.6	49.7	153.44	—	46.33	49.76
SBE1 4w A	67.1	49.5	171.56	—	39.14	42.05
SBE1 4w C	62.7	54.4	171.79	—	62.38	67
SBE1 4w F	63.8	51.5	153.18	—	35.38	38

Table B6 – DSC outputs for UV-treated PLA samples

Sample	Tg, 1st heating (°C)	Tg, 2nd heating (°C)	Tm (°C)	Tcc (°C)	Net ΔH (J/g)	Xc (%)
APLA 8hr	51.5	48.8	157.47	100.13	-2.55	0
APLA 24hr	45.7	39.3	139.79	100.79	7.94	8.53
CPLA 1hr	55.6	56.6	173.12	—	45.87	49.27
CPLA 2hr	54.8	55.8	171.79	—	47.5	51.02
CPLA 8hr	47.9	49.9	161.7	—	58.68	63.03
CPLA 24hr	43.4	43.8	153.43	—	46.16	49.58
FPLA 8hr	50.5	51.6	146.38	—	47	50.49
FPLA 24hr	45.8	44.1	139.65	—	47.71	51.25

Figure B7 – DSC first heating thermograms of amorphous PLA films after 8 and 24 hours of UV-C exposure

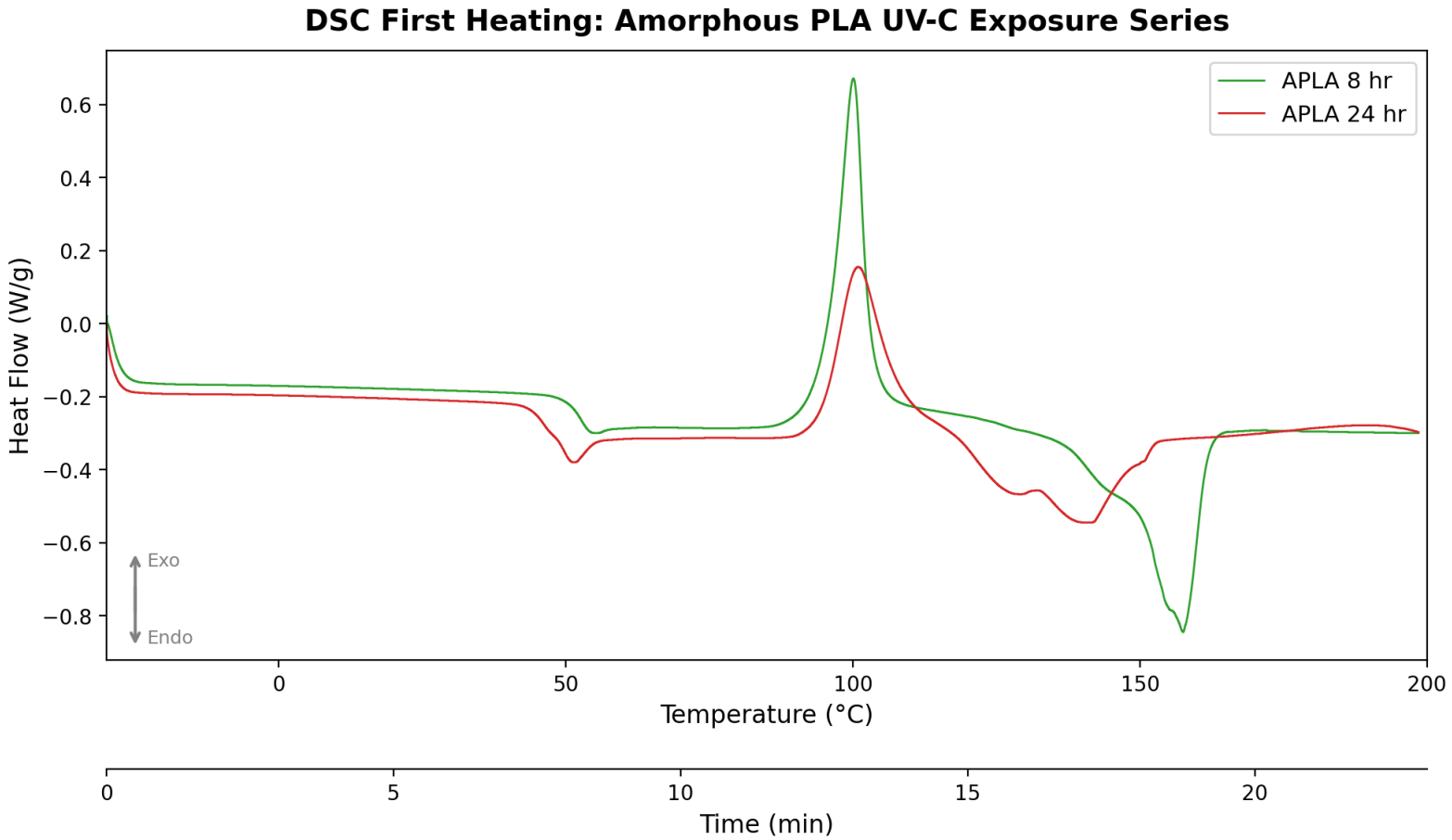

Figure B8 – DSC first heating thermograms of crystalline (annealed) PLA films after 0, 1, 2, 8, and 24 hours of UV-C exposure

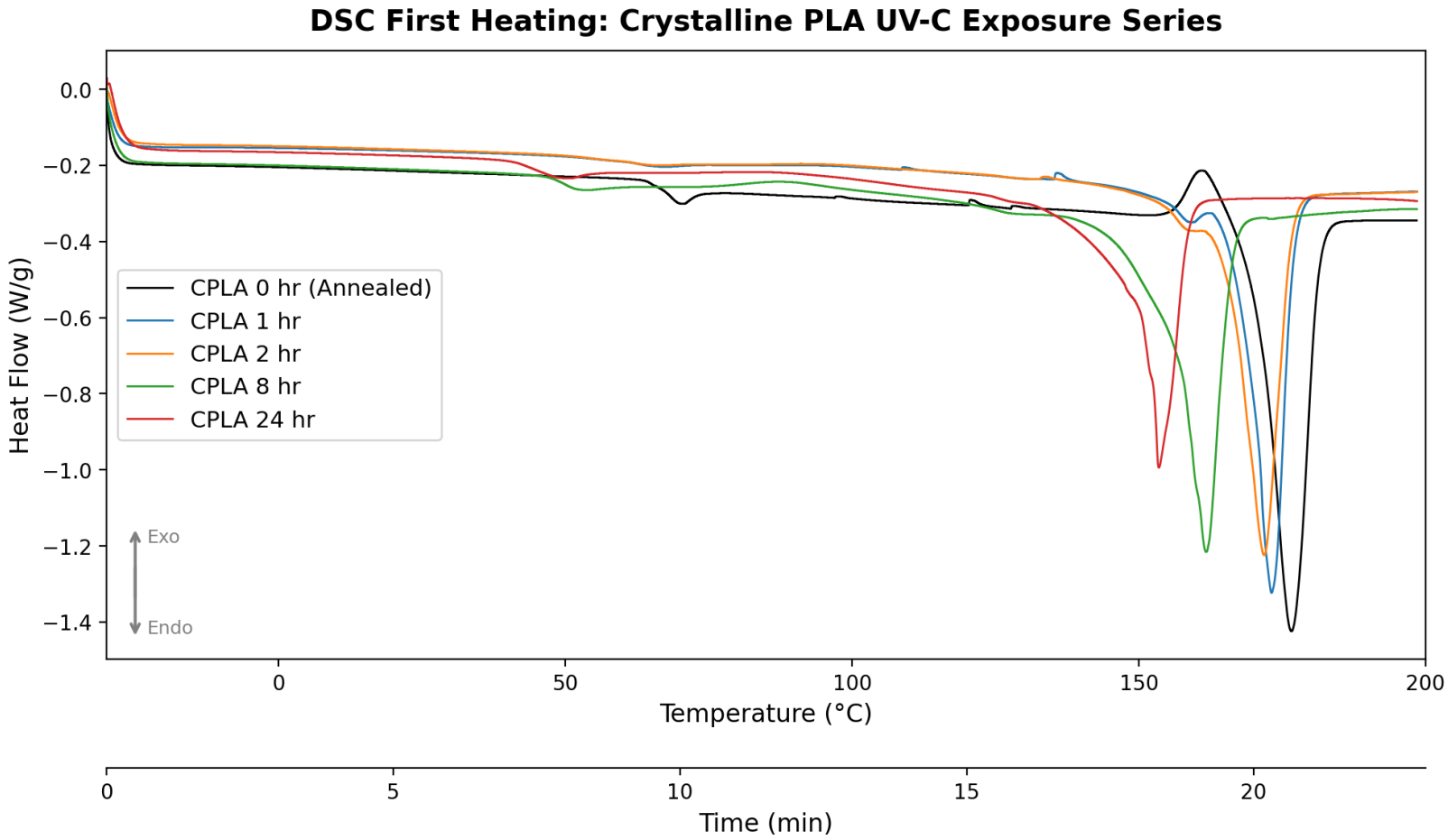

Figure B9 – DSC first heating thermograms of Forks PLA films after 0, 8, and 24 hours of UV-C exposure

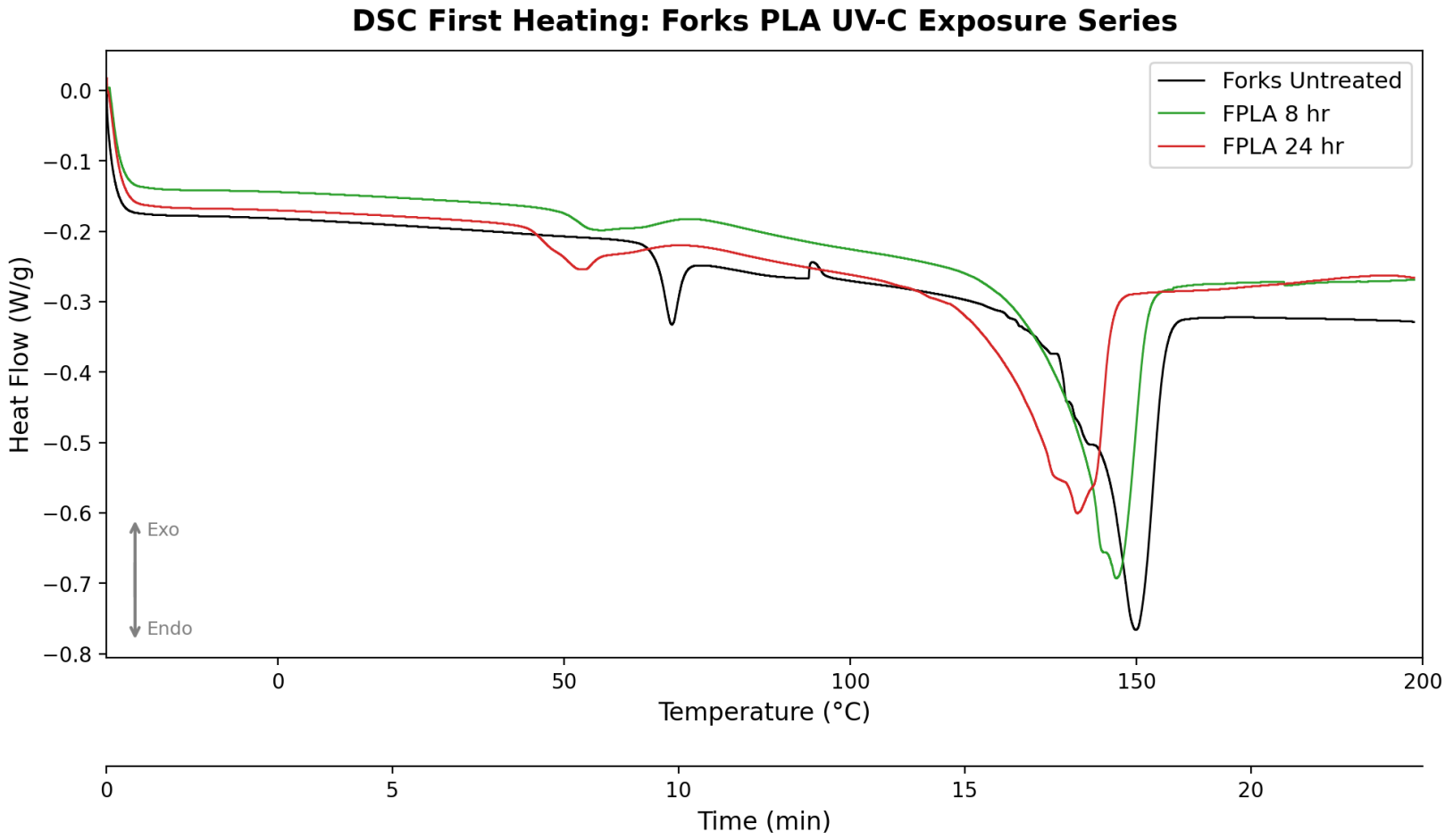

Figure B10 – DSC first heating thermograms of Forks PLA samples before and after 3 and 6 weeks in the Forks RDC

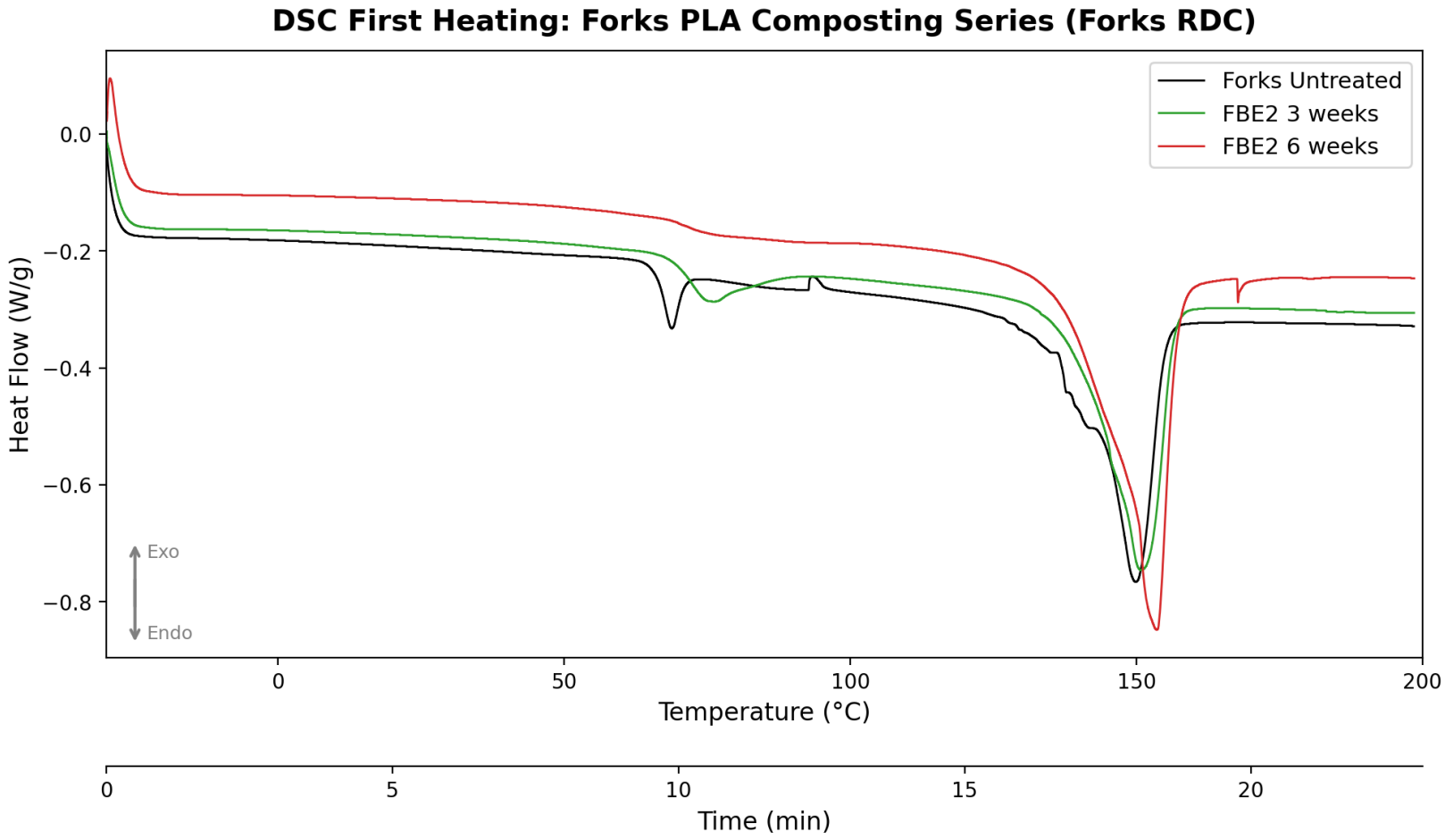

Figure B11 – DSC first heating thermograms of crystalline PLA recovered after 4 weeks in the SIAF RDC (SBE1 4w C).

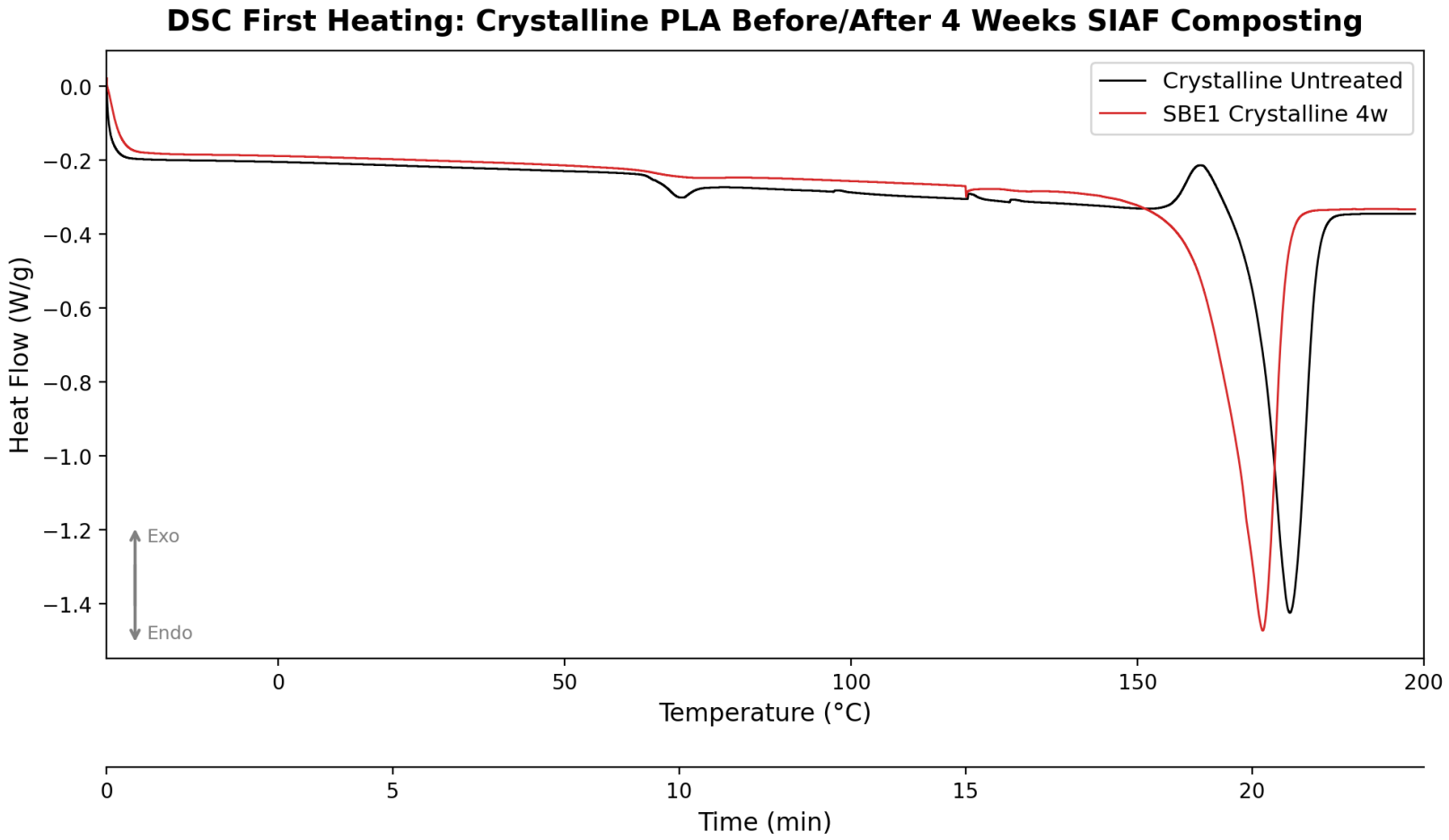

Figure B12 – DSC first heating thermograms of Forks PLA recovered after 4 weeks in the SIAF RDC (SBE1 4w F).

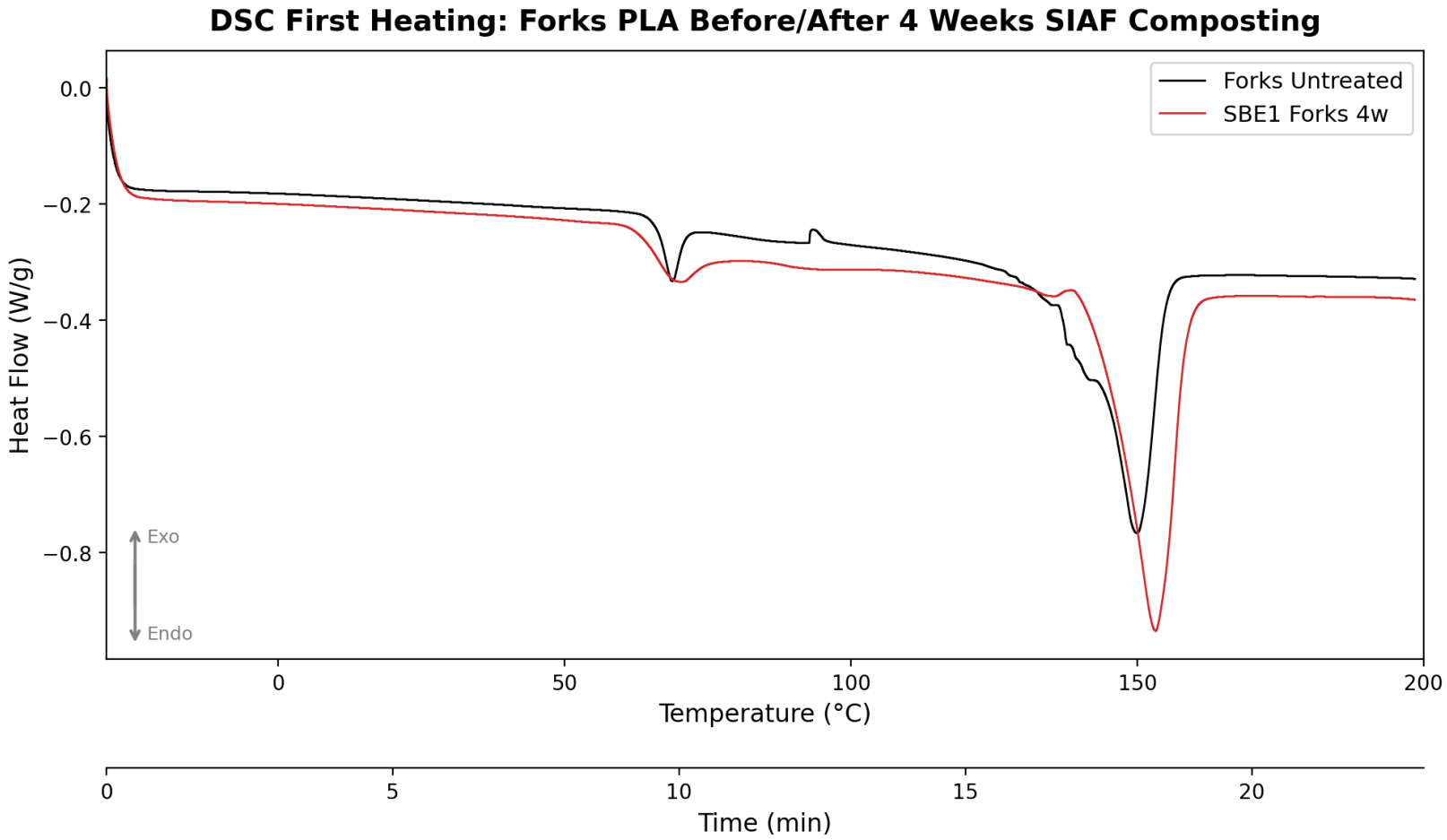

Figure B13 – DSC first heating thermogram of amorphous PLA recovered after 4 weeks in the SIAF RDC (SBE1 4w A).

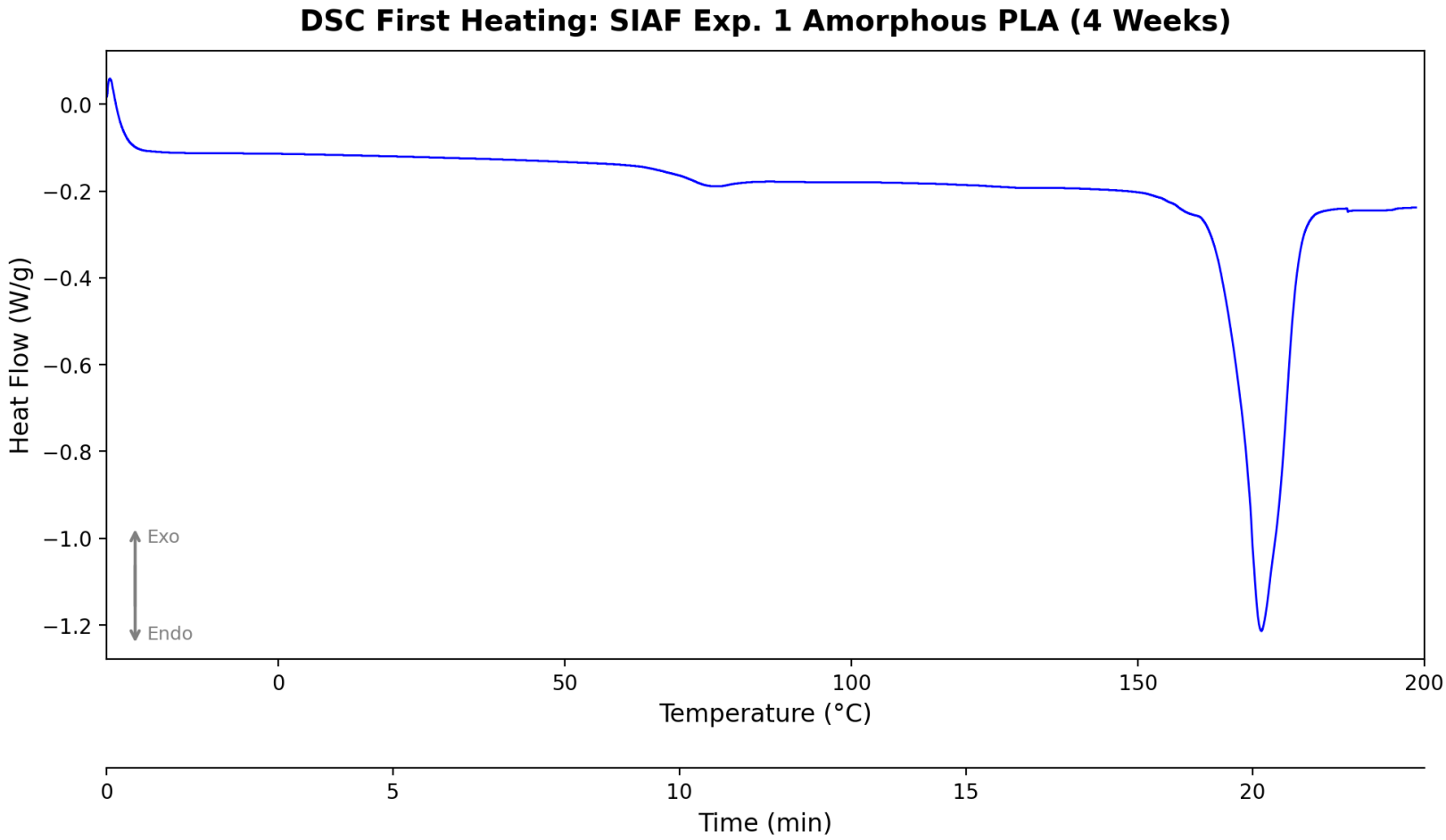

Appendix C – RDC Temperature Data

Table C1 – SIAF RDC Experiment 1 Daily Internal Temperature Data

Date	Day	Temp (°C)
2025-07-17	1	35
2025-07-18	2	39
2025-07-19	3	59
2025-07-20	4	61
2025-07-21	5	57
2025-07-22	6	51
2025-07-23	7	46
2025-07-24	8	50
2025-07-25	9	45
2025-07-26	10	49
2025-07-27	11	51
2025-07-28	12	47
2025-07-29	13	47
2025-07-30	14	40
2025-07-31	15	26
2025-08-01	16	28
2025-08-02	17	26
2025-08-03	18	23
2025-08-04	19	24
2025-08-05	20	25
2025-08-06	21	35
2025-08-07	22	45
2025-08-08	23	47
2025-08-09	24	55
2025-08-10	25	56
2025-08-11	26	54
2025-08-12	27	51
2025-08-13	28	49
2025-08-14	29	45
2025-08-15	30	45

2025-08-16	31	41
2025-08-17	32	40
2025-08-18	33	49
2025-08-19	34	54
2025-08-20	35	55
2025-08-21	36	56
2025-08-22	37	60
2025-08-23	38	55
2025-08-24	39	49
2025-08-25	40	44
2025-08-26	41	42
2025-08-27	42	42

Table C2 – SIAF RDC Experiment 2 Daily Internal Temperature Data

Date	**Day**	**Temp (°C)**
2025-09-18	1	20
2025-09-19	2	30
2025-09-20	3	41
2025-09-21	4	45
2025-09-22	5	46
2025-09-23	6	47
2025-09-24	7	51
2025-09-25	8	53
2025-09-26	9	51
2025-09-27	10	56
2025-09-28	11	55
2025-09-29	12	53
2025-09-30	13	52
2025-10-01	14	54
2025-10-02	15	51
2025-10-03	16	48
2025-10-04	17	46
2025-10-05	18	45

2025-10-06	19	40
2025-10-07	20	46
2025-10-08	21	49
2025-10-09	22	51
2025-10-10	23	52
2025-10-11	24	55
2025-10-12	25	57
2025-10-13	26	53
2025-10-14	27	54
2025-10-15	28	48
2025-10-16	29	42
2025-10-17	30	39
2025-10-18	31	45
2025-10-19	32	48
2025-10-20	33	50
2025-10-21	34	54
2025-10-22	35	55
2025-10-23	36	55
2025-10-24	37	53
2025-10-25	38	51
2025-10-26	39	50
2025-10-27	40	45
2025-10-28	41	44
2025-10-29	42	40

Table C3 – Forks RDC Experiment 2 Daily Internal Temperature Data

Date	**Chamber 1**	**Chamber 2**	**Chamber 3**
First three weeks			
9/25/2025	47	48	49
9/26/2025	46	45	42
9/27/2025	46	45	41
9/29/2025	44	42	39
October 1 2025	56	49	46
October 2 2025	55	50	45
October 8 2025	54	56	52
10-Oct	65	60	50
11-Oct	60	60	45
13-Oct	50	45	30
10/15/2025	42	40	37
Second three weeks			
10/20/2025	60	54	43
10/21/2025	54	54	43
10/22/2025	61	62	52
10/23/2025	60	63	54
10/24/2025	58	63	50
18-Oct	60	55	50
10/26/2025	64	60	48
19-Oct	65	65	50
25-Oct	65	60	55
10/27/2025	63	61	54
10/28/2025	58	47	43
10/29/2025	51	55	42
10/30/2025	47	57	43
01-Nov	40	40	40
10/2/2025	39	42	36
11/4/2025	44	45	39
11/5/2025	46	46	49
07-Nov	60	65	50
11/6/2025	61	52	50

Appendix D – Statistical outputs and calculation examples

Table D1 – Two-way ANOVA (58 °C respirometer)

Source	SS	DF	MS	F	P-value
Interaction	236.8	2	118.4	F(2,12) = 0.4566	0.6440
Row Factor (Gelatin)	320.0	1	320.0	F(1,12) = 1.234	0.2884
Column Factor (Substrate)	5777.0	2	2889.0	F(2,12) = 11.14	0.0018
Residual	3112.0	12	259.4		

Table D2 – One-way ANOVA (30 °C respirometer)

Condition	n	Mean CO2 (mg)	SD (mg)
Cellulose	3	122976	1116
Neg. Control	2	111843	540
Annealed PLA	3	114396	4215
Amorphous PLA	2	108538	6043
Cellulose + Gelatin	3	120621	1451
Neg. Control + Gelatin	3	113898	2805
Annealed PLA + Gelatin	3	109844	1312
Amorphous PLA + Gelatin	3	111112	4563

One-Way ANOVA (All Conditions)

Source	F	p-value	Significant
Between conditions	F(7, 14) = 7.347	0.0008	Yes

Table D3 – One-way ANOVA (30 °C inoculation experiment)

Treatment	n	Mean CO2 (mg)	SD (mg)
Neg. Control	3	107258	4117
Uninoculated PLA	3	111691	6698
Consortium 1	3	114057	4346
CA4	3	110750	2589

CA1	3	106444	4826
Strain 3.7	3	99333	2989
Strain 2.5	3	109379	3949
Strain 2.3	3	109048	3265

One-Way ANOVA (All Conditions Including Neg. Control)

Source	F	p-value	Significant
Between treatments	F(7, 16) = 3.220	0.025	Yes
Strain 2.3 vs Uninoculated	-0.758	0.9526	No

Table D4 – Tukey HSD pairwise comparisons (58 °C)

Comparison	P-value	Significant?
No Gelatin:Cellulose vs. No Gelatin:Annealed PLA	0.3662	No
No Gelatin:Cellulose vs. No Gelatin:Amorphous PLA	0.0264	Yes (*)
No Gelatin:Cellulose vs. Gelatin:Cellulose	0.9541	No
No Gelatin:Cellulose vs. Gelatin:Annealed PLA	0.0592	No
No Gelatin:Cellulose vs. Gelatin:Amorphous PLA	0.0319	Yes (*)
No Gelatin:Annealed PLA vs. No Gelatin:Amorphous PLA	0.5696	No
No Gelatin:Annealed PLA vs. Gelatin:Cellulose	0.8183	No
No Gelatin:Annealed PLA vs. Gelatin:Annealed PLA	0.8305	No
No Gelatin:Annealed PLA vs. Gelatin:Amorphous PLA	0.6334	No
No Gelatin:Amorphous PLA vs. Gelatin:Cellulose	0.1067	No
No Gelatin:Amorphous PLA vs. Gelatin:Annealed PLA	0.9960	No
No Gelatin:Amorphous PLA vs. Gelatin:Amorphous PLA	>0.9999	No
Gelatin:Cellulose vs. Gelatin:Annealed PLA	0.2238	No
Gelatin:Cellulose vs. Gelatin:Amorphous PLA	0.1274	No
Gelatin:Annealed PLA vs. Gelatin:Amorphous PLA	0.9989	No

Table D5 – Tukey HSD pairwise comparisons (30 °C)

Comparison	p-value	Significant
Cellulose vs Neg. Control	0.0278	Yes
Cellulose vs Annealed PLA	0.0714	No
Cellulose vs Amorphous PLA	0.0036	Yes

Cellulose vs Cellulose+Gel	0.9796	No
Cellulose vs Neg. Control+Gel	0.051	No
Cellulose vs Annealed+Gel	0.0031	Yes
Cellulose vs Amorphous+Gel	0.0073	Yes
Neg. Control vs Annealed PLA	0.9829	No
Neg. Control vs Amorphous PLA	0.9584	No
Neg. Control vs Cellulose+Gel	0.1156	No
Neg. Control vs Neg. Control+Gel	0.9951	No
Neg. Control vs Annealed+Gel	0.9958	No
Neg. Control vs Amorphous+Gel	1	No
Annealed PLA vs Amorphous PLA	0.4972	No
Annealed PLA vs Cellulose+Gel	0.3062	No
Annealed PLA vs Neg. Control+Gel	1	No
Annealed PLA vs Annealed+Gel	0.6509	No
Annealed PLA vs Amorphous+Gel	0.8948	No
Amorphous PLA vs Cellulose+Gel	0.0154	Yes
Amorphous PLA vs Neg. Control+Gel	0.5963	No
Amorphous PLA vs Annealed+Gel	0.9997	No
Amorphous PLA vs Amorphous+Gel	0.9821	No
Cellulose+Gel vs Neg. Control+Gel	0.2315	No
Cellulose+Gel vs Annealed+Gel	0.0157	Yes
Cellulose+Gel vs Amorphous+Gel	0.0379	Yes
Neg. Control+Gel vs Annealed+Gel	0.7591	No
Neg. Control+Gel vs Amorphous+Gel	0.9512	No
Annealed+Gel vs Amorphous+Gel	0.9995	No

Compact Letter Display

Condition	Group
Cellulose	a
Cellulose + Gelatin	a b
Annealed PLA	a b
Neg. Control + Gelatin	b
Neg. Control	b
Amorphous PLA + Gelatin	b
Annealed PLA + Gelatin	b
Amorphous PLA	b

Table D6 – Tukey HSD pairwise comparisons (inoculated study)

Comparison	p-value	Significant
Neg. Control vs No Inoc	0.8966	No
Neg. Control vs Consort1	0.5398	No
Neg. Control vs CA4	0.9675	No
Neg. Control vs CA1	1	No
Neg. Control vs Strain 3.7	0.3633	No
Neg. Control vs Strain 2.5	0.9982	No
Neg. Control vs Strain 2.3	0.9994	No
No Inoc vs Consort1	0.9965	No
No Inoc vs CA4	1	No
No Inoc vs CA1	0.7944	No
No Inoc vs Strain 3.7	0.0428	Yes
No Inoc vs Strain 2.5	0.997	No
No Inoc vs Strain 2.3	0.9932	No
Consort1 vs CA4	0.9757	No
Consort1 vs CA1	0.4088	No
Consort1 vs Strain 3.7	0.0116	Yes
Consort1 vs Strain 2.5	0.8697	No
Consort1 vs Strain 2.3	0.8278	No
CA4 vs CA1	0.9093	No
CA4 vs Strain 3.7	0.0708	No
CA4 vs Strain 2.5	0.9999	No
CA4 vs Strain 2.3	0.9996	No
CA1 vs Strain 3.7	0.4881	No
CA1 vs Strain 2.5	0.9875	No
CA1 vs Strain 2.3	0.9938	No
Strain 3.7 vs Strain 2.5	0.142	No
Strain 3.7 vs Strain 2.3	0.1666	No
Strain 2.5 vs Strain 2.3	1	No

Compact Letter Display

Condition	Group
Consortium 1	a

Uninoculated	a b
CA4	a b
Strain 2.5	a b
Strain 2.3	a b
Neg. Control	a b
CA1	a b
Strain 3.7	b

Dunnett's Test (vs. Uninoculated Control)

Comparison	Test Statistic	p-value
Neg. Control vs Uninoculated	-1.272	0.6825
Consortium 1 vs Uninoculated	0.679	0.9722
CA4 vs Uninoculated	-0.27	0.9999
CA1 vs Uninoculated	-1.505	0.5269
Strain 3.7 vs Uninoculated	-3.544	0.0146
Strain 2.5 vs Uninoculated	-0.663	0.9753
Strain 2.3 vs Uninoculated	-0.758	0.9526

Table D7 – Two-way ANOVA on Mv - 30 °C Experiment (Crystallinity × Gelatin)

Source	SS	df	MS	F	p-value
Crystallinity	270427096.3	1	270427096.3	14.436	0.0052
Gelatin	364563680.3	1	364563680.3	19.461	0.0023
Crystallinity × Gelatin	116937633.3	1	116937633.3	6.242	0.037
Residual	149866448.7	8	18733306.1		
Group Means					
Group	**Mean Mv (g/mol)**	**SD**			
Amorphous PLA	173366	4794			
Amorphous PLA + Gelatin	156099	2585			

Annealed PLA	157628	4569			
Annealed PLA + Gelatin	152848	4939			

Table D8 – Tukey HSD pairwise comparisons on Mv (30 °C Experiment)

Comparison	**Mean Difference**	**Adjusted p-value**	**Significant**
Amorphous PLA vs Amorphous PLA + Gelatin	-17267	0.0053	Yes
Amorphous PLA vs Annealed PLA	-15738	0.0092	Yes
Amorphous PLA vs Annealed PLA + Gelatin	-20518	0.0018	Yes
Amorphous PLA + Gelatin vs Annealed PLA	1529	0.9711	No
Amorphous PLA + Gelatin vs Annealed PLA + Gelatin	-3251	0.7954	No
Annealed PLA vs Annealed PLA + Gelatin	-4780	0.5586	No

Table D9 – One-way ANOVA on Mv - 30 °C Inoculation Experiment

Source	**SS**	**df**	**MS**	**F**	**p-value**
Treatment	914400260.2	2	457200130.1	5.177	0.0494
Residual	529892503.3	6	88315417.2		
Note: p = 0.049 is borderline. Alexander-Govern test (robust to unequal variances) gives p = 0.25.					
No pairwise comparison reached significance after Tukey HSD correction (all p > 0.06).					
Group	**Mean Mv (g/mol)**	**SD**			
No inoculum	166307	6596			
Consortium	164857	5753			
Strain 3.7	186927	13724			

Table D10 – Welch's t-test on Mv - Forks RDC (3 vs 6 weeks)

Timepoint	n	Mean Mv (g/mol)	SD
3 weeks	3	109582	2076
6 weeks	3	28851	5531
t-statistic	23.668		
df	4		
p-value	< 0.001		

Table D11 – Two-way ANOVA on Mv - UV-C 1h exposure (Material × Irradiance)

Source	SS	df	MS	F	p-value
Material	2338755.1	2	1169377.6	0.192	0.828
Irradiance	18388069.4	1	18388069.4	3.015	0.1081
Material × Irradiance	29527933.8	2	14763966.9	2.421	0.1309
Residual	73189628	12	6099135.7		
Material Means					
Material	**Mean Mv (g/mol)**				
Amorphous	60692				
Crystalline	60602				
Forks	61408				
Irradiance Means					
Irradiance	**Mean Mv (g/mol)**				
High	59890				
Low	61911				

Table D12 – Two-way ANOVA on Mv - UV-C 2h exposure (Material × Irradiance)

Source	SS	df	MS	F	p-value
Material	317950780.1	2	158975390.1	5.27	0.0228
Irradiance	197163462.7	1	197163462.7	6.535	0.0252

Material × Irradiance	197045828.8	2	98522914.4	3.266	0.0737
Residual	362021768.7	12	30168480.7		
Material Means					
Material	**Mean Mv (g/mol)**				
Amorphous	38793				
Crystalline	43940				
Forks	49088				
Irradiance Means					
Irradiance	**Mean Mv (g/mol)**				
High	40631				
Low	47250				

Table D13 – Two-way ANOVA on Mv - UV-C 8h exposure (Material × Irradiance)

Source	**SS**	**df**	**MS**	**F**	**p-value**
Material	30235314.3	2	15117657.2	3.665	0.0572
Irradiance	760.5	1	760.5	0	0.9894
Material × Irradiance	34110736.3	2	17055368.2	4.134	0.0431
Residual	49501977.3	12	4125164.8		
Material Means					
Material	**Mean Mv (g/mol)**				
Amorphous	15106				
Crystalline	17237				
Forks	18209				
Irradiance Means					
Irradiance	**Mean Mv (g/mol)**				
High	16857				

Low	16844				

Table D14 – Two-way ANOVA on Mv - UV-C 24h exposure (Material × Irradiance)

Source	**SS**	**df**	**MS**	**F**	**p-value**
Material	35800678.8	2	17900339.4	8.212	0.0057
Irradiance	8466612.5	1	8466612.5	3.884	0.0723
Material × Irradiance	2854470.3	2	1427235.2	0.655	0.5372
Residual	26158816	12	2179901.3		
Material Means					
Material	**Mean Mv (g/mol)**				
Amorphous	9864				
Crystalline	13276				
Forks	12035				
Irradiance Means					
Irradiance	**Mean Mv (g/mol)**				
High	11039				
Low	12411				

Table D15 – Tukey HSD pairwise comparisons on Material (UV-C, 24 h)

Comparison	**Mean Difference**	**Adjusted p-value**	**Significant**
Amorphous vs Crystalline	3412	0.0053	Yes
Amorphous vs Forks	2171	0.0751	No
Crystalline vs Forks	-1241	0.3857	No

Table D16 – Unconstrained kinetic model parameters

Unconstrained Fit of Cellulose Inducer

PLA degradation	
Best-fit values	
Lag	-3.24
Cmax	205.9
k	0.009463
95% CI (profile likelihood)	
Lag	-7.239 to -0.6603
Cmax	111.7 to ???
k	-0.003310 to 0.02248
Goodness of Fit	
Degrees of Freedom	43
R squared	0.9485
Sum of Squares	1040
Sy.x	4.918
Number of points	
# of X values	46
# Y values analyzed	46

Unconstrained Fit of Cellulose Untreated

	Biodegradation (%)
PLA degradation	
Best-fit values	
Lag	10.91
Cmax	62.56
k	0.09854
95% CI (profile likelihood)	
Lag	10.13 to 11.83
Cmax	59.04 to 66.52
k	0.08000 to 0.1259
Goodness of Fit	
Degrees of Freedom	43
R squared	0.9842
Sum of Squares	418.8
Sy.x	3.121
Number of points	
# of X values	46
# Y values analyzed	46

Unconstrained Fit of Amorphous PLA Inducer

	Biodegradation (%)
PLA degradation	
Best-fit values	
Lag	18.71
Cmax	122.6
k	0.1089

Unconstrained Fit of Amorphous PLA Untreated

	Biodegradation (%)
PLA degradation	
Best-fit values	
Lag	19.65
Cmax	138.7
k	0.06859

95% CI (profile likelihood)	
Lag	17.39 to 20.26
Cmax	110.7 to 137.5
k	0.07535 to 0.1632
Goodness of Fit	
Degrees of Freedom	43
R squared	0.9663
Sum of Squares	2932
Sy.x	8.258
Number of points	
# of X values	46
# Y values analyzed	46

Unconstrained Fit of Annealed PLA Inducer

	Biodegradation (%)
PLA degradation	
Best-fit values	
Lag	19.59
Cmax	125
k	0.08685
95% CI (profile likelihood)	
Lag	18.26 to 20.82
Cmax	112.5 to 148.8
k	0.05710 to 0.1258
Goodness of Fit	
Degrees of Freedom	43
R squared	0.9728
Sum of Squares	2103
Sy.x	6.993

95% CI (profile likelihood)	
Lag	19.12 to 20.45
Cmax	128.4 to 153.0
k	0.05603 to 0.08711
Goodness of Fit	
Degrees of Freedom	43
R squared	0.994
Sum of Squares	502.6
Sy.x	3.419
Number of points	
# of X values	46
# Y values analyzed	46

Unconstrained Fit of Annealed PLA Untreated

	Biodegradation (%)
PLA degradation	
Best-fit values	
Lag	21.72
Cmax	97.58
k	0.1193
95% CI (profile likelihood)	
Lag	20.42 to 22.95
Cmax	86.71 to 116.2
k	0.07452 to 0.1854
Goodness of Fit	
Degrees of Freedom	43
R squared	0.9653
Sum of Squares	2706
Sy.x	7.933

Number of points	
# of X values	46
# Y values analyzed	46

Number of points	
# of X values	46
# Y values analyzed	46

Table D17 – Constrained kinetic model parameters

Constrained Fit of Amorphous PLA Inducer	Biodegradation (%)
PLA degradation	
Best-fit values	
Lag	18.76
Cmax	100
k	0.1123
95% CI (profile likelihood)	
Lag	???
Cmax	86.39 to ???
k	0.09061 to ???
Goodness of Fit	
Degrees of Freedom	43
R squared	0.8915
Sum of Squares	9456
Sy.x	14.83

Constrained Fit of Amorphous PLA Untreated	Biodegradation (%)
PLA degradation	
Best-fit values	
Lag	20.87
Cmax	100
k	0.1407
95% CI (profile likelihood)	
Lag	20.00 to 22.70
Cmax	97.90 to ???
k	0.1297 to ???
Goodness of Fit	
Degrees of Freedom	43
R squared	0.9741
Sum of Squares	2180
Sy.x	7.12

Constraints		Constraints	
Cmax	Cmax < 100.00001	Cmax	Cmax < 100.00001

Number of points		Number of points	
# of X values	46	# of X values	46
# Y values analyzed	46	# Y values analyzed	46

Constrained Fit of Annealed PLA Inducer

	Biodegradation (%)
PLA degradation	Hit constraint
Best-fit values	
Lag	20.69
Cmax	~ 100.0
k	0.1612
95% CI (profile likelihood)	
Lag	19.64 to 21.95
Cmax	
k	0.1362 to ???
Goodness of Fit	
Degrees of Freedom	43
R squared	0.9588
Sum of Squares	3177
Sy.x	8.596
Constraints	
Cmax	Cmax < 100.00001
Number of points	
# of X values	46
# Y values analyzed	46

D18 – CO_2 → % biodegradation calculation example for Annealed PLA (Experiment 1)

STEP 1: Define Parameters

```
%C in CO₂ = 0.2729 (ratio of molecular weights: 12/44)
TOC value = 0.5 for PLA (50% carbon content)
Sample mass = 5 g
Moisture content = 5%
% dry weight = (1 - Moisture Content%/100) = (1 - 5/100) = 0.95
```

STEP 2: Calculate Theoretical Carbon Content (C_i)

C_i = TOC value × Sample mass (g) × % dry weight × 1000

$C_i = 0.5 \times 5 \times 0.95 \times 1000$

$C_i = 2375$ mg C

STEP 3: Obtain Raw CO_2 Evolution Data at Day 45

Negative control vessels (compost only):
- Channel 2: 72,499.21 mg CO_2
- Channel 6: 68,276.14 mg CO_2
- Channel 10: 71,723.48 mg CO_2

Annealed PLA vessels (sample + compost):
- Channel 3: 78,474.16 mg CO_2
- Channel 7: 78,305.24 mg CO_2
- Channel 11: 79,380.18 mg CO_2

STEP 4: Calculate Negative control Average

CO_2 negative control avg = (72,499.21 + 68,276.14 + 71,723.48) / 3

CO_2 negative control avg = 70,832.94 mg CO_2

STEP 5: Calculate % Biodegradation for Each Replicate

Formula:

$$\%\ \text{biodeg} = \frac{(\%C \text{ in } CO_2) \times (CO_2 \text{ sample} - CO_2 \text{ negative control avg})}{C_i} \times 100$$

Replicate 1 (Channel 3):

$$\%\ \text{biodeg} = \frac{0.2729 \times (78{,}474.16 - 70{,}832.94)}{2375} \times 100$$

$$= \frac{0.2729 \times 7{,}641.22}{2375} \times 100$$

$$= \frac{2{,}085.29}{2375} \times 100 = 87.8\%$$

Replicate 2 (Channel 7):

$$\%\ \text{biodeg} = \frac{0.2729 \times (78{,}305.24 - 70{,}832.94)}{2375} \times 100$$

$$= \frac{0.2729 \times 7{,}472.30}{2375} \times 100$$

$$= \frac{2{,}039.19}{2375} \times 100 = 85.9\%$$

Replicate 3 (Channel 11):

$$\%\ \text{biodeg} = \frac{0.2729 \times (79{,}380.18 - 70{,}832.94)}{2375} \times 100$$

$$= \frac{0.2729 \times 8{,}547.24}{2375} \times 100$$

$$= \frac{2{,}332.54}{2375} \times 100 = 98.2\%$$

STEP 6: Calculate Mean and Standard Deviation

Mean:

$$\text{Mean} = (87.8 + 85.9 + 98.2) / 3 = 90.6\%$$

Standard Deviation (population):

$$SD = \sqrt{\frac{(x_1 - \bar{x})^2 + (x_2 - \bar{x})^2 + (x_3 - \bar{x})^2}{n}}$$

Where $\bar{x} = 90.6\%$

$$(x_1 - \bar{x})^2 = (87.8 - 90.6)^2 = (-2.8)^2 = 7.97$$
$$(x_2 - \bar{x})^2 = (85.9 - 90.6)^2 = (-4.8)^2 = 22.70$$
$$(x_3 - \bar{x})^2 = (98.2 - 90.6)^2 = (7.6)^2 = 57.57$$

Sum of squared deviations = 88.24

$$SD = \sqrt{(88.24 / 3)} = \sqrt{29.41} = 5.4\%$$

Annealed PLA Biodegradation at Day 45 = 91 ± 5.4%

D19 – Intrinsic viscosity → Mark–Houwink molecular weight calculation example for Amorphous PLA (baseline)

STEP 1: Define parameters

Solvent: Chloroform

- Temperature: 25 °C
- Solvent flow time (t_0): 43.0 s

Mark–Houwink constants (PLA in chloroform, 25 °C):

- $K = 6.06 \times 10^{-4}$ dL/g
- $a = 0.64$

Mark–Houwink equation: $[\eta] = K \cdot M^a$

- Rearranged: **M = ([η]/K)^(1/a)**

STEP 2: Define solution concentrations

Sample mass and solvent volume:

- 15 mg in 15 mL → 1.00 mg/mL
- 30 mg in 15 mL → 2.00 mg/mL
- 45 mg in 15 mL → 3.00 mg/mL
- 60 mg in 15 mL → 4.00 mg/mL

Convert concentration units for viscometry: 1 mg/mL = 0.1 g/dL

Thus:

- c_1 = 0.10 g/dL
- c_2 = 0.20 g/dL
- c_3 = 0.30 g/dL
- c_4 = 0.40 g/dL

STEP 3: Calculate relative viscosity (η_r)

Formula: $\eta_r = t / t_0$

Mean flow times:

- c_1: 50.0 s
- c_2: 58.5 s
- c_3: 68.0 s
- c_4: 78.0 s

Calculations:

- c_1: 50.0 / 43.0 = 1.1628
- c_2: 58.5 / 43.0 = 1.3605
- c_3: 68.0 / 43.0 = 1.5814
- c_4: 78.0 / 43.0 = 1.8140

STEP 4: Calculate inherent viscosity (η_{inh})

Formula: $\eta_{inh} = \ln(\eta_r) / c$

(using c in g/dL)

c_1 (0.10 g/dL): $\eta_{inh} = \ln(1.1628) / 0.10 = 0.1508 / 0.10 = 1.51$ dL/g

c_2 (0.20 g/dL): $\eta_{inh} = \ln(1.3605) / 0.20 = 0.3078 / 0.20 = 1.54$ dL/g

c_3 (0.30 g/dL): $\eta_{inh} = \ln(1.5814) / 0.30 = 0.4583 / 0.30 = 1.53$ dL/g

c_4 (0.40 g/dL): $\eta_{inh} = \ln(1.8140) / 0.40 = 0.5956 / 0.40 = 1.49$ dL/g

STEP 5: Determine intrinsic viscosity [η]

Intrinsic viscosity is defined as: $[\eta] = \lim(c \rightarrow 0)\ \eta_{inh}$

A linear extrapolation of η_{inh} versus concentration yields an intercept of approximately:

$[\eta] \approx 1.52$ dL/g

STEP 6: Calculate Mark–Houwink molecular weight (Mη)

Substitute values into the Mark–Houwink equation:

M = ([η] / K)^(1/a)

$M = (1.52 / 6.06 \times 10^{-4})^{(1/0.64)}$

M = (2508)^1.5625

$M \approx 2.05 \times 10^5$ g/mol

FINAL RESULT

Amorphous PLA (baseline):

- Intrinsic viscosity: $[\eta] = 1.52$ dL/g
- Mark–Houwink estimated molecular weight: $M\eta \approx 2.05 \times 10^5$ g/mol

D20 – Single-point intrinsic viscosity estimate → Mark–Houwink molecular weight example for UV Experiment sample

Sample: Amorphous PLA High, 1 h, Rep 1

- Mean solution flow time (t): 51.0 s

Solvent: Chloroform

- Temperature: 25 °C
- Solvent flow time (t_0): 43.0 s

STEP 1: Define parameters

Mark–Houwink constants (PLA in chloroform, 25 °C):

- $K = 6.06 \times 10^{-4}$ dL/g
- $a = 0.64$

Mark–Houwink equation: $[\eta] = K \cdot M^a$

Rearranged: M = ([η]/K)^(1/a)

Important note (single-point method):

- With only one concentration, [η] cannot be determined by c→0 extrapolation.
- Instead, a single-point estimate can be used.

STEP 2: Calculate concentration in g/dL

Given:

- Mass = 36.1 mg
- Solvent volume = 15 mL
- Concentration = 2.41 mg/mL (given)

Convert to g/dL: 1 mg/mL = 0.1 g/dL

$c = 2.41 \times 0.1 = 0.241$ g/dL

STEP 3: Calculate relative viscosity (η_r)

$\eta_r = t / t_0 = 51.0 / 43.0 = 1.1860 \approx 1.19$

STEP 4: Calculate single-point viscosity estimate (η_{inh})

Single-point inherent viscosity: $\eta_{inh} = \ln(\eta_r) / c$

$\ln(\eta_r) = \ln(1.1860) = 0.1706$

$\eta_{inh} = 0.1706 / 0.241 = 0.708 \approx 0.71$ dL/g

For this single-point example, use: $[\eta] \approx \eta_{inh} = 0.71$ dL/g

STEP 5: Calculate Mark–Houwink molecular weight (Mη)

$M = ([\eta] / K)^{(1/a)} = (0.71 / 6.06\times10^{-4})^{(1/0.64)}$

$0.71 / 6.06\times10^{-4} = 1172.4$

$M = (1172.4)^{1.5625} \approx 6.22 \times 10^4$ g/mol

STEP 6: Calculate relative drop (%)

Using baseline starting polymer molecular weight: $M_0 = 2.05 \times 10^5$ g/mol

Relative drop: $\%\ \text{Drop} = (1 - M/M_0) \times 100$

$\%\ \text{Drop} = (1 - 62229/205000) \times 100 = (1 - 0.3036) \times 100 = 69.6\% \approx 69\%$

FINAL RESULT

UV Experiment – Amorphous PLA High 1 h Rep 1 (single-point estimate):

- $[\eta] \approx 0.71$ dL/g (single-point inherent viscosity estimate)
- $M\eta \approx 6.22 \times 10^4$ g/mol
- Relative drop vs baseline (2.05×10^5 g/mol): ~69%